UNIVERSITY OF SOUTHAMPTON

FACULTY OF ENGINEERING AND THE ENVIRONMENT

Dynamic topology optimization of plate for vibration suppression

by

Li Zhu

Thesis for the degree of Master of Philosophy

March 2019

UNIVERSITY OF SOUTHAMPTON

ABSTRACT

FACULTY OF ENGINEERING AND THE ENVIRONMENT

Thesis for the degree of Master of Philosophy

DYNAMIC TOPOLOGY OPTIMIZATION OF PLATE FOR VIBRATION SUPPRESSION

Li Zhu

Structural vibration control has always received considerable attentions for the unpleasant motions and environmental noise pollutions. Engineers and researchers have been looking for the more suitable and efficient methods to reduce structural vibration. Topology optimization method, as one design tool which could provide designers a design space with substantially more freedoms than size and shape optimization, has the potential to solve the long-standing problems. Stemming from this idea, the aim of this project is to apply topology optimization method to structural attenuation design.

In this thesis, the optimal distribution of damping material on vibrating structures by using topology optimization method has been investigated. Four topology optimization models for bi-material plate, free damping layer plate and constrained damping layer plate are established respectively to achieve structure vibration suppression design. In the bi-material case, both the sensitivity expressions for power flow response and dynamic compliance are derived. The comparison of these two objective functions illustrates minimization of power flow response also has great effect on the vibration suppression. In free damping layer plate topology optimization case, by comparing the optimal topology pattern with the steady-state responses of the structure, a rapid strategy to obtain a feasible damping material layout is proposed. Also in this research, an interface finite element is introduced to build the viscoelastic layer of constrained damping layer which reduces the computation cost of optimization procedure in constrained damping layer plate topology optimization case. One conclusion can be drawn that a better performance of vibration suppression can be achieved by increasing the thickness of viscoelastic layer or constrained layer. But with the increase of thickness of the constrained layer, the vibration amplitude decrease continuously while the same phenomenon is not that obvious for viscoelastic layer. The relationship between the constrained damping patch distribution and mode shape of the structure is also discovered in this case. In addition, a convenient implementation framework written by Python is developed for implement topology optimization method in Abaqus. Further extensions such as new topology optimization model, new objective functions and different optimizers could be easily built.

Contents

List of Figures

List of Tables

Declaration of Authorship

I, *Li Zhu*, declare that this thesis and the work presented in it are my own and has been generated by me as the result of my own original research.

Dynamic topology optimization of plate for vibration suppression

I confirm that:

1. This work was done wholly or mainly while in candidature for a research degree at this University;

2. Where any part of this thesis has previously been submitted for a degree or any other qualification at this University or any other institution, this has been clearly stated;

3. Where I have consulted the published work of others, this is always clearly attributed

4. Where I have quoted from the work of others, the source is always given. With the exception of such quotations, this thesis is entirely my own work;

5. I have acknowledged all main sources of help;

6. Where the thesis is based on work done by myself jointly with others, I have made clear exactly what was done by others and what I have contributed myself;

7. Parts of this work have been published as listed in publications.

Signed: ……

Date: ……27/112017……

Acknowledgements

Firstly, I gratefully acknowledge the help from my supervisors Associate Prof. Yeping Xiong and Prof. Atul Bhaskar. Without your advice, encouragement and patience, this thesis would not reach its present level. Another special acknowledgement goes to Yeping for all the suggestions on my project work during my MPhil study.

I would like to thanks my colleagues in this research group, Dr. Linghan Li and Mr Wei Wang for the helpful discussions. I would also like to express my gratitude to my friend Dr. Ping Lu and Dr. Yi Qu for your kind encouragement and viva mock before my transfer viva.

The financial support from the Faculty of Engineering and the Environment (FEE) and the China Scholarship Council is gratefully acknowledged. I would extend my sincere thanks to Yeping for her encouragement and great help to my applications for these scholarships.

Finally, I would like to thank my wife and my parents and my sister for their love and great encouragement through all these years.

Thank you all very much!

Li

Nomenclature

Symbol	Meaning
ρ	Material density
E	Young's modulus
h	Thickness
G	Shear modulus
Q	Shear forces
ω	Angular frequency
κ	Shear correction factor
$\boldsymbol{J}$	Jacobian matrix
M	Moments in Chapter 6
$\boldsymbol{M}$	Mass matrix
B	Strain-displacement matrix
D	Stress-strain matix
$\boldsymbol{C}$	Damping matrix
$\boldsymbol{K}$	Stiffness matrices
$\boldsymbol{Z}$	Impedance matrix
$\boldsymbol{S}$	Dynamic stiffness matrix
$\boldsymbol{F}$	Load magnitude vector
$\boldsymbol{f}$	External force vector
α	Mass damping coefficients
β	Stiffness damping coefficients
p, q	Penalty factor
η_r	Modal loss factor.
η_v	Loss factor of viscoelastic core
μ	Poissons' ratio
$\boldsymbol{\Phi}$	Mode shapes vectors
λ	Eigenvalue
θ	Rotation displacement
ϕ	Rotation of the normal to the mid-lane of the viscoelastic

	core layer
V	Material volume
f_v	Volume fraction ratio
$u,\ v,\ w$	Longitudinal displacements along x-, y-, z-axis
$\boldsymbol{W}$	Out-of-plane deflection
$\boldsymbol{U}$	Steady-state nodal displacement vector
$\boldsymbol{V}$	Steady-state nodal velocity vector
$\boldsymbol{d_e}$	Elemental nodal displacements vector
$\boldsymbol{\chi}$	Displacement field
$\widehat{U},\widehat{V},\widehat{W}$	Normal coordinates
a_r	Associated weighting factor
ψ	Linear interpolation functions
φ	Hermite cubic interpolation functions
Π	Objective function
C_d	Dynamic compliance
ε	Normal strain
σ	Normal stress
τ	Shear stress
γ	Shear strain
$\xi,\ \eta$	Normalised coordinate
N	Shape functions
A_j	Displacement amplitude of each degree of freedom
X	Displacement vector (in Chapter 6)
$q(t)$	Time-average power flow

Abbreviation

Abbreviation	Full Version
SIMP	Solid isotropic material with penalization
RAMP	Rational approximation of material properties
ESO	Evolutionary structural optimization method
MMA	Method of moving asymptotes
MAC	Modal assurance criterion
MDR	Modal damping ratio
GCMMA	Global convergence method of moving asymptotes
FE	Finite element
ASI	ABAQUS Scripting Interface
FLD	Free layer damping
PCLD	Passive constrained layer damping

Chapter 1 Introduction

1.1 Background

Structural vibration is a common problem in the field of engineering which would cause unpleasant vibration, noises and damages of the structure life. For many years, vibration suppression has been an urgent problem for engineers and scientists. Meanwhile, structure attenuation design, as one of the solutions for vibration reduction, has long been of concern for researchers.

Many strategies including active[1], semi-active control and passive control[2] have been proposed to address these problems. Among those control methods, passive vibration control, as a conventional approach, is advantageous for its simplicity and ease of implementation and has been widely applied in various fields, such as civil engineering[3] and aircraft industry[4]. Representative examples include minimization of the vibration amplitude of key structural components for fatigue damage reasons[5], and reduction of acoustic noise levels[6][7].

Structural design and materials distribution have great impact on the structural dynamic characterization which is essential for passive vibration control. Topology optimization, firstly proposed by Bendsøe and Kikuchi[8], is a suitable method to address this problem. This method was developed for determining the distribution of materials within an admissible design domain to yield an optimal structure which satisfies the required performance. Compared with the traditional size and shape optimization, this method provides the designers a design space with substantially more freedoms in the initial stage, which implies that much more efficient structures may be obtained. Thus topology optimization method gradually become a useful structure design tool to achieve higher performance, lower costs and lightweight structures.

This research is concern on optimizing structural topology layout by topology optimization method to achieve the better performance of vibration suppression. A systematic research involving both free damping layer structure and sandwich structure topology optimization for vibration suppression is performed. For the objective functions, topology optimization methods, design variables and optimization algorithms have a visible impact on the optimization effect for vibration reduction, thus it's necessary to compare and analyses the impact of these factors in topology optimization to find out the applicable methods for different engineering problems

and to guide engineering practice. In addition, an effective and efficient topology optimization tool will be developed in this research to implement topology optimization method and experiments will be designed to validate the effect of the optimized model.

1.2 Aims of this Thesis

The primary aim of this MPhil project is to apply topology optimization method to structural design for the better performance of passive vibration suppression. This project will explore the feasible topology optimization models to improve the performance of structural suppression design. Meanwhile the mechanism of vibration suppression and factors affecting the efficiency of suppressing vibration will be investigated. In order to expand topology optimization method to a wide range of engineering problems, a topology optimization package will be developed for commercial finite element software.

1.3 Achievement of this Thesis

1) A three-layer framework code is proposed to implement topology optimization method in Finite Element commercial software Abaqus. By taking advantage of the modelling capability of Abaqus, topology optimization method can be expanded to more engineering problems. Meanwhile, customized objective function is available for research purpose.
2) The power flow response is firstly proposed as the objective function in topology optimization to achieve vibration suppression. Both the sensitivity expression of power flow response and dynamic compliance as the objective function are derived. These results of comparison between the two cases provide numerical evidence that topology optimization with respect to minimum power flow response also has a strong improving effect on the vibration suppression.
3) An artificial damping material model for free damping layer plate that has a similar form as in the Solid isotropic material with penalization method (SIMP) approach is suggested with the sensitivity expression of steady-state vibration amplitude be given. The analysis of the results illustrates that there is no constant positive relationship between the performance of vibration suppression and the area of damping layer laid. By comparing the optimal topology pattern with the steady-state responses of the structure, a rapid strategy to obtain a feasible damping material layout is proposed.
4) Based on the analytical solution of constrained damping layer plate model established in thesis, vibration reduction effects with respect to different viscoelastic layer thicknesses and constrained layer thickness are compared. The results illustrate the difference of contributions to vibration suppression between constrained layer and the viscoelastic layer,

which plays a helping role in design of constraint damping layer structures

5) An interface finite element is introduced to build the viscoelastic layer of constrained damping layer which reduce the computation cost of optimization procedure. Based on the topology optimization model with respect to maximize modal damping ratio, the results discovered the relationship between the constrained damping patch distribution and mode shape of the structure.

1.4 Structure and content of this Thesis

For a comprehensive view of the field of topology optimization it is necessary to bring together three key areas of elasticity theory, engineering and optimization theory. This thesis begins by covering these areas before moving on to showing the work in the subsequent chapters. Hence the thesis is organised as follows:

Chapter 2 highlights a number of key issues in the field of structural optimization including the basic concept of topology optimization, widely used numerical solvers for topology optimization, numerical instability issue in topology optimization, applications of structural dynamics topology optimization and development of topology optimization codes.

Chapter 3 presents the FE modelling method for topology optimization models considering in this thesis. For the extensibility of topology optimization method, the framework and design process of Python topology optimization package based on solid isotropic material with penalization method for Abaqus has been detailed.

Chapter 4 shows case studies on dynamic topology optimization of bi-material plate structure for vibration suppression. The mathematical formulation of topology optimization is established based on power flow response and bi-material solid isotropic material with SIMP model. The results of numerical examples and comparison of optimal results between two topological designs with minimum power flow response and minimum dynamic compliance verified the efficiency of this method.

Chapter 5 investigates topology optimization model of vibrating structure with damping layer under harmonic excitations. An artificial damping material mode with penalization that has a similar form as in the SIMP approach is suggested. Numerical examples are given for illustrating the applicability and efficiency of the present approach. Optimal topologies obtained under different excitation frequencies and damping coefficients are also compared.

Chapter 6 derived the analytical solution of constrained damping layer plate model and

vibration reduction effects of this sandwich structure has also been discussed. The results indicate the reason why the constrained damping layer model could achieve a better performance of vibration energy dissipation than the free damping layer model. Then a topology optimization approach was proposed to design of the constrained damping layer treatments on flat base plates. In the proposed approach, an interface finite element is introduced to modelling the viscoelastic layer of constrained damping layer treatment to simplify the FE model in the optimization procedure. The SIMP interpolation scheme is applied to generate the mass and stiffness matrices of the structure. The optimal layout obtained in optimization achieve a remarkable effect on vibration suppression with 50% reduction of weight.

Finally, Chapter 7 concludes the thesis by recounting the achievements and limitations of the work. Ideas for future work are set out as possible topics for investigation.

Chapter 2 Literature review

This chapter presents some general concepts related to structural optimization with topology optimization method. The basic concept of topology optimization is introduced in the Section 2.1. A short development history of topology optimization is reviewed followed by the introduction of widely used numerical solvers for topology optimization. Optimizer is also critical part in the process of optimization. This part is detailed in Section 2.4. The problem of numerical instability is inevitable especially when you are dealing with optimization under multiple non-linear constraints. Section 2.5 presents the development of techniques to avoid numerical instability in topology optimization. Topology optimization method of structural dynamics is reviewed in Section 2.6 and last, the research related to topology optimization codes is presented in Section 2.7.

2.1 Basic concept of topology optimization

Generally, design variables, objective functions and constraints form an integral part of an optimization problem. Each of these three plays an important role in structural optimization. Among them, design variable is the main factor used to distinguish optimization methods. As a result, there are several structural optimization techniques in terms of the dimensions of design variables: sizing, shape, and topology optimizations. **Fig 2.1** shows the examples that three main structural optimization techniques are applied to a beam problem.

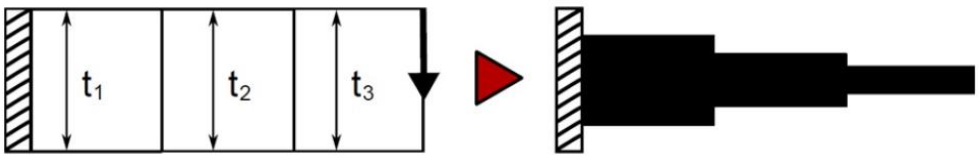

(a) Size Optimization

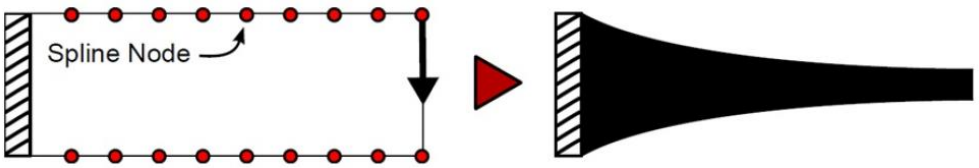

(b) Shape Optimization

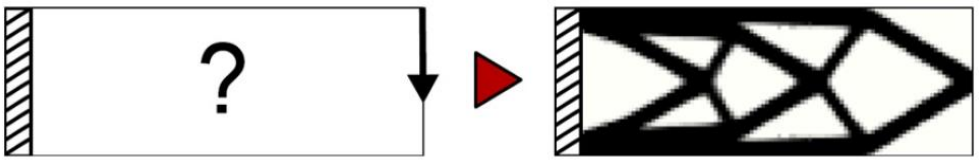

(c) Topology Optimization

Fig 2.1 *Difference between Size, Shape and Topology optimization*[9]

Size optimization aims to search the optimal size parameters in design space while keeping shape and topology unchanged. Usually this method employs discrete design variables as shown in **Fig 2.1 a)**. The thickness of each of the three portions is considered as the design variable and is optimized. This technique has been widely applied to real world problems because of its ease of use and mature theory and algorithm. Shape optimization aims to search the optimal boundary and geometry of structure while only keeping the topology of the structure unchanged. As shown in **Fig 2.1 b)**, specifically employs geometrical entities such as surfaces or edges. The edges are defined using spline nodes which can be freely moved up or down in order to maximize/minimize an objective function such as maximum deflection or maximum stress and so on.

Different from size optimization and shape optimization, topology optimization method aims to search the optimal topological pattern of the structure, in other words, an art to find the best locations for cavities in a given design domain. In topology optimization, not only the boundary shape of the structure is changed, but also the material distribution in the structure are totally reorganized. Obviously, this method allows greater design freedom than sizing and shape optimization. This topic has been intensively investigated in the past three decades. At present, it is mainly used in the applications such as the force path in the mechanics, the heat conduction channel in the heat conduction structure, and the waveguide design in the wave propagation and so on.

2.2 Overview of structural topology optimization

Structural topology optimization is one of the most advanced and challenging subjects in the field of structural optimization, which is a multidisciplinary research subject including topology theory, mechanics, computer science and optimization theory. The origin of structural topology optimization can be traced back to 1904 when Michell[10] adopted the analytic method to study the topology optimization design of truss structures under stress constraints. The condition that the lightest weight truss configuration should meet is known as the Michell criterion, and the truss satisfying the Michell criterion is called the Michell Truss. In 1981, the study of Olhoff and Cheng Gengdong[11] on the material distribution of solid plates obtained a global optimal plate design with infinite ribs. This work is considered to be the pioneer of topology optimization of modern continuum structures. Later, Bendsøe and Kikuchi[8] firstly proposed the homogenization method for topology optimization, in which identifying the optimal topology of a structure is transformed to a size optimization problem with the geometry parameters describing the microstructure of materials as design variables. Although the milestone laid the foundation for the later development of topology optimization method, the

homogenization method requires great computational effort because elastic properties of the porous material and the geometry parameters of its microstructure with complex geometries need to be established in applying this approach. On the basis of previous works, a number of different methods has been developed from the original homogenization approach concept, including Solid Isotropic Material with Penalisation (SIMP) and Evolutionary Structural Optimization (ESO) approaches and Level Set Method

The early structural optimization algorithms are mainly based on the intuitive criterion method, such as full stress criterion and full strain criterion, but the nonlinear mathematical programming method has better robustness and adaptability. However, topology optimization problems often require the computation of objective functions, constraint equations and their derivatives[15], and the computational time depends on the number of design variables. This means that when the number of design variables increases, these mathematical programming methods will become very time-consuming and inefficient [16]. In topology optimization, especially the topology optimization based on the finite element method, the number of design variables is proportional to the number of finite elements in the design area. In order to overcome the efficiency problem of topology optimization, the Optimality Criteria (OC) method appeared in 1960s. OC method is an effective method for solving topology optimization. Its advantage lies in its fast convergence speed, high computational efficiency, simple concept and easy implementation. Later Svanberg proposed Method of Moving Asymptotes（MMA[17]）based on Sequential Convex Programming in 1987 which has become one of the most popular optimization method for topology optimization. With the development of artificial intelligence, there are more and more non-gradient optimization algorithms be applied in topology optimization such as neutral network and genetic algorithm.

2.3 Numerical methods of topological optimization

2.3.1 Homogenisation Method

In 1988, Bendsøe and Kikuchi[8] firstly introduced the homogenization method into the structural topology optimization problem. Since then, the topology optimization theory has been developed rapidly. By introducing material microstructure model with cavity into the macrostructure, topological design problem is transformed into a relatively simple material size optimization problem. Then, the homogenization method is used to solve the macroscopic materials characteristics with different microstructure configurations. The optimal structure macroscopic topology can be obtained by optimizing the microstructure size because the relationship between the macroscopic characteristics and the microstructure size has been obtained. Suzhki[18] studied structural shape and topology optimization collaborative design

based on homogenization method. In his paper, a structural topology optimization algorithm considering multiple working conditions was proposed. Tenek etc.[22] adapted the mathematical programming algorithm as the optimization solver for structural topology design based on homogenization theory. Hassani and Hinton[23] systematically summarized the topology optimization theory and algorithm based on homogenization method, and proposed the mathematical topology optimization model based on homogenization method. With the help of homogenization theory, topology optimization problem is transferred to size optimization to some extent which greatly reduces the difficulty of searching optimal solution.

2.3.2 Solid isotropic material with penalization method

Shortly after the homogenization approach to topology optimization was introduced, Bendsøe[24] and later others[25] suggested the solid isotropic material with penalization(SIMP) approach, 'which first was meant as an easy but artificial way of reducing the complexity of the homogenization approach and improving the convergence to 0-1 solutions.' Compared with the homogenization method, the model can obtain the relationship between the material density and the elastic modulus without computation burden which reduces the amount of the optimization design variables and also simplifies the optimization process.

The distributed function of design variables in SIMP method is interpreted as the material density of each finite element ρ_e. 'usually the density variables are penalized with a basic power law (whose value is finite) and multiplied onto physical quantities such as material stiffness and density'[9], see **Eq. (2.1)**.

$$E(\rho_e) = \rho_e{}^p E_0 \tag{2.1}$$

where p is the penalization parameter and E_0 is the Young's modulus of solid material. The values of density range as $0 \leq \rho_e \leq 1$ where 0 corresponds to a void element, 1 to a solid element.

In 1999, Bendsøe and Sigmund[26] proved the existence of microstructure of the intermediate density elements in the process of continuum structure topology optimization which further completed SIMP method theoretically. Since then, the SIMP method entered a period of rapid development. Sigmud[27] in 2001 published a Matlab program and then Tchernika and Sigmud[28]developed the topology optimization program on web pages so that more scholars and engineers have the access to understand and use the SIMP method. In 2003, Sigmud and Bendsøe in 2003 published an important book[9] which systematically introduced the theory and applications of topology optimization method.

In the process of the development of SIMP model, Sigmud and Olhoff have also made

outstanding contributions to the application of this method, including compliant mechanism[29], geometric nonlinear structure[30], phononic crystal structure[31][32], phononic crystal band gap material[33]. reliability based topology optimization[34] and continuum vibration problems[35][36][37]. In addition, due to the development and progress of commercial finite element software (Opti Struct, Genesis, MSC / Nastran, Ansys, Tosca, etc.), topology optimization has been widely used in the fields of automobile, aerospace industry. SIMP method has also become a must-have option in most of commercial softwares for structural optimization.

2.3.3 Evolutionary structural optimization method

Evolutionary optimization method (ESO) is based on the idea of evolution to gradually remove invalid or inefficient materials to achieve topology optimization of continuum structures, thus avoiding the solution of multivariable mathematical programming. The study of this algorithm was first developed by Xie and Stephen[38]. Manickarajah et al. [39] proposed a ESO optimization method for buckling of thin plates based on stress criterion. Li et al. [40][41]carried out the shape optimization and topology optimization design of heat conduction structure based on ESO method and applied the filtering algorithm in his research. Yang et al. [42]proposed a bidirectional evolutionary structural optimization algorithm(BESO), which not only can be deleted, but also can be added, which is a good way to improve the single direction evolutionary algorithm. Huang et al. [43] pointed out that the BESO method has a great advantage in terms of computational efficiency and optimization ability compared with previous method.

2.3.4 Level set approach

Compared with the optimization process of homogenization method, evolutionary optimization method and solid isotropic material with penalization method, level set method is mainly developed from the field of boundary propagation and based on implicit functions that define structural boundaries rather than an explicit parameterization of the design domain. **Fig 2.2** b) demonstrates an implicit representation where the structural boundary is implicitly specified as a contour line of the field Φ, which is a function of x.

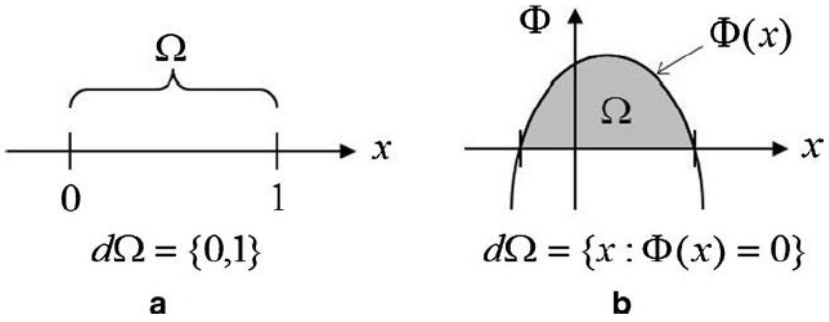

Fig 2.2 a) *Explicit versus* ***b)*** *Implicit representation of a design domain and boundaries (from Deaton et al[44])*

In 2001, Osher and Santosa[46] used the level set function to describe the geometric boundary of the structure. In their research, the variational principle and gradient projection method were used to derive the velocity function and the optimal design of the structure self-vibration problem was studied. Allaire[47][48][49] applied the level set approach to the static problems, dynamic problems and multiple loadings problems including maximum stiffness design of linear and nonlinear problems. The capability for topology design for stiffness under a volume constraint was demonstrated. Additional discussion of multiple material level set method can be found in Wang et al. [50] and Wang et al.[51]. However, as the Hamilton–Jacobi equation is employ to evolve the level set function and lack of the mechanism to insert holes into the design regions, the convergence rate of the traditional level set method is slower than that of conventional method. This difficulty can be overcome by topological derivative technique which was firstly proposed by Eschenauer et.al [52]. By employing this hole insertion mechanism, the efficiency of the level set method can be greatly enhanced and the initial design-dependency of the optimal topologies can be alleviated.

2.4 Update schemes

As a highly developed tool for structural design, topology optimization plays an important role in mechanical, automotive and aerospace industries[54]. Optimizer, as a critical part in topology optimization process, undoubtedly deserves more attention. So far, a large number of different design update schemes have been suggested for topology optimization problems, which can be roughly divided into two categories: gradient-based topology optimization algorithms and non-gradient approaches.

2.4.1 Gradient-based topology optimization algorithm

Gradient-based topology optimization algorithms for continuum topology optimization problems has been applied to almost all topology optimization methods such as solid isotropic material with penalization approach [16][24], level set approach[50][55], evolutionary structural

optimization approach[56], etc.

Compliance minimization problem with a volume constraint is very common in static topology optimization. However, this case is very special because the gradients of the objective function have same sign during each iteration, so basically any rigorous mathematical methods and even intuitive criterion methods (eg. Optimality Criteria) work well for this kind of optimization. Once more difficult problems such as the non-selfadjoint problems are considered, varying signs on gradients or more than one non-linear constraint will lead to fail of majority of the intuitive criterion methods.

A large number of studies have shown that the sequential convex programming method has strong adaptability to solve the topology optimization problem. The Method of Moving Asymptotes (MMA) proposed by Svanberg[17] belongs to a classical method of convex programming method. Currently, the MMA and global convergence version GCMMA [58] have become one of the most widely used method in topology optimization. The basic idea of MMA is to produce a strict convex approximation sub-problem in each iteration step and to solve them. This sub-problem is controlled by the so-called moving asymptotes which greatly improve the stability and efficiency of the iterative process. So far, more advanced mathematical programming tools [59][60] have emerged and tested; however, they have not been proven to be more effective or reliable than Method of Moving Asymptotes methods [61].

2.4.2 Non-gradient-based topology optimization algorithm

Besides the development of gradient-based topology optimization algorithms, another type of optimization approach based on random processes was continuously proposed by scholars. Such methods encompass Genetic Algorithms[65][66][67], Artificial Immune Algorithms[68], and Differential Evolution schemes[69]. These methods only use objective function evaluations to converge to a reasonable solution. Sigmund[70] compares the gradient-based and non-gradient topology optimization algorithms technologies systematically. Although non-gradient topology optimization algorithms may solve extremely coarse problems quite well, it is obvious that it cannot solve even slightly larger problems since the number of possible combinations grows exponentially with respect to increase in design variables[70]. And non-gradient topology optimization algorithms cannot guarantee obtaining the global optimum in every case. Thus gradient-based topology optimization technologies, so far, are still the most efficient and reliable technology to achieve the optimal design for topology optimization[70].

2.5 Numerical instability of topological optimization

The topology optimization theory of continuum has been well developed[71][72] and applied in

the structure, material, mechanical, electromagnetic and other industrial fields, but there is still instability phenomenon during the optimization process such as checkerboard structure and mesh dependence and so on[73].

2.5.1 Checkerboards problems

Checkerboards refers to the formation of adjacent solid-void elements arranged in a checkerboard pattern as shown in **Fig 2.3**. **Fig 2.3**. a) shows typical checkerboards problem occurring in topology optimization. **Fig 2.3**. b) and **Fig 2.3**. c) are the optimal results for different discretization.

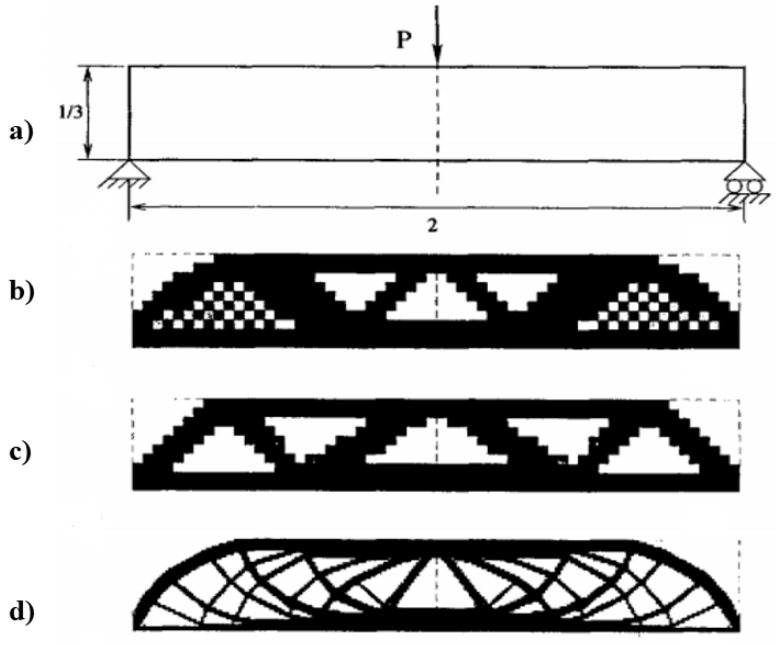

Fig 2.3 *Numerical instability; (a) Design problem (b) Example of checkerboards (c) Solution for 600 elements discretization (d) Solution for 5400 elements discretization (Deaton et. al 2014)*

The chessboard format in the topology optimization results in the difficulty of manufacturing, so the chessboard structure in the topology optimization should be avoided as much as possible. The main processing methods of chessboard structure are as follows:

(1) Smoothing: that is image post-processing[77]. However, this method ignores the problem itself and should be avoided in practical engineering.

(2) High-order Finite Elements: literature[78] pointed out that the finite element model with 8 or 9 nodes can suppress checkerboard structure to a great extent. The disadvantage of this method is the increasing computation load due to the use of higher-order element models.

(3) Filter: Based on the filtering technology in image processing, Sigmund[79][80] proposed a checkerboard structure filtering technology by modifying the design sensitivity of each element in which the sensitivity of an element is decided by all adjacent elements in the

filter radius range instead of itself. Literature[81] pointed out that the ability to suppress chessboard structure was improved by using this method.

2.5.2 Mesh dependence

Mesh dependence means that the optimal topological structure of the same optimization problem will change if the number of elements increase, meanwhile the geometric complexity of the optimal topological structure is also increasing. As shown in Fig. 2.3, (c) the optimization results obtained by using 600 finite elements; (d) the optimization results obtained by using 5400 finite elements. Document[82] pointed out that the reason for mesh dependency of topology optimization is that the optimal solution does not exist or exists, but is not unique. Zhou and other[83] pointed out that the chessboard format is a form of meshing dependency, so the designers can eliminate the meshing dependency by using the checkerboard pattern filtering technology.

2.6 Topology optimization method of structural dynamics

The early structural optimization design mainly focuses on the static strength of the structure, however, a great deal of engineering experience shows that the structural accidents are often related to the dynamic stiffness of structures. Therefore, performing dynamic optimization design of structures is necessary. Because the structure dynamic performance is much more complex compared to static performance, so there are a variety of indicators for structural dynamic performance evaluation, mainly include: natural frequency of structure, frequency response, dynamic compliance, power flow response, modal loss factor and so on.

The natural frequency characteristics of structures can often be used to effectively describe the dynamic characteristics of structures. For example, in low frequency vibration, the dynamic response of the structure depends mainly on the fundamental frequency and the first order mode of the structure. So, in general, the design and optimization of structural natural frequencies is often considered to be able to improve the dynamic performance of structures. Therefore, the research on the optimization of structural natural frequencies is the earliest, the most comprehensive in the development of structural dynamics optimization. There are mainly two kinds of frequency optimization problems in the traditional sense: one is the minimization of the structure weight under a certain frequency; the other is the maximization of the fundamental frequency or frequencies gap of the structure under the constraint of a given weight. For these objectives, sensitivity of the eigenvalue and eigenvector analysis is very important, so a large number of scholars dedicated to the research on this problem.

Allaire et al. [84]presented a procedure that maximized the first eigenvalues of a combination of

two elastic materials in a bounded domain, extended the homogenization method, originally developed for compliance optimization, to frequency optimization problems. Subjected to a volume constraint for the rigid material, the optimal materials distribution of admissible design domain was achieved for two- and three-dimensional problems. Du J. and Olhoff N. [84] discussed dynamic topology optimization problems involving simple and multiple eigenfrequencies of linearly elastic structures without damping. In that paper, the maximization of the fundamental eigenfrequency of beam-like 2D structure and plate-like 3D structures were investigated. The results represented a feasible approach to move structural resonance frequencies far away from external excitation frequencies and thereby avoid high vibration levels. For avoiding the artificial localized modes occurred in areas where elements are assigned with lower density values, Du and Olhoff[86] modified the interpolation formulation to place a heavy penalty on the mass of elements to avoid the occurrence of spurious, localized eigenmodes. In their paper, the design objective functions are to maximize the distances (gaps) between two consecutive eigenfrequencies of the structures. Madeira et al.[88] employed a genetic algorithm to achieve the maximization of the stiffness and the maximization of the first and the second eigenfrequencies of a plate. Compared with classical gradient optimizer based on SIMP method, genetic algorithm avoid grey areas for only integer design variables are interpreted. However, although avoiding the calculation of objective sensitivity, a much larger iteration is required by using Genetic Algorithm.

In many cases, the structure may work at a specific frequency or frequency range for a long period of time (such as engine), so study on the specified frequency response of structure is also very important. The common structural dynamic responses include displacement, acceleration, velocity and so on. In addition to frequency response of a specified position of the structure, a global structural frequency response indicator can also be used to evaluate dynamic performance of structure, such as the concept of compliance in the static optimization which has applied to the dynamic optimization, named "dynamic compliance and this concept is currently has been widely accepted.

Dynamic compliance was firstly introduced into topology optimization with density method by Jog [89]. In his paper, dynamic compliance was treated as the objective function to reduce the vibrations in an overall. Du and Olhoff[93] dealt with the topological design problem with structures that are subjected to time-harmonic, design-independent (or –dependent) dynamic loading by the same objective function. Jensen[94] proposed an efficient procedure for topology optimization of dynamics based on frequency responses represented by Padé approximants. An accurate approximation of the frequency response and design sensitivities was given and the accuracy of the Padé approximants is studied for simple 1-D and 2-D systems.

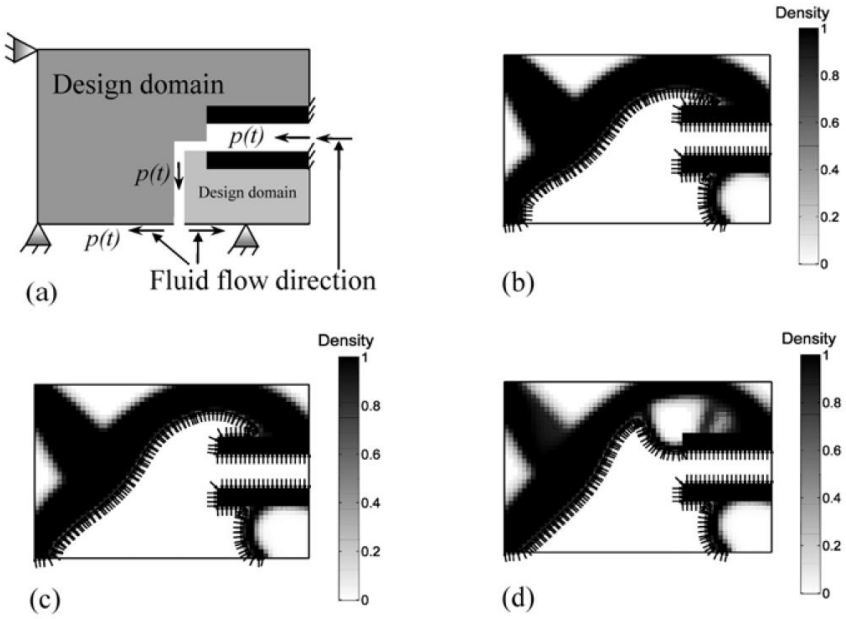

Fig 2.4 *Optimized topologies (40% volume fraction) and loading boundaries of 2D inlet for three different loading frequencies. (a) Admissible design domain, loading and support conditions. (b)* ω_p *= 0 rad/s. (c)* ω_p *= 800 rad/s (d)* ω_p *= 1000 rad/s. (From Olhoff and Du 200*[6][93]*)*

More recently, a concurrent topology optimization methodology was proposed by Vicente W.M.[95] to conduct designs of the macro and micro structures simultaneously. In their model, macro structure and micro structure are coupled using the homogenization theory. It is assumed that the macro structure is composed of a periodic material and the effective properties of this material obtained from the micro structure is used in finite element analysis. Bi-directional ESO method is applied to find the optimum layout on both macro and micro scales of the structure, with the objective of minimizing the frequency response in the macro structure. For a structure with a non-dominant damping effect, modal loss factor method can be used as a convenient way to measure structure's ability to absorb vibration, thus modal loss factors are often chosen as objective functions in the optimization of constrained damping layer structures. Mohammed[99] studied the optimal layout of damping materials with maximum energy dissipation as objective function. In his paper, the shear strain energy of the viscoelastic damping materials is designed by the inverse mean - square method. The position and shape optimization of the material damping layer on the surface of the structure to reduce the vibration in a frequency band is studied by Alvelid[99].

2.7 Topology optimization codes

Several educational articles[99][104] were published aimed at introducing fundamentals of various algorithms by presenting computer program implementations since topology optimization method has received more attentions. The first topology optimization method Matlab codes based on SIMP method was published by Sigmund[99]. The 99 lines codes provide a compact

implementation of solid isotropic material with penalization method to obtain the optimal structure under various boundaries. An 88-line Matlab code was later developed by Andreassen et al. [106] as an extension to Sigmund's 99-line Matlab code with improved efficiency. Huang and Xie [105] published a Matlab code for 2D compliance minimization using the Bi-directional evolutionary structure optimization method. Later a discrete topology optimization method code using the level-set method was presented by Challis [107] in 2010. However, the codes provided by these papers are only for 2D optimization problems. Inspired by the previous work, Liu K. and Tovar A. [108] presented a Matlab implementation using a modified SIMP model for 3D topology optimization for linear structures with regular 8-noded elements. Niels Aage et al. [109] proposed a parallel framework for topology optimization method. In his work, the widely used MMA optimization algorithm is parallelized as a fundamental part of framework. Zuo Z.H. and Xie Y. M. [110] presented a simple Python topology optimization code for general 2D and 3D structures based on Abaqus /CAE. With simple modifications, the basic Python code has been extended to enhance computational efficiency and to consider multiple load cases and nonlinearities. So far, most of work on the implementation of topology optimization method require the researchers to write their own finite element code for the optimization problems. However, we know that many mature commercial finite element software, such as ANSYS and Abaqus, have been widely used in many engineering fields. So how to make better use of these resources for topology optimization is also a problem worthy of attention.

2.8 Motivation for current work

In a summary, current research on the passive vibration control by using topology optimization method is still in its infancy. Most of their work mainly focused on taking intrinsic properties of the structures like fundamental eigenfrequencies, frequency response or dynamic compliance as objective function, but the possibility of using other objective to achieve the vibration reduction still exits. These attempts research are very limited in current work. In addition, there is a lack of systematic research on different vibration reduction strategies for plate structures by using topology optimization method. Thus a comprehensive study and comparison on different strategies to achieve the purpose of plate vibration reduction is necessary. Moreover, a convenient platform to run topology optimization is not available at present. Researchers usually need to write optimization algorithms or finite element codes by themselves, which has a certain impact on the development of research work.

To achieve deeper and more comprehensive understanding of applying the topology optimization method in vibration suppression design of plate structure forms the foundational motivation of this MPhil project. This thesis mainly focuses on the aspects associated with the

passive vibration control of plate structure by using topology optimization method, including:

1. Proposing a SIMP model based on power flow response to achieve dynamic topology optimization for plate vibration deduction.

2. Proposing topology optimization models based on different strategies for vibration deduction and evaluating the efficiency.

3. Developing Python package works with commercial finite element software Abaqus to apply topology optimization method

Chapter 3 Finite element modelling for topology optimization

FE method is a necessary tool to implement topology optimization method. In this chapter, the method of modelling four-node Mindlin[131] plate element and eight-node 5 degrees of freedom interface element are given. In addition, a code framework to implement topology optimization method based on Abaqus are presented. All these works pave the way for the case studies and applications in the following chapters.

3.1 Finite element modelling of Mindlin plates

3.1.1 Introduction of Mindlin plate theory

Before we start to introduce of the modelling details, the background of our model adapted is discussed here. In this thesis, plate is the main object to adapt the topology optimization for vibration suppression. In terms of the relationship of thickness and length(width), plates might be classified as thin if thickness/min(length, width)< 1/20 and thick if thickness/min(length, width)< 1/10[131] . Correspondingly, different theories need to be adopted in modelling.

The Kirchhoff-Love[131] plate theory is applicable to thin plate. The following assumptions are made:

(i) The middle plane of the plate remains free of in-plane stress/strain. Bending of the plate will cause material above and below this mid-plane to deform in-plane.

(ii) Line elements lying perpendicular to the middle surface of the plate remain perpendicular to the middle surface during deformation,

(iii) Line elements lying perpendicular to the mid-surface do not change length during deformation, so that γ_{zz} throughout the plate.

When the plate is relatively thick, one is advised to use a more exact theory, for example one of the shear deformation theories: Mindlin plate theory. The Mindlin plate theory was developed in the mid-1900s to allow for possible transverse shear strains. In this theory, there is the added complication that vertical line elements before deformation do not have to remain perpendicular to the mid-surface after deformation, although they do remain straight. Thus shear strains γ_{xz} and γ_{yz} are generated, constant through the thickness of the plate. In this Chapter, both Kirchoff and Mindlin theories are adapted and the models are also subject to the assumptions for these two theories.

3.1.2 Finite element discretization

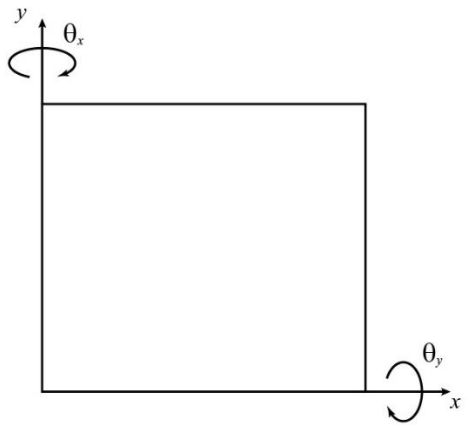

Fig 3.1 *Mindlin plate: illustration of geometry, degrees of freedom*

We consider the assumed displacement field $\boldsymbol{\chi}$ as below:

$$\boldsymbol{\chi} = \begin{Bmatrix} u \\ v \\ w \end{Bmatrix} = \begin{Bmatrix} z\phi_x \\ z\phi_y \\ w \end{Bmatrix} \tag{3.1}$$

Where z denotes the poison in z-axis. ϕ_x and ϕ_y are the rotations along y- and x-axis. u, v are the displacements in x- and y- direction. w is the longitudinal displacements in the mid-plane. Then bending strains field $\boldsymbol{\varepsilon_f}$ can be obtained as

$$\boldsymbol{\varepsilon_f} = \begin{Bmatrix} \varepsilon_x \\ \varepsilon_y \\ \gamma_{xy} \end{Bmatrix} = \begin{Bmatrix} \dfrac{\partial u}{\partial x} \\ \dfrac{\partial v}{\partial y} \\ \dfrac{\partial u}{\partial y} + \dfrac{\partial v}{\partial x} \end{Bmatrix} = \begin{Bmatrix} z\dfrac{\partial \phi_x}{\partial x} \\ z\dfrac{\partial \phi_y}{\partial y} \\ z\left(\dfrac{\partial \phi_y}{\partial x} + \dfrac{\partial \phi_x}{\partial y}\right) \end{Bmatrix} \tag{3.2}$$

Where $\varepsilon_x, \varepsilon_y$ and γ_{xy} are the strain components in three directions. And transverse shear deformations field $\boldsymbol{\varepsilon_c}$ are obtained as:

$$\boldsymbol{\varepsilon_c} = \begin{Bmatrix} \gamma_{xz} \\ \gamma_{yz} \end{Bmatrix} = \begin{Bmatrix} \dfrac{\partial w}{\partial x} + \dfrac{\partial u}{\partial z} \\ \dfrac{\partial w}{\partial y} + \dfrac{\partial v}{\partial z} \end{Bmatrix} = \begin{Bmatrix} \dfrac{\partial w}{\partial x} + \phi_x \\ \dfrac{\partial w}{\partial y} + \phi_y \end{Bmatrix} \tag{3.3}$$

After both bending and shear deformations are defined, the strain energy P of the Mindlin plate can be given as

$$P = \frac{1}{2}\int_V \boldsymbol{\sigma_f^T}\,\boldsymbol{\varepsilon_f} dV + \frac{\kappa}{2}\int_V \boldsymbol{\sigma_c^T}\,\boldsymbol{\varepsilon_c} dV \tag{3.4}$$

$\boldsymbol{\sigma_f}$ and $\boldsymbol{\sigma_c}$ are bending stress and shear stress respectively. κ is a shear correction factor which takes the value $5/6$ for the rectangle section in this case.

For homogeneous isotropic material and plane stress problem are considering here, thus the constitutive relations can be reduced to the plane stress approximation as below:

$$\boldsymbol{\varepsilon_f} = \begin{bmatrix} \varepsilon_x \\ \varepsilon_y \\ \gamma_{xy} \end{bmatrix} = \frac{1}{E} \begin{bmatrix} 1 & -\mu & 0 \\ -\mu & 1 & 0 \\ 0 & 0 & 2(1+\mu) \end{bmatrix} \boldsymbol{\sigma_f} \tag{3.5}$$

μ is Poissons' ratio and E is Young's modulus, which has the inverse:

$$\boldsymbol{\sigma_f} = \frac{E}{(1-\mu^2)} \begin{bmatrix} 1 & \mu & 0 \\ \mu & 1 & 0 \\ 0 & 0 & \dfrac{1-\mu}{2} \end{bmatrix} \boldsymbol{\varepsilon_f} \tag{3.6}$$

Similarly, transverse shear stresses

$$\boldsymbol{\sigma_c} = \begin{bmatrix} G & 0 \\ 0 & G \end{bmatrix} \boldsymbol{\varepsilon_c} \tag{3.7}$$

Introducing these concepts into the strain energy, we obtain

$$P = \frac{1}{2} \int_V \boldsymbol{\varepsilon_f^T D_f \varepsilon_f} dV + \frac{\kappa}{2} \int_V \boldsymbol{\varepsilon_c^T D_c \varepsilon_c} dV \tag{3.8}$$

Where:

$$\boldsymbol{D_f} = \frac{E}{(1-\mu^2)} \begin{bmatrix} 1 & \mu & 0 \\ \mu & 1 & 0 \\ 0 & 0 & \dfrac{1-\mu}{2} \end{bmatrix}, \qquad \boldsymbol{D_c} = \begin{bmatrix} G & 0 \\ 0 & G \end{bmatrix} \tag{3.9}$$

G is the shear modulus, and the interpolation functions of the displacements in mid-plane can be given as follow:

$$\begin{aligned} w(x,y,t) &= \sum_{k=1}^{4} w_k(t)\psi_k(x,y) \\ \phi_x(x,y,t) &= \sum_{k=1}^{4} \phi_{xk}(t)\psi_k(x,y) \\ \phi_y(x,y,t) &= \sum_{k=1}^{4} \phi_{yk}(t)\psi_k(x,y) \end{aligned} \tag{3.10}$$

ψ_k $(k = 1,2,3,4)$ are the shape functions of a bilinear four-node Q4 element., which can be expressed as:

$$\psi_k = \frac{1}{4}(1+\xi\xi_k)(1+\eta\eta_k) \tag{3.11}$$

Rewrite the equations in matrix form as follow:

$$[\boldsymbol{\chi}]_{\mathbf{3\times1}} = [\boldsymbol{N}]_{3\times12}[\boldsymbol{d^e}]_{12\times1} \tag{3.12}$$

Where $\boldsymbol{d}_e^{(i)}$ is the elemental nodal displacements vector:

$$\boldsymbol{d^e} = [w_k, \phi_{xk}, \phi_{yk}]^T{}_{12\times1} \quad (k = 1,2,3,4) \tag{3.13}$$

$$\boldsymbol{N} = [N_1 \quad N_2 \quad N_3 \quad N_4]_{3\times12} \tag{3.14}$$

$$\boldsymbol{N_k} = \begin{bmatrix} 0 & \psi_k & 0 \\ 0 & 0 & \psi_k \\ 0 & \psi_k & \psi_k \end{bmatrix}_{3\times3} \tag{3.15}$$

According to linear elastic stress-strain relations and use **Eq. (3.5)**, the strains can be written in matrix form as follow:

$$\left[\boldsymbol{\varepsilon_f}\right]_{\mathbf{3\times1}} = \begin{bmatrix} \varepsilon_x \\ \varepsilon_y \\ \gamma_{xy} \end{bmatrix} = \begin{bmatrix} z\dfrac{\partial \phi_x}{\partial x} \\ z\dfrac{\partial \phi_y}{\partial y} \\ z\left(\dfrac{\partial \phi_y}{\partial x} + \dfrac{\partial \phi_x}{\partial y}\right) \end{bmatrix} = z[\boldsymbol{B}_s]_{3\times12}[\boldsymbol{d^e}]_{12\times1} \tag{3.16}$$

Where $\boldsymbol{B}_s$ is strain-displacement matrix for bending contributions

$$\boldsymbol{B}_s = [\boldsymbol{B}_{s1} \;\; \boldsymbol{B}_{s2} \;\; \boldsymbol{B}_{s3} \;\; \boldsymbol{B}_{s4}]_{3\times12} \tag{3.17}$$

$$\boldsymbol{B}_{sk} = \begin{bmatrix} 0 & \dfrac{\partial \psi_k}{\partial x} & 0 \\ 0 & 0 & \dfrac{\partial \psi_k}{\partial y} \\ 0 & \dfrac{\partial \psi_k}{\partial y} & \dfrac{\partial \psi_k}{\partial x} \end{bmatrix}_{3\times3} \qquad k = 1,2,3,4 \tag{3.18}$$

According to linear elastic stress-strain relations and use **Eq. (3.7)**, the strains can be written in matrix form as follow:

$$\boldsymbol{\varepsilon_c}_{\;\mathbf{2\times1}} = \begin{bmatrix} \gamma_{xz} \\ \gamma_{yz} \end{bmatrix} = \begin{bmatrix} \dfrac{\partial w}{\partial x} + \phi_x \\ \dfrac{\partial w}{\partial y} + \phi_y \end{bmatrix} = [\boldsymbol{B}_v]_{2\times12}[\boldsymbol{d^e}]_{12\times1} \tag{3.19}$$

Where $\boldsymbol{B}_v$ is strain-displacement matrix for shear contributions

$$\boldsymbol{B}_v = [\boldsymbol{B}_{v1} \;\; \boldsymbol{B}_{v2} \;\; \boldsymbol{B}_{v3} \;\; \boldsymbol{B}_{v4}]_{2\times12} \tag{3.20}$$

$$\boldsymbol{B}_{vk} = \begin{bmatrix} \dfrac{\partial \psi_k}{\partial x} & \psi_k & 0 \\ \dfrac{\partial \psi_k}{\partial y} & 0 & \psi_k \end{bmatrix}_{2\times3} \qquad k = 1,2,3,4 \tag{3.21}$$

We then obtain the plate strain energy as:

$$U_e = \frac{1}{2}\boldsymbol{d}^{\boldsymbol{e}^T}\int_V \int_z z^2 \boldsymbol{B}_s^T \boldsymbol{D}_f \boldsymbol{B}_s dz dV \boldsymbol{d}^e + \frac{\kappa}{2}\boldsymbol{d}^{\boldsymbol{e}^T}\int_V \int_z \boldsymbol{B}_v^T \boldsymbol{D}_c \boldsymbol{B}_v dz dV \boldsymbol{d}^e \tag{3.22}$$

So stiffness element matrix is described as follow:

$$[\boldsymbol{K^e}]_{\mathbf{12\times12}} = \frac{h^3}{12}\int_V [\boldsymbol{B_s^T}]_{12\times3}\,[\boldsymbol{D_f}]_{\mathbf{3\times3}}[\boldsymbol{B_s}]_{\mathbf{3\times12}}dV + \kappa h\int_V [\boldsymbol{B_v^T}]_{12\times2}\,[\boldsymbol{D_c}]_{2\times2}[\boldsymbol{B_c}]_{\mathbf{2\times12}}dV \tag{3.23}$$

Where h is the thickness of the plate. The stiffness matrix integrals are computed by numerical integration. The stiffness integral is solved by considering for the Q4 element, 2 ×2 Gauss points for the bending contribution and 1 Gauss point for the shear contribution. This selective integration proved to be one of the simplest remedies for avoiding shear locking.

By using the kinetic energy for the plate

$$T_e = \frac{1}{2}\dot{\boldsymbol{d}}^{\boldsymbol{e}^T}\int_V \rho \boldsymbol{N}^T \begin{bmatrix} h & 0 & 0 \\ 0 & \frac{h^3}{12} & 0 \\ 0 & 0 & \frac{h^3}{12} \end{bmatrix} \boldsymbol{N}\, dV\, \dot{\boldsymbol{d}}^{\boldsymbol{e}} \tag{3.24}$$

We may compute the mass matrix as:

$$[\boldsymbol{M^e}]_{\mathbf{12\times12}} = \int_V \rho[\boldsymbol{N^T}]_{12\times3} \begin{bmatrix} h & 0 & 0 \\ 0 & \frac{h^3}{12} & 0 \\ 0 & 0 & \frac{h^3}{12} \end{bmatrix}_{3\times3} [\boldsymbol{N}]_{\mathbf{3\times12}}\, dV \tag{3.25}$$

3.1.3 Model validation

A standard FE approach is used to set up discretized equations:

$$\boldsymbol{SU} = \boldsymbol{F} \tag{3.26}$$

Where

$$\boldsymbol{S} = -\omega^2\boldsymbol{M} + i\omega\boldsymbol{C} + \boldsymbol{K} \tag{3.27}$$

in which $\boldsymbol{M}$, $\boldsymbol{C}$ and $\boldsymbol{K}$ are the mass-, damping- and stiffness matrices, respectively, $\boldsymbol{U}$ is a vector containing the complex nodal variables and $\boldsymbol{F}$ is a load vector. The matrices $\boldsymbol{M}$, $\boldsymbol{C}$ and $\boldsymbol{K}$ are collected in the dynamic stiffness matrix $\boldsymbol{S}$.

The analytical solutions and numerical solutions obtained by present FE model of square plate are compared. A plate with dimensions of 1m ×1m ×0.01 m and four simply supported edges is chosen as validation case. The material properties are Young's modulus $E = 2.1\text{GPa}$, density is $\rho = 7800\text{Kg/m}^3$ and Poisson's ratio μ=0.3.

***Table** 3.1 Comparison of the eigenfrequencies of present FE model analytical solution*

Methods	Mode Frequency (Hz)					
	m=1, n=1	**m=1, n=2**	**m=2, n=1**	**m=2, n=2**	**m=1, n=3**	**m=2, n=3**
Analytical Solution	4.9	12.3	12.3	19.7	24.7	32.1
Present FE Model	4.9	12.4	12.4	19.8	25.2	32.5

The first six eigenfrequencies of present FE model shown in

Table 3.1which agree well with those calculated by analytical solutions which indicate the present FE model in this Chapter is acceptable.

3.2 Finite element modelling of constrained damping layer plate

Accurate evaluation of damped sandwich plate vibration requires careful analysis of the shear deformation field of the viscoelastic core. This shear deformation requires to be modelled correctly in order to accurately quantify the increased damping capacity of the sandwich plate. In conventional FE model, all three layers are modelled with Mindlin shell elements and he coupling between the shell elements are handled by kinematic constraints (Ling Z. et al. [111]). In this chapter, a more efficient model is introduced. In this model, the viscoelastic layer is modelled using a special interface element with eight nodes (shown in **Fig** 3.2 b)) that can couples two plate elements layers using Kirchhoff-Love plate theory together directly. Only 20 degrees of freedom are required for each element. We also assume no slip happened between the cover layer and viscoelastic layer.

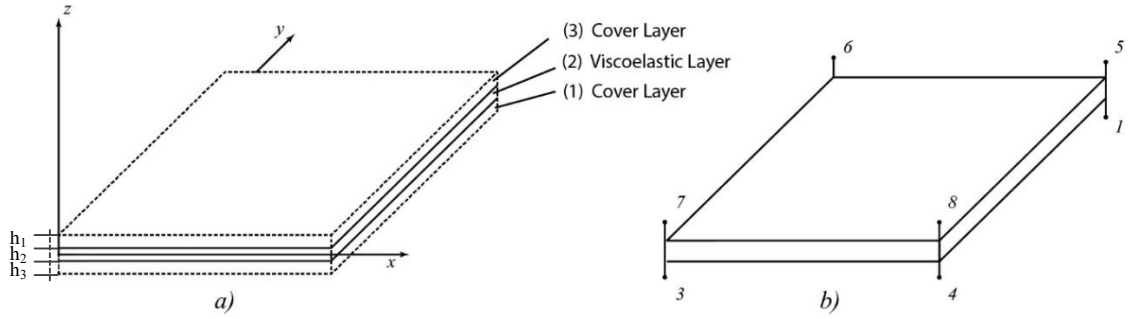

***Fig** 3.2 Schematic of finite element model. a) constrained damping layer; b) interface element for viscoelastic core*

Based on the classical Kirchhoff-Love plate theory, the displacement field of the face-layers can be written as:

$$
\begin{aligned}
u_i(x,y,z,t) &= u_{0i}(x,y,t) - z\frac{\partial w}{\partial x} \\
v_i(x,y,z,t) &= v_{0i}(x,y,t) - z\frac{\partial w}{\partial y} \qquad i = 1{,}3 \\
w_i(x,y,z,t) &= w(x,y,t)
\end{aligned} \tag{3.28}
$$

Where u_i, v_i, w are the longitudinal displacements along x-, y-, z-axis. u_{0i}, v_{0i} and w are the longitudinal displacements in the midplane. $\partial w/\partial x$ and $\partial w/\partial y$ are the rotations along x- and y-axis. z is the poison in z-axis. As shown in **Fig** 3.2 b), each node of this interface element has three translational and two rotational degrees of freedom. The transverse and longitudinal displacements of the element are then expressed in terms of the elemental nodal displacements vector:

$$
\boldsymbol{\chi}^{(i)} = \begin{bmatrix} u_i \\ v_i \\ w_i \end{bmatrix} = \begin{bmatrix} 1 & 0 & 0 & -z & 0 \\ 0 & 1 & 0 & 0 & -z \\ 0 & 0 & 1 & 0 & 0 \end{bmatrix} \begin{Bmatrix} u_{0i} \\ v_{0i} \\ w \\ \dfrac{\partial w}{\partial x} \\ \dfrac{\partial w}{\partial y} \end{Bmatrix} \quad i = 1,3 \tag{3.29}
$$

where i in **Eq. (3.29)** denotes the layer index in sandwich model as shown in **Fig** 3.2. $\boldsymbol{\chi}$ denotes displacement field. The interpolation functions of the displacements in mid-plane can be given as follow:

$$
\begin{aligned}
u_{0i}(x,y,t) &= \sum_{k=1}^{4} u_{0k}(t)\psi_k(x,y) \\
v_{0i}(x,y,t) &= \sum_{k=1}^{4} v_{0k}(t)\psi_k(x,y) \\
w(x,y,t) &= \sum_{k=1}^{4} [w_k(t)\varphi_{k1}(x,y) + \frac{\partial w_k}{\partial x}\varphi_{k2}(x,y) + \frac{\partial w_k}{\partial y}\varphi_{k3}(x,y)]
\end{aligned} \tag{3.30}
$$

$\psi_k \ (k = 1,2,3,4)$ and $\varphi_{kl} \ (k = 1,2,3,4$ and $l = 1,2,3)$ are the linear and Hermite cubic interpolation functions, respectively, which can be expressed as

$$
\begin{aligned}
\psi_k &= \frac{1}{4}(1+\xi\xi_k)(1+\eta\eta_k) \\
\varphi_{k1} &= \frac{1}{8}(1+\xi\xi_k)(1+\eta\eta_k)(2+\xi\xi_k+\eta\eta_k-\xi^2-\eta^2) \\
\varphi_{k2} &= \frac{1}{8}\xi_k(1+\xi\xi_k)^2(\xi\xi_k-1)(1+\eta\eta_k)a \\
\varphi_{k3} &= \frac{1}{8}\eta_k(1+\eta\eta_k)^2(\eta\eta_k-1)(1+\xi\xi_k)b
\end{aligned} \tag{3.31}
$$

where a and b are the half length of the rectangular element along the x- and y-directions, respectively. Rewrite the equations in matrix form as follow:

$$[\boldsymbol{\chi}^{(i)}]_{3\times1} = [\boldsymbol{H}]_{\mathbf{3\times5}}[\boldsymbol{N_s}]_{\mathbf{5\times20}}[\boldsymbol{d}_e^{(i)}]_{20\times1} \qquad k = 1,3 \tag{3.32}$$

Where $\boldsymbol{d}_e^{(i)}$ is the elemental nodal displacements vector

$$\boldsymbol{d}_e^{(i)} = [u_{0k}, v_{0k}, w_k, \frac{\partial w_k}{\partial x}, \frac{\partial w_k}{\partial y}]^T_{\ 20\times1} \quad (k = 1,2,3,4) \tag{3.33}$$

$$\boldsymbol{H} = \begin{bmatrix} 1 & 0 & 0 & -z & 0 \\ 0 & 1 & 0 & 0 & -z \\ 0 & 0 & 1 & 0 & 0 \end{bmatrix}_{3\times5} \tag{3.34}$$

$$\boldsymbol{N_s} = [N_{s1} \quad N_{s2} \quad N_{s3} \quad N_{s4}]_{5\times20} \tag{3.35}$$

$$\boldsymbol{N_{sk}} = \begin{bmatrix} \psi_k & 0 & 0 & 0 & 0 \\ 0 & \psi_k & 0 & 0 & 0 \\ 0 & 0 & \varphi_{k1} & \varphi_{k2} & \varphi_{k3} \\ 0 & 0 & \frac{\partial \varphi_{k1}}{\partial x} & \frac{\partial \varphi_{k2}}{\partial x} & \frac{\partial \varphi_{k3}}{\partial x} \\ 0 & 0 & \frac{\partial \varphi_{k1}}{\partial y} & \frac{\partial \varphi_{k2}}{\partial y} & \frac{\partial \varphi_{k2}}{\partial y} \end{bmatrix} \tag{3.36}$$

According to linear elastic stress-strain relations and use **Eq. (3.16)**, the strains for each layer can be written in matrix form as follow:

$$[\boldsymbol{\varepsilon_s}^{(i)}]_{3\times1} = \begin{bmatrix} \varepsilon_x^{(i)} \\ \varepsilon_y^{(i)} \\ \gamma_{xy}^{(i)} \end{bmatrix} = \begin{bmatrix} \partial u_i/\partial x \\ \partial v_i/\partial y \\ \partial u_i/\partial y + \partial v_i/\partial x \end{bmatrix} = [\boldsymbol{B}_s]_{3\times20}[\boldsymbol{d}_e^{(i)}]_{20\times1} \tag{3.37}$$

Where $\boldsymbol{B}_s$ is strain-displacement matrix

$$\boldsymbol{B}_s = [\boldsymbol{B}_{s1} \ \ \boldsymbol{B}_{s2} \ \ \boldsymbol{B}_{s3} \ \ \boldsymbol{B}_{s4}]_{3\times20} \tag{3.38}$$

$$\boldsymbol{B}_{sk} = \begin{bmatrix} \frac{\partial \psi_k}{\partial x} & 0 & \frac{\partial^2 \varphi_{k1}}{\partial x^2} & \frac{\partial^2 \varphi_{k2}}{\partial x^2} & \frac{\partial^2 \varphi_{k3}}{\partial x^2} \\ 0 & \frac{\partial \psi_k}{\partial y} & \frac{\partial^2 \varphi_{k1}}{\partial y^2} & \frac{\partial^2 \varphi_{k2}}{\partial y^2} & \frac{\partial^2 \varphi_{k3}}{\partial y^2} \\ \frac{\partial \psi_k}{\partial y} & \frac{\partial \psi_k}{\partial x} & \frac{\partial^2 \varphi_{k1}}{\partial x \partial y} & \frac{\partial^2 \varphi_{k2}}{\partial x \partial y} & \frac{\partial^2 \varphi_{k3}}{\partial x \partial y} \end{bmatrix}, k = 1,2,3,4 \tag{3.39}$$

The kinetic energies and potential energies of base layer and constrained layer are:

$$\begin{aligned} T_e^{\ (1,3)} &= \frac{1}{2}\int_{V_e} \rho \dot{\boldsymbol{\chi}}^{(1,3)^T} \dot{\boldsymbol{\chi}}^{(1,3)} dV \\ U_e^{\ (1,3)} &= \frac{1}{2}\int_{V_e} \boldsymbol{\varepsilon_s}^{(1,3)^T} \boldsymbol{D_f} \boldsymbol{\varepsilon_s}^{(1,3)} dV \end{aligned} \tag{3.40}$$

Where:

$$\boldsymbol{D_s} = \frac{E}{(1-\mu^2)}\begin{bmatrix} 1 & \mu & 0 \\ \mu & 1 & 0 \\ 0 & 0 & \dfrac{1-\mu}{2} \end{bmatrix} \tag{3.41}$$

So the mass element matrix and stiffness element matrix describe as follow

$$\begin{aligned} [\boldsymbol{M}_e^{(1),(3)}]_{20\times20} &= \iiint_{V_e^{(1),(3)}} \rho_e^{(1),(3)} [\boldsymbol{N}_s^T]_{20\times5} [\boldsymbol{N}_s]_{5\times20} dV \\ [\boldsymbol{K}_e^{(1),(3)}]_{20\times20} &= \iiint_{V_e^{(1),(3)}} [\boldsymbol{B}_s^T]_{20\times3} [\boldsymbol{D}_s]_{3\times3} [\boldsymbol{B}_s]_{3\times20} dV \end{aligned} \tag{3.42}$$

Where ρ_e is element material density and V_e is element volume.

3.2.1 Modelling of the viscoelastic layer

To better measure the tensile and shear deformation of viscoelastic layer, solid element is adopted here and at the same time we assume no slip occurs at the interfaces of the layers the shear. Requiring continuity of the displacements at the adjacent layers and assuming the displacements is small related to the model size, the displacement field of viscoelastic layer can be expressed in linear interpolation. So the displacement field shown as below(see **Fig** 3.2Error! Reference source not found..):

$$\begin{aligned} u_2 &= \frac{1}{2}(u_1 + u_3) - \frac{z}{h_2}(u_1 - u_3) \\ v_2 &= \frac{1}{2}(v_1 + v_3) - \frac{z}{h_2}(v_1 - v_3) \\ w_2 &= \frac{1}{2}(w_1 + w_3) - \frac{z}{h_2}(w_1 - w_3) \end{aligned} \tag{3.43}$$

Rewrite **Eq. (3.43)** in matrix form as follow:

$$[\boldsymbol{\chi}^{(2)}]_{3\times1} = [\boldsymbol{T}_1 \ \ \boldsymbol{T}_2]_{3\times6} \left[\boldsymbol{\chi}^{(1)} \ \ \boldsymbol{\chi}^{(3)}\right]^T_{6\times1} \tag{3.44}$$

Where

$$\boldsymbol{T}_1 = \begin{bmatrix} \dfrac{1}{2} - \dfrac{z}{h_2} & 0 & 0 \\ 0 & \dfrac{1}{2} - \dfrac{z}{h_2} & 0 \\ 0 & 0 & \dfrac{1}{2} - \dfrac{z}{h_2} \end{bmatrix}_{3\times3} \qquad \boldsymbol{T}_2 = \begin{bmatrix} \dfrac{1}{2} + \dfrac{z}{h_2} & 0 & 0 \\ 0 & \dfrac{1}{2} + \dfrac{z}{h_2} & 0 \\ 0 & 0 & \dfrac{1}{2} + \dfrac{z}{h_2} \end{bmatrix}_{3\times3} \tag{3.45}$$

where $\boldsymbol{\chi}^{(1)}$, $\boldsymbol{\chi}^{(2)}$ and $\boldsymbol{\chi}^{(3)}$ are the displacement field of the top surface of the base layer, both surfaces of viscoelastic layer and the bottom surface of the constrained layer, respectively. By

introducing **Eq. (3.45)** to **Eq. (3.44)** and combining **Eq. (3.32)**, the displacement field of the viscoelastic layer is derived as the following equation:

$$[\boldsymbol{\chi}^{(2)}]_{3\times1} = [\boldsymbol{N_v}]_{3\times40}\left[\boldsymbol{d}_e^{(1)} \quad \boldsymbol{d}_e^{(3)}\right]^T_{40\times1} \tag{3.46}$$

$$[\boldsymbol{N_v}]_{3\times40} = [\boldsymbol{T}_1 \ \ \boldsymbol{T}_2]_{3\times6}\begin{bmatrix} \boldsymbol{H}_{\left(z=\frac{h_1}{2}\right)} & \boldsymbol{0} \\ \boldsymbol{0} & \boldsymbol{H}_{\left(z=-\frac{h_3}{2}\right)} \end{bmatrix}_{6\times10}\begin{bmatrix} \boldsymbol{N_s} & \boldsymbol{0} \\ \boldsymbol{0} & \boldsymbol{N_s} \end{bmatrix}_{10\times40} \tag{3.47}$$

where $\boldsymbol{H}$ and $\boldsymbol{N_s}$ are defined in equation **Eq. (3.34)** and **Eq. (3.35)**, $\boldsymbol{T_1}$ and $\boldsymbol{T_2}$ are defined in **Eq. (3.45)**. $\boldsymbol{d}_e^{(1)}$ and $\boldsymbol{d}_e^{(3)}$are nodal displacement vectors of the base layer and constrained layer, respectively. According to linear isotropic elastic stress-strain relations in three dimensions:

$$\left[\boldsymbol{\varepsilon}_s{}^{(2)}\right]_{6\times1} = \begin{bmatrix} \varepsilon_x \\ \varepsilon_y \\ \varepsilon_z \\ \gamma_{xy} \\ \gamma_{yz} \\ \gamma_{zx} \end{bmatrix} = \begin{bmatrix} \frac{\partial u}{\partial x} \\ \frac{\partial v}{\partial y} \\ \frac{\partial w}{\partial z} \\ \frac{\partial u}{\partial y}+\frac{\partial v}{\partial x} \\ \frac{\partial v}{\partial z}+\frac{\partial w}{\partial y} \\ \frac{\partial w}{\partial x}+\frac{\partial u}{\partial z} \end{bmatrix} = \begin{bmatrix} \frac{\partial}{\partial x} & 0 & 0 \\ 0 & \frac{\partial}{\partial y} & 0 \\ 0 & 0 & \frac{\partial}{\partial z} \\ \frac{\partial}{\partial y} & \frac{\partial}{\partial x} & 0 \\ 0 & \frac{\partial}{\partial z} & \frac{\partial}{\partial y} \\ \frac{\partial}{\partial z} & 0 & \frac{\partial}{\partial x} \end{bmatrix}_{6\times3} \left[\boldsymbol{\chi}^{(2)}\right]_{3\times1} \tag{3.48}$$

Substitute the **Eq. (3.47)** into **Eq. (3.48)** to obtain

$$\left[\boldsymbol{\varepsilon}_s{}^{(2)}\right]_{6\times1} = [\boldsymbol{B}_v]_{6\times40}\left[\boldsymbol{d}_e^{(1)} \quad \boldsymbol{d}_e^{(3)}\right]^T_{40\times1} \tag{3.49}$$

Where

$$[\boldsymbol{B}_v]_{6\times40} = \begin{bmatrix} \frac{\partial}{\partial x} & 0 & 0 \\ 0 & \frac{\partial}{\partial y} & 0 \\ 0 & 0 & \frac{\partial}{\partial z} \\ \frac{\partial}{\partial y} & \frac{\partial}{\partial x} & 0 \\ 0 & \frac{\partial}{\partial z} & \frac{\partial}{\partial y} \\ \frac{\partial}{\partial z} & 0 & \frac{\partial}{\partial x} \end{bmatrix}_{6\times3} [\boldsymbol{N}_v]_{3\times40} \tag{3.50}$$

The kinetic energies and potential energies of base layer and constrained layer are:

$$T_e{}^{(2)} = \frac{1}{2}\int_{V_e} \rho \dot{\boldsymbol{\chi}}^{(2)^T} \dot{\boldsymbol{\chi}}^{(2)} dV$$
$$U_e{}^{(2)} = \frac{1}{2}\int_{V_e} \boldsymbol{\varepsilon_s}^{(2)^T} \boldsymbol{D_v} \boldsymbol{\varepsilon_s}^{(2)} dV \tag{3.51}$$

Where:

$$\boldsymbol{D_v} = \frac{E}{1+\mu}\begin{bmatrix} \frac{1-\mu}{1-2\mu} & \frac{\mu}{1-2\mu} & \frac{\mu}{1-2\mu} & 0 & 0 & 0 \\ \frac{\mu}{1-2\mu} & \frac{1-\mu}{1-2\mu} & \frac{\mu}{1-2\mu} & 0 & 0 & 0 \\ \frac{\mu}{1-2\mu} & \frac{\mu}{1-2\mu} & \frac{1-\mu}{1-2\mu} & 0 & 0 & 0 \\ 0 & 0 & 0 & 1 & 0 & 0 \\ 0 & 0 & 0 & 0 & 1 & 0 \\ 0 & 0 & 0 & 0 & 0 & 1 \end{bmatrix}_{6\times 6} \tag{3.52}$$

Similar to the cover layer element, the mass element matrix and stiffness element matrix can be written as:

$$\left[\boldsymbol{M}_e^{(2)}\right]_{40\times 40} = \iiint_{V_e^{(2)}} \rho_e^{(2)} [\boldsymbol{N}_v^T]_{40\times 3} [\boldsymbol{N}_v]_{3\times 40} dV$$
$$\left[\boldsymbol{K}_e^{(2)}\right]_{40\times 40} = \iiint_{V_e^{(2)}} [\boldsymbol{B}_v^T]_{40\times 6} [\boldsymbol{D}_v]_{6\times 6} [\boldsymbol{B}_v]_{6\times 40} dV \tag{3.53}$$

The present interface element directly couples the two cover layers modelled with shell elements to the viscoelastic layer in between with no extra nodes added. Then, the matrix of elemental interpolation functions is determined and the strain-displacement matrix can be obtained by differentiating the interpolation function matrix with respect to the local element coordinates. Appling the principal of virtual work, the mass matrix and stiffness matrix of the element can be readily calculated.

3.2.2 Model validation

To validate the model proposed in last section, we compare the natural frequencies and modal loss factors for first six modes with the solutions published by Johnson C.D.et al.[112] . Natural frequencies are the frequency at which an elastic body make free vibration. Loss factor is a factor which when multiplied by energy lost at time of peak and the number of load periods will give overall average energy lost. It is calculated as the ratio of the average load loss to the peak load loss. Both natural frequencies and modal loss factors are important characteristics to describe vibration.

***Table** 3.2* The natural frequencies and modal loss factors of a plate with passive constrained damping layer

Mode m , n	Analytical solution (Johnson C.D. et al. [112])		NASTRAN/MSE (Johnson C.D. et al. [112])		Present solution	
	Frequency (Hz)	Loss factor	Frequency (Hz)	Loss factor	Frequency (Hz)	Loss factor
1 , 1	60.3	0.190	57.4	0.176	59.1	0.206
1 , 2	115.4	0.203	113.2	0.188	113.9	0.211
2 , 1	130.6	0.199	129.3	0.188	129.1	0.206
2 , 2	178.7	0.181	179.3	0.153	176.8	0.185
1 , 3	195.7	0.174	196.0	0.153	194.1	0.177

As seen in **Table 3.2** The natural frequencies and modal loss factors of a plate with constrained damping layer, both the natural frequencies and loss factors of present solution are a slight higher than the analytical solution. One possible explanation for this is that the elastic modulus of the viscoelastic core is considered in this finite element model but not in the analytical solution. Thus the whole model is stiffer than the model in analytical case which lead to higher natural frequency. Also as the in-plane deformation of viscoelastic core layer has been taken into account, the loss factor is larger than the analytical solution. Compared to the simulation results in **NASTRAN/MSE**, this interface finite element model is more accurate on the loss factors especially for the mode (2,2) and (1,3). The loss factors of these two modes in **NASTRAN/MSE** model is much lower than the analytical solution.

3.3 Topology optimization method code development for Abaqus based on SIMP model

A topology optimization python package based on SIMP model has been discussed in this Section. This package provides a convenient platform to imply topology optimization method in Abaqus. By taking the advantage of the modelling power of the commercial finite element software, more complex structures, material properties and contact conditions which are more close to the real engineering problems can be taken into account. Besides that, different objective functions can be defined flexibly according to the needs of research and engineering problems with simple modifications.

Recently, Zuo, et al [110]presented a simple Python code for topology optimization of general 2D and 3D structures in Abaqus based on bi-directional evolutionary structural optimization

method. They integrate the optimization algorithm into the FE analysis process which provide convenience for implementation. But there are still some places can be improved in their work. First, Abaqus build-in Python kernel is usually not the latest version which means some useful packages of Python, such as Scipy, Matplotlib etc. which cover calculation, visualization, and analysis optimization fields are not accessible. Without these useful tools may limit the extension of re-development of Abaqus. Second, performance is always a drawback for an advanced dynamic script language. Pure Python is not a good solution for high density calculation task. A common answer for this issue is to separate the heavy calculation step from main cycle and call external library written by low-level but high efficiency language like C or FORTRAN. At last, the objective functions they choose are limited to the outputs field provided by Abaqus, more flexible definition objective of functions are required for various optimization problems. Inspired by their work, a new framework for topology optimization is proposed to integrate the Abaqus kernel as FE solver into the optimization process. The details of implementation of the code are shown in the follow sections.

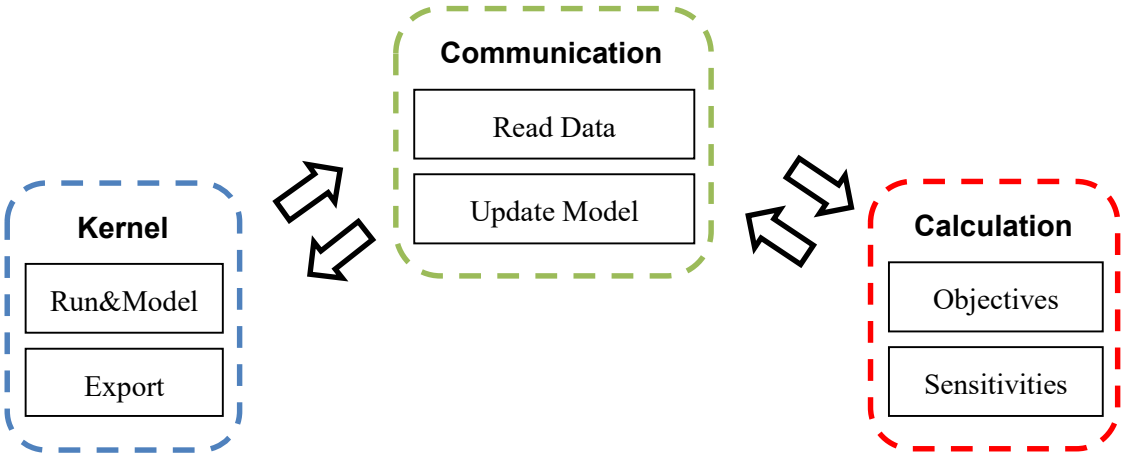

Fig 3.3 *Framework of topology optimization code in Abaqus*

3.3.1 Framework of the code

Different from the previous work that integrating topology optimization algorithm into Abaqus, this framework imports Abaqus as external FE solver. The framework proposed in this thesis is built up by three layers as shown in **Fig 3.4.**

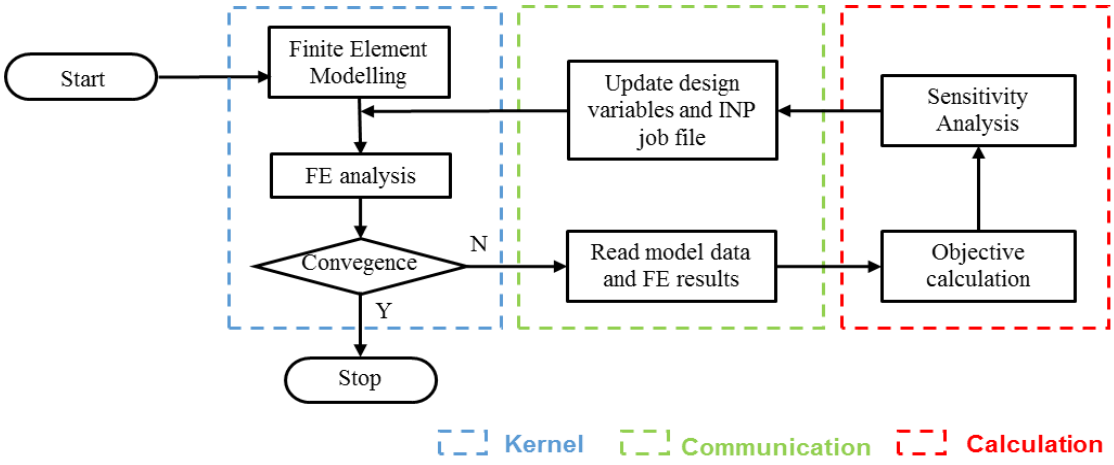

Fig 3.4 *Flowchart of topology optimization implementation in Abaqus*

To introduce Abaqus as finite element solver into the topology optimization process, an interface is needed to communicate with the kernel for modelling, we call it "Kernel Layer". Fortunately, Abaqus already provides a tool to handle this kind of job and name it as Abaqus Scripting Interface(ASI) which is an extension of the Python language. One obvious advantage for ASI is that we can execute the whole optimization process using one single language rather than maintain different versions of codes. As a standard component of the Abaqus software, ASI provides convenient interfaces of the models and results. With the interfaces provided by Abaqus (shown in **Fig** 3.5 *Python interface structure*), a complex structure can be built by several lines of Python code. ASI also help user define or retrieve model data and analysis

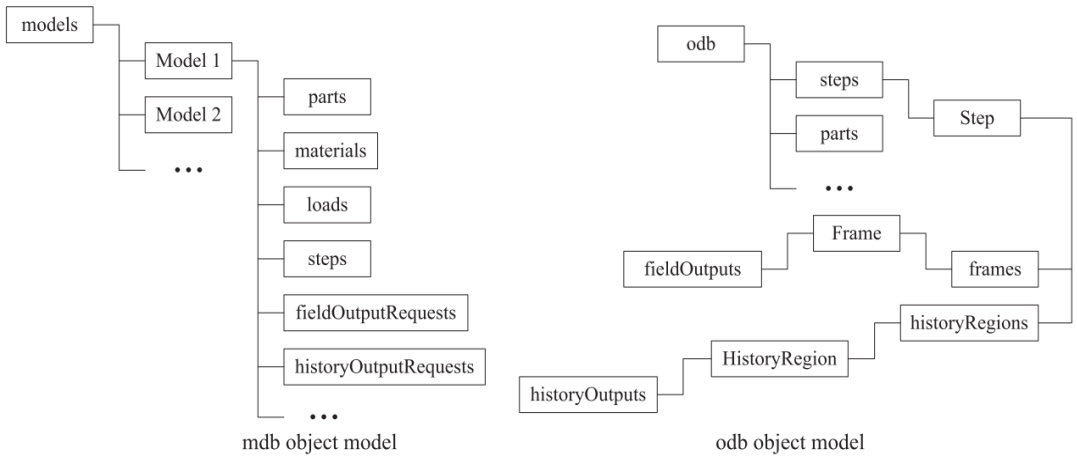

Fig *3.5* Python interface structure

results in the FE analysis process.

Second layer called "Communication Layer" which is responsible for retrieving results and updating model. Usually there may be hundreds of iterations during an optimization case, the data produced during the process is also very important for the analysis afterwards, thus we

need a database to store the intermediate datasets. In this package, a database named by model is created to store the model data, optimization parameters, FE analysis results and optimization history. Also the database is the source for the objective calculation and sensitivity analysis. In this framework, according to the requirement of sensitivity analysis and objective function, the output data could be displacement, velocity, element stiffness/mass matrix and gross stiffness/mass matrix.

Besides retrieving intermediate data, "Communication Layer" is also responsible for model updating. Solid isotropic material with penalization method is a density-based approach in which each element has an independent density variable in optimization process so that tens or even hundreds of thousands of materials and sections will be created depending on the numbers of elements in the finite element model. To avoid the low efficiency operations in Abaqus /CAE GUI, finite element model is updated by modifying *.INP file directly which greatly improve the efficiency of optimization especially when the model is complex. *.INP file is the input file generated by Abaqus before running the FE analysis which contains comprehensive model information including node coordinates, element mesh, material properties, loads definition and boundary conditions, etc. so any change of FE model can be realized by modifying this input file. Based on the study on the file structure of INP file, a 'Updating_INP' function in the "Communication Layer" is developed to modify material information and boundary conditions.

The last layer is "Calculation Layer" which focus on objective and sensitivities calculation. Obviously, "Calculation Layer" is the most time-consuming step during the optimization process. Introducing this layer is to define arbitrary objective functions with proper efficiency. So far, the sensitivities analysis for four objective functions: dynamic compliance, power flow response, displacement and modal damping ratio have been developed in this thesis. Python libraries also provide the possibility of further visualization and analysis in post-process step. In addition, to improve the efficiency of optimization, optimizers and sensitivities analysis for objective functions have been written in FORTRAN dynamic library for higher performance.

3.3.2 Advantages of this framework

The main advantages of this package are as follows:

1) Abaqus is a reliable FE analysis software which has been widely applied to the static, dynamic, heat analysis in many areas during last decades. The wide range of elements are available to solve various engineering problems. So by importing Abaqus as finite element solver, this package is capable of modelling more complex structures for the topology optimization models.
2) Highly extendable framework for topology optimization. Its extensibility can be seen

in two aspects. Firstly, this thesis proposed a SIMP topology optimization model for vibration suppression, which is widely accepted method in many topology optimizations filed. However, this framework is also compatible with the Bi-directional evolutionary structural optimisation method or level-set method which are also applied to other topology optimization problems. On the other hand, Python is one kind of complete programming languages which has many mature libraries for computing, graph and optimization. The accessibly of Python various packages enables this framework to execute data analysis and visualization in one single script which provides a convenient platform for topology optimization research work.

3) Abaqus has its own topology optimization module called ATOM which only support optimization problem taking displacement as objective function. However, in this package, the objective functions are highly customizable because the "Calculation Layer" is completely independent of Abaqus kernel so there is no limit on the objective functions definition.
4) More efficient and less memory is required. Compared to the topology optimization case with self-written finite element code, this package has more advantages in computing speed and stability by integrating Abaqus as finite element solver. To achieve higher efficiency of optimization, a Fortran version of MMA algorithm is introduced to replace Python one. Different from the Abaqus ATOM module which stores all sections and nodes data after each iteration during optimization process, this framework will re-call Abaqus FE solver at each iteration and clear all intermediate data from memory and dump the results to the database. Therefore, this mechanism can guarantee memory occupation will be released in time and maintain high execution efficiency. At the same time, the stability has been greatly improved and the unexpected errors has been greatly reduced.

3.4 Summary

This chapter presents the FE modelling method for topology optimization in this report. Four-node Mindlin plate and eight-node interface element are derived. For the extensibility of topology optimization method, Python topology optimization package for Abaqus based on SIMP model has been developed. This new topology optimization framework integrates Abaqus as external finite element solver to achieve better extensibility and performance. With simple modifications, the basic Python code can be extended to enhance computational efficiency and to consider a wide range of engineering problems.

Chapter 4 Case study: bi-material square plate

A numerical case study is investigated in this Chapter which aim to establish a complete topology optimization model including FE modelling, material interoperation function definition, sensitivity analysis and implementation of optimization algorithm. The mathematical formulation of topology optimization is established based on power flow response and bi-material solid isotropic material with penalization(SIMP) model. Optimum results between topological design of minimum power flow response and minimum dynamic compliance are compared, showing that the power flow response has strong adaptability for structural dynamic topology optimization problems.

4.1 Minimization of power flow response using topology optimization

4.1.1 Introduction of power flow analysis

A power flow analysis provides a technique to describe the dynamic behaviour of vibrational structures by considering not only the amplitudes of force and velocity vectors, but also the phase relationship of the two quantities. The approach focuses on the flow of vibrational energy rather than the detailed spatial pattern of the structural response. The fundamental concept of power flow, which is originally devised by Belov, et al[125], is discussed by Goyder, et al [126]. From a more generic viewpoint of continuum mechanics, Xing, et al[129], developed a power flow analysis method based on continuum dynamics. Compared with a mobility based power flow model, a power flow mode theory based on a system's damping distribution, proposed by Xiong, et al[130], provides a new technique to describe the dynamic behaviour of complex structures and coupled systems.

In a dynamical analysis, harmonic quantities are often represented mathematically in complex mathematical forms. For example, a real harmonic force $f(t)$ with amplitude F and frequency ω, or a real velocity $v(t)$ with amplitude V , frequency ω and relative phase angle θ, are given by

$$\begin{aligned} \tilde{f}(t) &= F\ e^{i\omega t} = \tilde{F}e^{i\omega t} \\ \tilde{v}(t) &= V\ e^{i(\omega t+\theta)} = \tilde{V}e^{i\omega t} \end{aligned} \tag{4.1}$$

In this notation, the tilde denotes a complex quantity. For equivalence of representations, either the real part Re or imaginary part Im of the complex quantity is chosen. Herein, we use the real part of a complex quantity to represent the corresponding measurable quantity such that

$$\tilde{f}(t) = Re\{\tilde{f}(t)\} = \frac{1}{2}(\tilde{f} + \tilde{f}^H)$$
$$\tilde{v}(t) = Re\{\tilde{v}(t)\} = \frac{1}{2}(\tilde{v} + \tilde{v}^H) \tag{4.2}$$

where the superscript $\tilde{v}$ denotes the complex conjugate.

In power flow analysis, the power is defined as the rate at which work is done and therefore it is a practical measurable quantity. Thus the real power at time t is given by

$$q(t) = Re\{\tilde{f}(t)\}Re\{\tilde{v}(t)\} = \frac{1}{4}(\tilde{f} + \tilde{f}^H)(v + \tilde{v}^H) \tag{4.3}$$

Thus, the time-average of this real power over a period of vibration $\omega/2\pi$, i.e. the mean power, is given by

$$< q >= \frac{\omega}{2\pi}\int_0^{\omega/2\pi} Re\{\tilde{f}(t)\}Re\{\tilde{v}(t)\}dt = \frac{1}{2}|\tilde{F}\tilde{V}|cos\theta \tag{4.4}$$

Mathematically, an instantaneous complex power may be defined as

$$\tilde{q}(t) = \tilde{f}(t)\tilde{v}(t) = \tilde{F}\tilde{V}e^{2i\omega t} \tag{4.5}$$

Although it has some applications in vibrational experiments, its mean value

$$< \tilde{q} >= \frac{\omega}{2\pi}\int_0^{\omega/2\pi} \tilde{f}\tilde{v}dt = 0 \tag{4.5}$$

This result clearly conveys the essential difference between a physical power and a complex power. Therefore, real power is the primary quantity considered in a total time-average power flow analysis. In this section, a bi-material square plate topology optimization model discussed in this section which takes the phase relationship of force and velocity vectors into account and formulates directly with the design objective of minimizing the power flow response, which is another angle to represent the physical insight of structural vibration.

4.1.2 SIMP model of bi-material plate

In this Chapter, a bi-material plate subjected to a harmonic force with prescribed amplitude and frequency is investigated. A bi-material plate (see **Fig 4.1**) indicates two different materials distributing in a single layer, one is stiffer material and the other one is relative soft. By searching the optimal topology pattern for the plate structure, better performance of the vibration suppression can be achieved. Here we assume the two materials are perfectly ideal contacted, so strict constraints are applied to the elements of both materials in all degree of freedom.

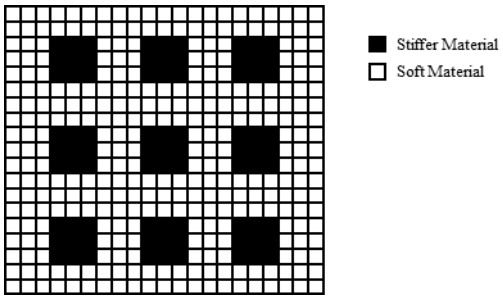

Fig 4.1 *A bi-material plate configuration*

Following Bendsøe and Sigmund[113], the SIMP model for single-material can be easily extended to bi-material design by using the rule of mixtures. The element stiffness matrix and mass matrix of the bi-material model may be stated in a similar way as follows:

$$\begin{aligned} \boldsymbol{M_e}(\rho_e) &= {\rho_e}^q \boldsymbol{M_e^s} + (1 - {\rho_e}^q)\boldsymbol{M_e^w} \\ \boldsymbol{K_e}(\rho_e) &= {\rho_e}^p \boldsymbol{K_e^s} + (1 - {\rho_e}^p)\boldsymbol{K_e^w} \end{aligned} \tag{4.6}$$

where $\boldsymbol{M_e^s}$ and $\boldsymbol{K_e^s}$ are the element mass and stiffness matrices of stiffer material, $\boldsymbol{M_e^w}$ and $\boldsymbol{K_e^w}$ are the element mass and stiffness matrices of weak material . It is known that a pertinent value of the power q is 1 in design for the maximization of eigenfrequencies because the penalization of the ratio between stiffness and mass (representing the squared eigenfrequencies) is an important aspect in such a topology design problem[114][115]. The design objective functions (i.e., the dynamic compliance) in this Chapter depends mainly on the dynamic stiffness matrix of the structure, especially in the case of high loading frequencies. Thus, the same penalization is applied simultaneously to the stiffness and mass. For a given element in **Eq** (4.6), $\rho_e = 1$ implies that the element fully consists of the solid material, whereas $\rho_e = 0$ means that the element is void.

4.1.3 Power flow modelling

Taking the form $\dot{\boldsymbol{U}} = \boldsymbol{V}e^{i\omega t}$ in which $\boldsymbol{V}$ is the real velocity vector and ω is excitation frequency in rad/s, then the dynamic governing equation can be expressed as:

$$\boldsymbol{ZV} = \boldsymbol{F} \tag{4.7}$$

Where $\boldsymbol{Z}$ denotes the impedance matrix, and can be expressed as:

$$\boldsymbol{Z} = i\omega\boldsymbol{M} + \boldsymbol{C} \ + \frac{\boldsymbol{K}}{i\omega} \tag{4.8}$$

Real-life systems are not undamped but possess some kind of energy dissipation mechanism or damping. In order to apply modal analysis of undamped systems to damped systems, it is common to assume the proportional damping, a special type of viscous damping such as the Rayleigh damping[116], which can be expressed as a linear combination of $\boldsymbol{M}$ and $\boldsymbol{K}$:

$$\boldsymbol{C} = \alpha\boldsymbol{M} + \beta\boldsymbol{K} \tag{4.9}$$

where α and β denote the mass damping and stiffness damping coefficients, respectively. With this formulation the damping ratio is the same for axial, bending and torsional response. Rayleigh damping results in different damping ratios for different response frequencies, according to the equation

$$\xi = \frac{1}{2}(\frac{\alpha}{\omega} + \beta\omega) \tag{4.10}$$

Where ξ is the damping ratio and ω is the response frequency in rad/s. It can be seen from this that the mass proportional term gives a damping ratio inversely proportional to response frequency and the stiffness proportional term gives a damping ratio linearly proportional to response frequency. One limitation of Rayleigh damping is the damping ratio varies with the frequency but in many real systems display hysteretic damping which is largely independent of frequency. Despite the limitation, Rayleigh damping can and has been used as a heuristic, as opposed to strictly physical, attenuation mechanism.

The total time-averaged power flow response by all excitation forces applied to the structure is given by the expression[130]:

$$\boldsymbol{P} = \frac{\mathbf{1}}{\mathbf{2}} Re(\boldsymbol{F^H V}) \tag{4.11}$$

In this thesis, the material layout is represented by the distribution of two prescribed linearly elastic materials in the admissible design domain for the structure. The optimization problem is formulated as follows:

$$min \quad \Pi = \frac{\mathbf{1}}{\mathbf{2}} \boldsymbol{Re}(\boldsymbol{F^H V}) \tag{4.12}$$

$$s.t. \quad \boldsymbol{R} = \boldsymbol{ZV} - \boldsymbol{F} = \mathbf{0},$$

$$\sum_{e=1}^{N_e} \rho_e V_e - f_v \sum_{e=1}^{N_e} V_e \leq 0, \tag{4.13}$$

$$0 \leq \rho_e \leq 1, \qquad e = 1, \cdots, N_e$$

Symbol Π represents the optimization objective. In the bi-material design problem, we are aim to find the optimal topology layout to minimize power flow response subject to a volume limit. where ρ_e is the volumetric density of the stiffener material in element e and plays the role of the design variable in the problem. The symbol f_v denotes the volume fraction limit of the stiffener material.

4.1.4 Design sensitivity analysis

As usual, the optimization problem **Eq. (4.12)** is solved by a gradient-based mathematical programming algorithm, which necessitates sensitivity analysis of the objective function with respect to the design variables. In what follows, the objective function Π only explicitly

depending on the amplitudes of the velocity response $\boldsymbol{V}$ is considered. The sensitivity analysis scheme for Π is derived by using the adjoint variable method which is more efficient than the direct variable method in the problems involving a large number of design variables but only a few behaviour functions, as in the case of a topology optimization.

Considering the vibration equation and its conjugate equation, we can rewrite the function Π as follows:

$$\Phi = \Pi + \boldsymbol{\Upsilon_1}^T(\boldsymbol{ZV} - \boldsymbol{F}) + \boldsymbol{\Upsilon_2}^T(\overline{\boldsymbol{Z}}\overline{\boldsymbol{V}} - \overline{\boldsymbol{F}}) \tag{4.14}$$

where $\overline{\boldsymbol{Z}}$ and $\overline{\boldsymbol{F}}$ denote the conjugates of the impedance matrix $\boldsymbol{Z}$ and the force amplitude vector $\boldsymbol{F}$, respectively; $\boldsymbol{V}$ and $\overline{\boldsymbol{V}}$ denote the velocity response and conjugates of the velocity response; $\boldsymbol{\Upsilon_1}$ and $\boldsymbol{\Upsilon_2}$ are the adjoint vectors. Differentiating **Eq. (4.13)** with respect to the eth design variable leads to

$$\begin{aligned}\frac{d\Phi}{d\rho_e} &= \boldsymbol{\Upsilon_1}^T\frac{\partial \boldsymbol{Z}}{\partial \rho_e}\boldsymbol{V} + \boldsymbol{\Upsilon_2}^T\frac{\partial \overline{\boldsymbol{Z}}}{\partial \rho_e}\overline{\boldsymbol{V}} \\ &+ \left(\frac{\partial \Pi}{\partial \boldsymbol{V_R}} + \boldsymbol{\Upsilon_1}^T\boldsymbol{Z} + \boldsymbol{\Upsilon_2}^T\overline{\boldsymbol{Z}}\right)\frac{\partial \boldsymbol{V_R}}{\partial \rho_e} \\ &+ \left(\frac{\partial \Pi}{\partial \boldsymbol{V_I}} + i\boldsymbol{\Upsilon_1}^T\boldsymbol{Z} - i\boldsymbol{\Upsilon_2}^T\overline{\boldsymbol{Z}}\right)\frac{\partial \boldsymbol{V_I}}{\partial \rho_e}\end{aligned} \tag{4.15}$$

where $\boldsymbol{V_I}$ and $\boldsymbol{V_R}$ represent the real part and image part of vector $\boldsymbol{V}$, respectively.
Let the adjoint variables $\boldsymbol{\Upsilon_1}$ and $\boldsymbol{\Upsilon_2}$ satisfy the following equations:

$$\begin{aligned}\left(\frac{\partial \Pi}{\partial \boldsymbol{V_R}} + \boldsymbol{\Upsilon_1}^T\boldsymbol{Z} + \boldsymbol{\Upsilon_2}^T\overline{\boldsymbol{Z}}\right) &= 0 \\ \left(\frac{\partial \Pi}{\partial \boldsymbol{V_I}} + \mathrm{i}\boldsymbol{\Upsilon_1}^T\boldsymbol{Z} - i\boldsymbol{\Upsilon_2}^T\overline{\boldsymbol{Z}}\right) &= 0\end{aligned} \tag{4.16}$$

We can obtain equations as follow:

$$\begin{aligned}\boldsymbol{\Upsilon_1}^T\boldsymbol{Z} &= \frac{1}{2}\left(\ i\frac{\partial \Pi}{\partial \boldsymbol{V_I}} - \frac{\partial \Pi}{\partial \boldsymbol{V_R}}\right) \\ \boldsymbol{\Upsilon_2}^T\overline{\boldsymbol{Z}} &= \frac{1}{2}\left(-i\frac{\partial \Pi}{\partial \boldsymbol{V_I}} - \frac{\partial \Pi}{\partial \boldsymbol{V_R}}\right)\end{aligned} \tag{4.17}$$

It can be seen from **Eq. (4.17)** that $\boldsymbol{\Upsilon_1} = \overline{\boldsymbol{\Upsilon}}_{\boldsymbol{2}}$. Therefore, it is sufficient to solve **Eq. (4.16)** to determine the adjoint vectors in **Eq. (4.15)**. Then **Eq. (4.15)** becomes

$$\begin{aligned}\frac{d\Phi}{d\rho_e} &= \boldsymbol{\Upsilon_1}^T\frac{\partial \boldsymbol{Z}}{\partial \rho_e}\boldsymbol{V} + \boldsymbol{\Upsilon_2}^T\frac{\partial \overline{\boldsymbol{Z}}}{\partial \rho_e}\overline{\boldsymbol{V}} \\ &= 2Re\left(\boldsymbol{\Upsilon_1}^T\frac{\partial \boldsymbol{Z}}{\partial \rho_e}\boldsymbol{V}\right) \\ &= 2\mathrm{Re}(\boldsymbol{\Upsilon_1}^T\left(i\omega\frac{\partial \boldsymbol{M}}{\partial \rho_e} + \frac{\partial \boldsymbol{C}}{\partial \rho_e} + \frac{1}{i\omega}\frac{\partial \boldsymbol{K}}{\partial \rho_e}\right)\mathbf{V})\end{aligned} \tag{4.18}$$

Assuming design load is real and independent, then $\boldsymbol{F} = \overline{\boldsymbol{F}}$ and considering the total time-averaged power flow response as:

$$\Pi = \frac{1}{2} Re(\boldsymbol{F}^H \boldsymbol{V}) = \frac{1}{2} (\boldsymbol{F}_R^T \boldsymbol{V}_R + \boldsymbol{F}_I^T \boldsymbol{V}_I) \tag{4.19}$$

So the expression with respect to real part and imagine part of velocity are:

$$\frac{\partial \Pi}{\partial \boldsymbol{V}_R} = \frac{1}{2} \boldsymbol{F}_R^T, \qquad \frac{\partial \Pi}{\partial \boldsymbol{V}_I} = \frac{1}{2} \boldsymbol{F}_I^T \tag{4.20}$$

Then $\boldsymbol{\Upsilon_1}$ can be obtained from **Eq. (4.17)**:

$$\boldsymbol{\Upsilon_1}^T \boldsymbol{Z} = \frac{1}{4} \left(i \boldsymbol{F}_I^T - \boldsymbol{F}_R^T \right) = -\frac{1}{4} \boldsymbol{F}^H \tag{4.21}$$

Comparing **Eq. (4.21)** to **Eq. (4.7)** we can obtain that:

$$\boldsymbol{\Upsilon_1}^T = -\frac{1}{4} \boldsymbol{V}^H \tag{4.22}$$

Substituting **Eq. (4.22)** into **Eq. (4.18)** then the sensitivity of dynamic compliance can be expressed as follow:

$$\frac{d\Phi}{d\rho_e} = -\frac{1}{2} Re(\boldsymbol{V}^H \left(i\omega \frac{\partial \boldsymbol{M}}{\partial \rho_e} + \frac{\partial \boldsymbol{C}}{\partial \rho_e} + \frac{1}{i\omega} \frac{\partial \boldsymbol{K}}{\partial \rho_e} \right) \boldsymbol{V}) \tag{4.23}$$

The derivatives of the mass matrix, the damping matrix and the stiffness matrix with respect to the design variables can be easily calculated at the elemental level with the following relations:

$$\frac{\partial \boldsymbol{M}}{\partial \rho_e} = q * {\rho_e}^{q-1} \boldsymbol{M_e^s} - q * {\rho_e}^{q-1} \boldsymbol{M_e^w}) \tag{4.24}$$

$$\frac{\partial \boldsymbol{K}}{\partial \rho_e} = p * {\rho_e}^{p-1} \boldsymbol{K_e^s} - p * {\rho_e}^{p-1} \boldsymbol{K_e^W}) \tag{4.25}$$

$$\frac{\partial \boldsymbol{C}}{\partial \rho_e} = \alpha \frac{\partial \boldsymbol{M}}{\partial \rho_e} + \beta \frac{\partial \boldsymbol{K}}{\partial \rho_e} \tag{4.26}$$

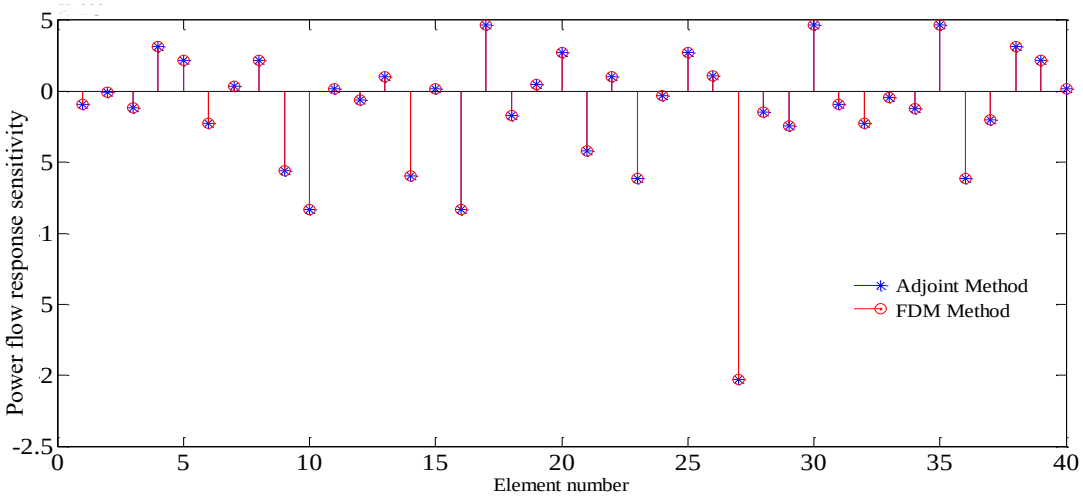

***Fig** 4.2 Sensitivity analysis results of power flow response at the loading point with respect to the element relative density*

In order to verify the finite element model and sensitivity analysis procedures, we first calculate a square plate with 4 edges simply supported and discretized with 400 uniform-sized square elements. Such a coarse mesh is used here for ease of graphical illustration of the sensitivity analysis results. The total number of degrees of freedom is n = 1323. As an initial design of later topology optimization, the relative densities are given random value from 0 to 1. The sensitivity of 40 elements picked from all 400 elements by random have been calculated by both adjoint method and finite difference method to verify the sensitivities. The results in **Fig** 4.2 show that the sensitivities obtained by these two methods agree well.

4.1.5 Numerical study

In this section, we show the example of bi-material plate optimized with the objective of minimizing the power flow response given by **Eq. (4.12)**. The plate we discuss here is made of two materials with different properties, one of which has relatively larger Yong's modulus to ensure the strength requirements of the structure. The other material is relatively soft which is aim to increase the energy dissipation. The aim of this case study is mainly to perform a complete topology optimization process with FE analysis and numerical optimization so that the feasibility of applying topology optimization method to passive structure vibration control can be verified. Thus, the materials properties adopted here may not have a very solid engineering background, but the topology optimization model still could be applied to realistic engineering problem with proper material parameters. In addition, we also assume these two materials are ideal contacted.

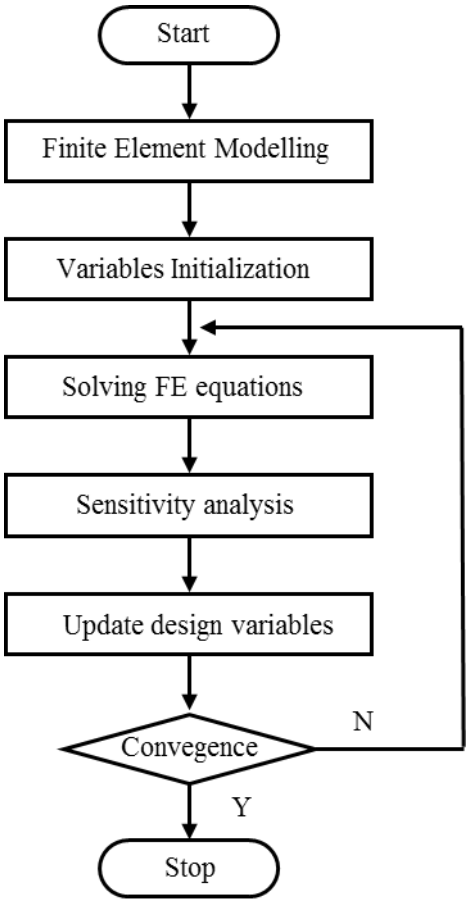

***Fig** 4.3 Flow chart of optimization procedure*

The simply supported square plate has a geometrical dimension of $a = 0.5\ m$ and the thickness $t = 0.003\ m$. Four-node Mindlin plate element is used in the finite element modelling. An external force $\boldsymbol{F}e^{i\omega t}$ is applied at centre point. Young's modulus, Poisson's ratio and the mass density of the stiffer material(metal-like material) are $\mathrm{E}_s = 1.0 \times 10^{11}\ N/m^2$, $\mu_s = 0.3$ and $\rho_s = 7800\ \mathrm{kg/m^3}$, respectively, while the properties of soft material(rubber-like material) are $\mathrm{E}_w = 1.0 \times 10^{10}\ N/m^2$, $\mu_w = 0.3$ and $\rho_w = 780\ \mathrm{kg/m^3}$, respectively. Rayleigh damping

is one kind of common damping model which is adopted in this case for its mathematical convenience. The damping coefficients of the damping material are given as $\alpha = 1 \times 10^{-4}, \beta = 1 \times 10^{-5}$. Obviously, the overall damping ratio is mainly contributed by the stiffness proportion in this case.

In order to ensure the accuracy of result by FE method at high frequency level, the FE model is meshed into 100×100. The optimization procedure will be stopped when the relative difference of the objective function values between two adjacent iteration steps satisfies $|\Phi_{new} - \Phi_{old})/\Phi_{old}| < 0.005$ or iteration >100. Although with filter technology, the optimized topology layout is still with large grey area leading to a non 0-1 distribution. One way to handle this problem was proposed by Sigmund[61]. The Matlab script in that paper is intended as a post-processing step that converts a grey scale design. This technology is also adopted in this thesis. The iteration history of topology optimization for load frequency $\omega = 531.0\text{Hz}$ has been shown in **Fig** 4.4. A dramatic decrease of the power flow response between the initial design and the optimum design can be observed. The unstable fluctuation in the iteration curve might be explained as the process of global searching. In this explanation, each suddenly raise means jumping out of a local optimal.

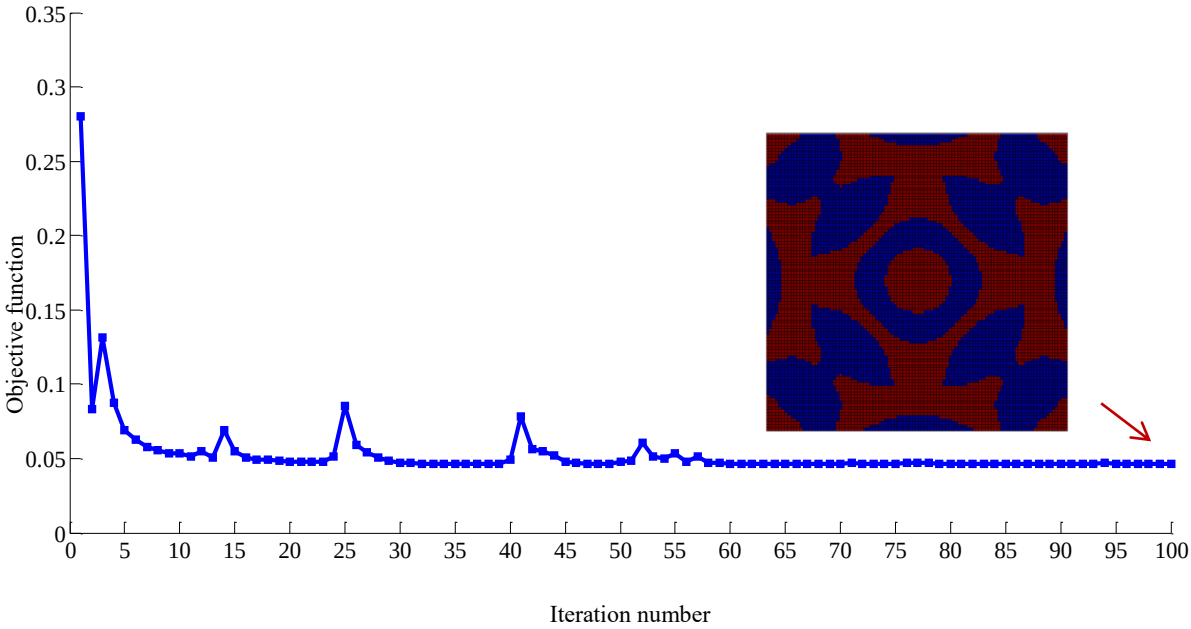

***Fig** 4.4 The optimal topology layout and iteration history of the design objective function for $\omega = 531.0Hz$*

We consider five different loading frequencies ranging from a low frequency level to high frequency level here. The optimal topologies are shown in **Fig 4.5 a)** to **Fig 4.5 d)** in which brown and blue areas in topology pattern represent stiffer material and soft material respectively.

When looking at the optimized topology layouts we can notice that they all have stiffer material of different size or shape at the centre of plate. The reason might be that the load applied to plate is a central force, therefore it is necessary to place stiffer material at the centre to resistant

the external force. With the loading frequencies increase, the central stiffer materials (see **Fig 4.5 a)**) are spreading to the edges and the optimal shape also become more complex. That probably because at lower frequency level, the mode shape of plate is simple, for example, the mode shape of the first loading frequency is like large funnel. The largest deformation is happened at the centre of plate, which leads to the all stiffer material concentrate on the centre of the plate. Similarly, as the loading frequency increases, the optimal layouts of the stiffer materials become spatially more complex as the mode shape changed. A similar tendency was also reported in the study of Du and Olhoff[117]. This is natural since a higher loading frequency will excite higher order of eignemodes, which typically have more localized features.

***Fig** 4.5 Optimum topologies of simply supported bi-material Mindlin plate obtained by minimization of the input power flow subject to five different loading frequencies with central forece loading is applied to the upper surface of the plate.*

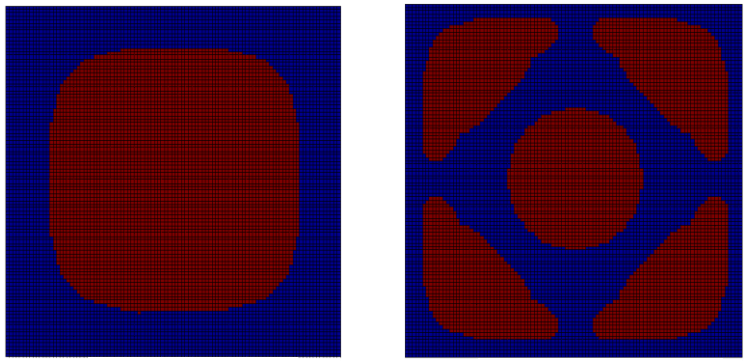

a) ω=40.7 Hz

b) ω=205.0 Hz

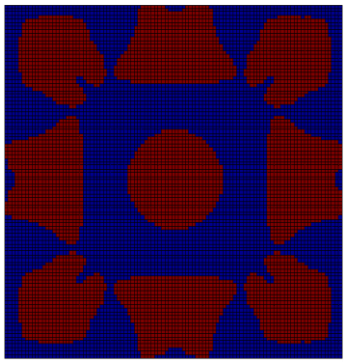

c) ω=367.0 Hz

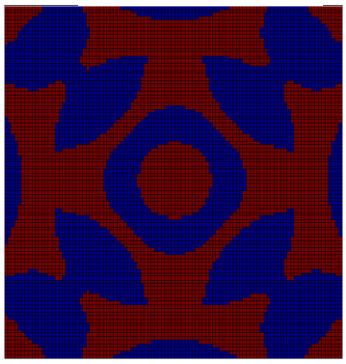

d) ω=693.0 Hz

After obtaining the optimal topology layouts for five different loading frequencies, the new optimized finite element models are used to re-calculate the power flow responses for comparison. The power flow responses have been shown in **Fig 4.6 a)** to **Fig 4.6 d)**. It is noted that, compared to the initial designs, the power flow responses have a remarkable decrease. The reason is that all the given excitation frequencies are very close to the natural eigenfrequencies of the initial design. For the optimal design **Fig. 4.6 b)**, we find that its second and third eigenfrequencies of free vibrations are $\omega_2 = 167.3\ \ Hz$ and $\omega_3 = 317.2\ \ Hz$, which are far away from the given excitation frequency $\omega_p = 205\ \ Hz$. This demonstrates that large displacement amplitudes have been avoided effectively at the excitation frequency $\omega_p = 205\ \ Hz$ with the optimal design.

We could also observe a large reduction at the excitation frequencies. This reduction has been obtained because the eigenfrequencies are moved away from the excitation frequencies. The lowest point of the response curve is now located close to the excitation frequency and a relative large span around this frequency exists where the power flow response is small.

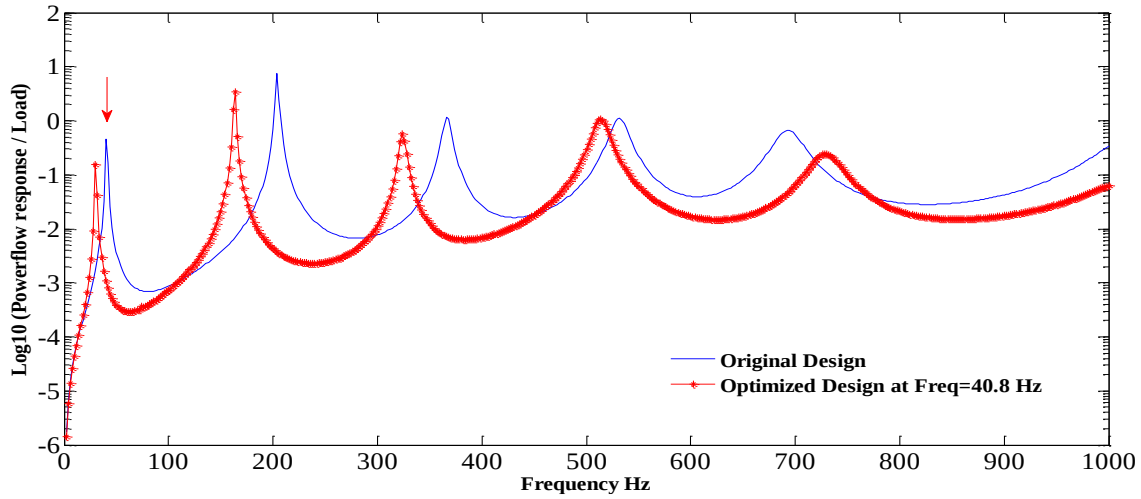

a) Power flow response at optimization frequency=40.8 Hz

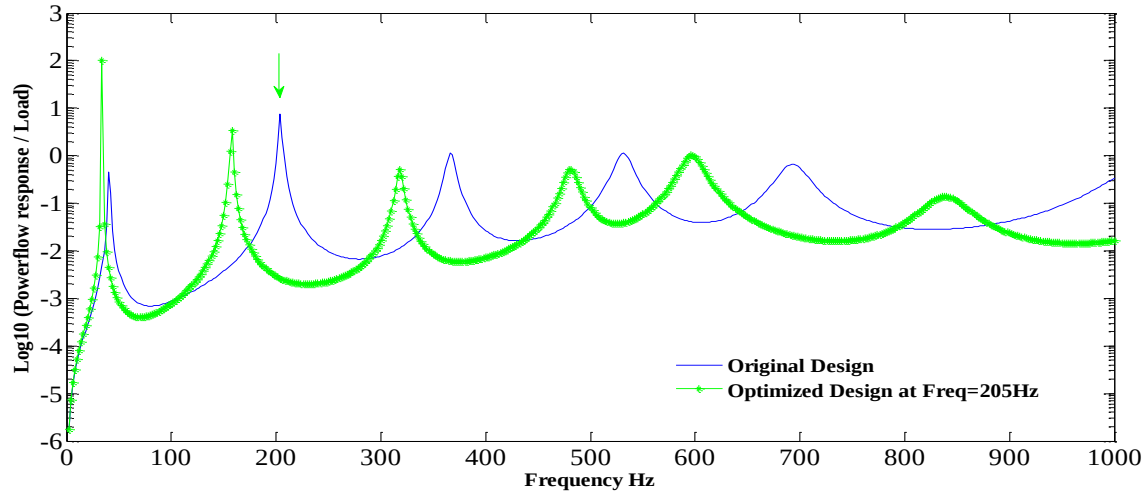

b) Power flow response at optimization frequency=205.0Hz

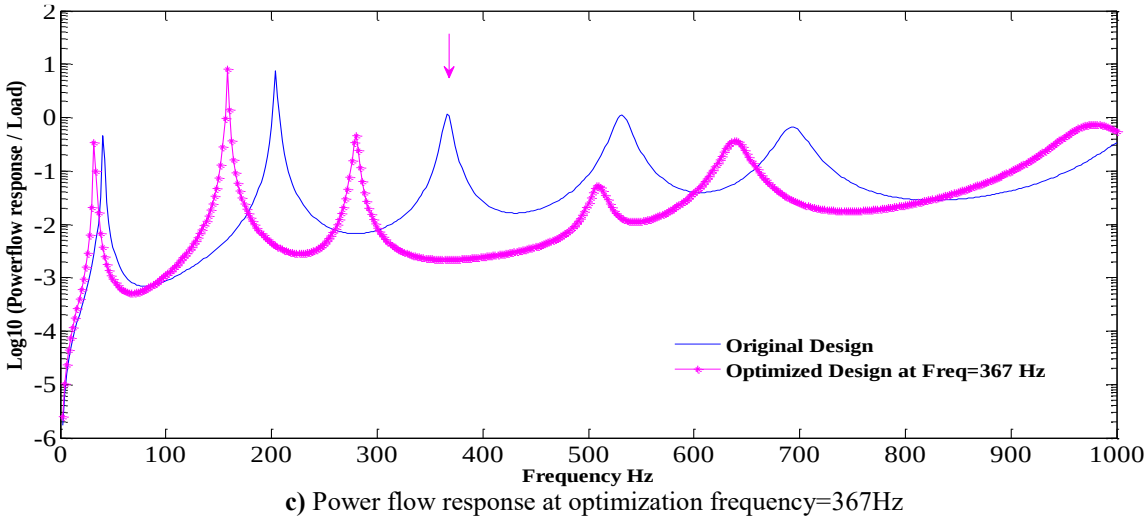

c) Power flow response at optimization frequency=367Hz

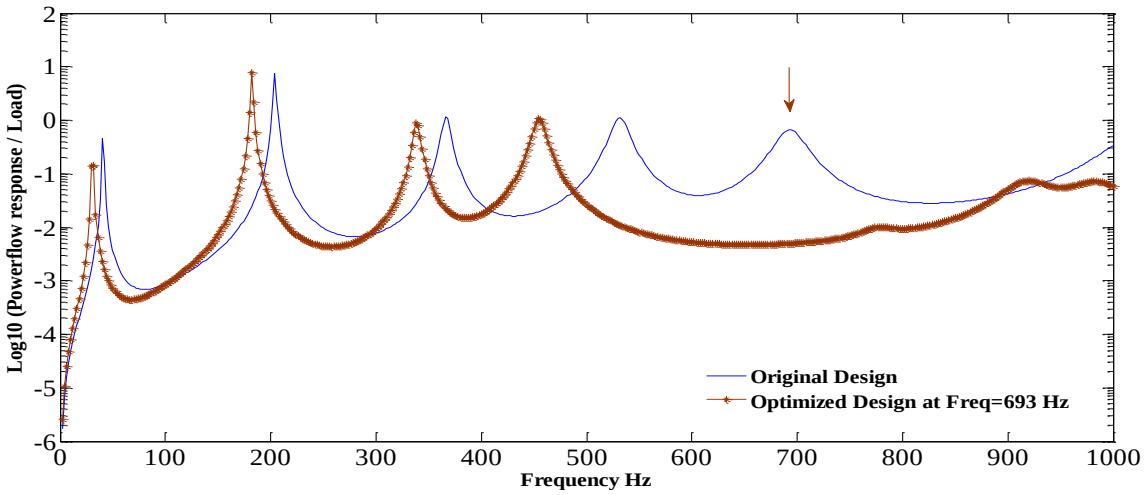

d) Power flow response at optimization frequency=693Hz

***Fig** 4.6 Power flow responses of five optimum layouts finite element plate model with excitation frequency from 0 Hz to 1000Hz*

4.1.6 Damping effect

As we know, structural damping, even with a small value, probably has a remarkable effect on the structural dynamic behaviour. Therefore, in this section, the impact of structural damping on optimal layouts of the plate is investigated. Here, the structural damping is considered as Rayleigh damping. Taking the same problem settings as in **Section 4.1.1**. Considering the contribution of mass damping coefficient α is quite small, we only investigate the effect of stiffness damping coefficient β. A small value is assigned to the mass damping coefficient ($\alpha = 1 \times 10^{-5}$) with respect to different stiffness damping coefficients in a certain range ($\beta = 1 \times 10^{-5} \sim 0.5 \times 10^{-3}$). According to **Eq. (4.10)**, that means the damp ratios of the plate range from 0.37 to 1.88 correspondingly. Through the comparison, it can be observed that the effect of different damping levels on the topology layout is significant. The results are shown in **Fig 4.7**. As we expected, the effect of the stiffness damping on the optimal topology is quite remarkable. That is because the elastic modulus of stiffness matrix is approximately 10^9 larger than material density in mass matrix. Thus, it is less surprise that the stiffness damping coefficient has more remarkable effect on the result of topology optimization than the mass damping coefficient does. Higher damping ratio means more energy will be dissipated during the vibration, so it also can be observed that the volume of stiffer material in $\beta = 0.5 \times 10^{-3}$ case is obviously less than 50%. That probably because higher capability to dissipate energy lead less strong material is required.

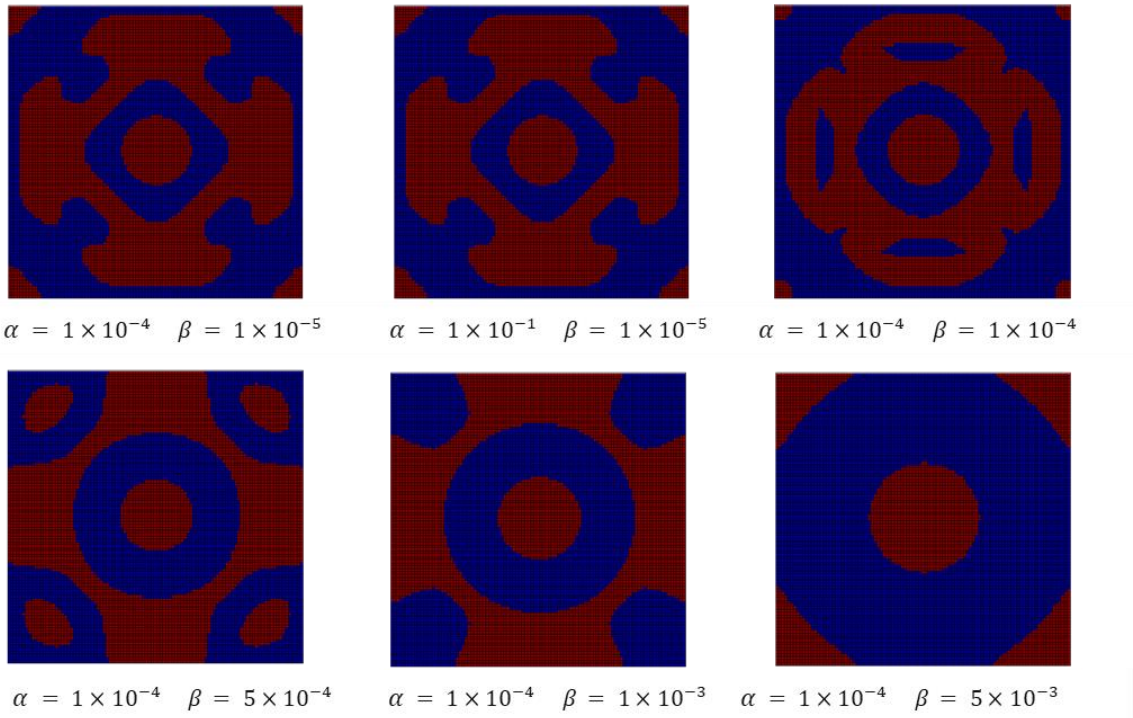

Fig 4.7 *Effect of the stiffness damping coefficient on the topology design* ($\omega_p = 600$Hz)

In the second case, the damping coefficients are fixed at larger values $\alpha = 1\times10^{-4}$ and $\beta = 1\times10^{-3}$, the optimal bi-material topologies with respect to different excitation frequencies are given in **Fig 4.8**. It is found that the optimal design is insensitive to the change of the excitation frequency within a broad frequency interval when the structural damping, especially the stiffness damping, is large. There are not remarkable changes between the optimal topologies

Fig *4.8 Optimal bi-material topologies at different excitation frequencies with large structural damping* ($\alpha = 1\times10^{-4}, \beta = 1\times10^{-3}$)

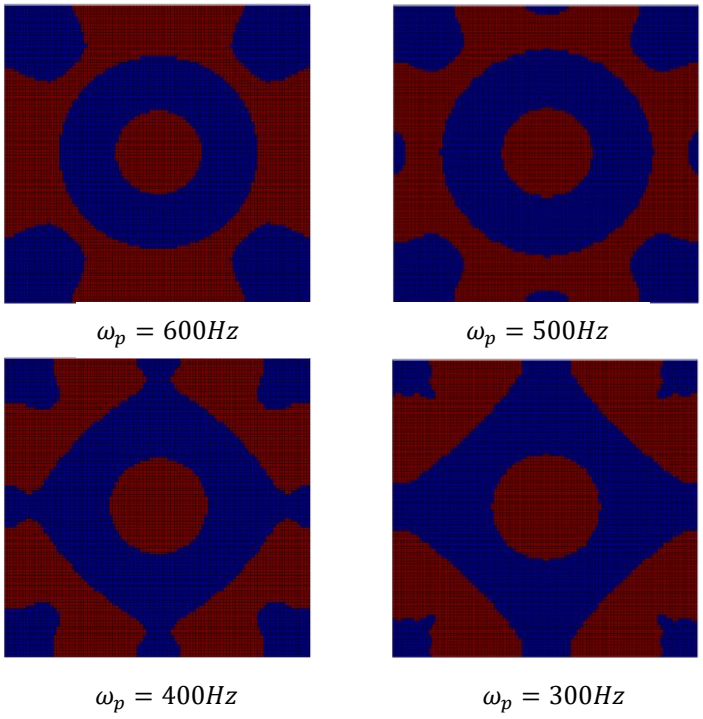

for different frequencies. Moreover, the iteration process becomes more stable even at the high excitation frequency as the structural damping increases.

4.2 Minimization of dynamic compliance based on topology optimization

4.2.1 Objective function for topology optimization

The problem of optimizing the topology of a continuum structure for minimum value of the integral dynamic structural compliance can be formulated in a discrete form as follows:

$$\begin{aligned} min \quad & \mathrm{C}_d = |\boldsymbol{F}^T\boldsymbol{U}| = |\boldsymbol{U}^T\boldsymbol{S}\boldsymbol{U}| \\ s.t. \quad & \boldsymbol{S}\boldsymbol{U} = \boldsymbol{F} \\ & \boldsymbol{S} = \boldsymbol{K} + i\omega_p\boldsymbol{C} - \omega_p^2\boldsymbol{M} \\ & \sum_{e=1}^{N_e} \rho_e V_e - f_v \sum_{e=1}^{N_e} V_e \le 0, \\ & 0 \le \rho_e \le 1, \qquad e = 1, \cdots, N_e \end{aligned} \tag{4.27}$$

In this bi-material design problem, we are aim to find the optimal topology layout to minimize dynamic compliance subject to a volume limit. Where C_d represents the optimization objective dynamic compliance which is equal to the work done by the external dynamic forces against corresponding displacements, $\boldsymbol{U}$ denotes the steady-state amplitude vector and $\boldsymbol{F}$ denotes the load magnitude vector. The harmonic external loading vector $\boldsymbol{f}(t)$ with the given excitation frequency ω_p can then be expressed as $\boldsymbol{f}(\boldsymbol{t}) = \boldsymbol{F}e^{i\omega t}$ and the displacement response vector as $\boldsymbol{u}(t) = \boldsymbol{U}e^{i\omega t}$. The symbols $\boldsymbol{K}$ and $\boldsymbol{M}$ represent the structural stiffness and mass matrix, where N is the number of DOFs. The symbol $\boldsymbol{C}$ is Rayleigh damping where α and β denote the mass damping and stiffness damping coefficients, respectively. Here, the same bi-material optimization model as last case is used for this one. The volumetric densities of two materials play the role of the design variable in the problem.

4.2.2 Design sensitivity analysis

In what follows, the objective function C_d only explicitly depending on the amplitudes of the velocity response $\boldsymbol{U}$ is considered. The sensitivity analysis scheme for C_d is derived by using the adjoint variable method which is more efficient than the direct variable method in the problems involving a large number of design variables but only a few behaviour functions, as in the case of a topology optimization.

Considering the vibration equation and its conjugate equation, we can rewrite the function:

$$\Phi = C_d + \boldsymbol{\Upsilon_1}^T(\boldsymbol{SU} - \boldsymbol{F}) + \boldsymbol{\Upsilon_2}^T(\overline{\boldsymbol{S}}\,\overline{\boldsymbol{U}} - \overline{\boldsymbol{F}}) \tag{4.28}$$

where $\overline{\boldsymbol{S}}$ and $\overline{\boldsymbol{F}}$ denote the conjugates of the dynamic stiffness matrix $\boldsymbol{S}$ and the force amplitude vector $\boldsymbol{F}$, respectively; $\boldsymbol{U}$ and $\overline{\boldsymbol{U}}$ denote the steady-state amplitude vector and its conjugate respectively; $\boldsymbol{\Upsilon_1}$ and $\boldsymbol{\Upsilon_2}$ are the adjoint vectors. Differentiating **Eq. (4.28)** with respect to the eth design variable leads to

$$\begin{aligned}\frac{d\Phi}{d\rho_e} &= \boldsymbol{\Upsilon_1}^T\frac{\partial \boldsymbol{S}}{\partial \rho_e}\boldsymbol{U} + \boldsymbol{\Upsilon_2}^T\frac{\partial \overline{\boldsymbol{S}}}{\partial \rho_e}\overline{\boldsymbol{U}} \\ &+ \left(\frac{\partial C_d}{\partial \boldsymbol{U_R}} + \boldsymbol{\Upsilon_1}^T\boldsymbol{S} + \boldsymbol{\mu_2}^T\overline{\boldsymbol{S}}\right)\frac{\partial \boldsymbol{U_R}}{\partial \rho_e} \\ &+ \left(\frac{\partial C_d}{\partial \boldsymbol{U_I}} + i\boldsymbol{\Upsilon_1}^T\boldsymbol{S} - i\boldsymbol{\Upsilon_2}^T\overline{\boldsymbol{S}}\right)\frac{\partial \boldsymbol{U_I}}{\partial \rho_e}\end{aligned} \tag{4.29}$$

where $\boldsymbol{U_R}$ and $\boldsymbol{U_I}$ represent the real part and image part of vector $\boldsymbol{U}$, respectively.
Let the adjoint variables satisfy the following equations:

$$\begin{aligned}\left(\frac{\partial C_d}{\partial \boldsymbol{U_R}} + \boldsymbol{\Upsilon_1}^T\boldsymbol{S} + \boldsymbol{\Upsilon_2}^T\overline{\boldsymbol{S}}\right) &= 0 \\ \left(\frac{\partial C_d}{\partial \boldsymbol{U_I}} + \mathrm{i}\boldsymbol{\Upsilon_1}^T\boldsymbol{S} - i\boldsymbol{\Upsilon_2}^T\overline{\boldsymbol{S}}\right) &= 0\end{aligned} \tag{4.30}$$

We can obtain equations as follow:

$$\begin{aligned}\boldsymbol{\Upsilon_1}^T\boldsymbol{S} &= \frac{1}{2}\left(i\frac{\partial C_d}{\partial \boldsymbol{U_I}} - \frac{\partial C_d}{\partial \boldsymbol{U_R}}\right) \\ \boldsymbol{\Upsilon_2}^T\overline{\boldsymbol{S}} &= \frac{1}{2}\left(-i\frac{\partial C_d}{\partial \boldsymbol{U_I}} - \frac{\partial C_d}{\partial \boldsymbol{U_R}}\right)\end{aligned} \tag{4.31}$$

It can be seen from **Eq. (4.31)** that $\boldsymbol{\Upsilon_1} = \overline{\boldsymbol{\Upsilon}}_{\boldsymbol{2}}$. Therefore, it is sufficient to solve **Eq. (4.30)** to determine the adjoint vectors in **Eq. (4.29)**. Then **Eq. (4.29)** becomes

$$\begin{aligned}\frac{d\Phi}{d\rho_e} &= \boldsymbol{\Upsilon_1}^T\frac{\partial \boldsymbol{S}}{\partial \rho_e}\boldsymbol{U} + \boldsymbol{\Upsilon_2}^T\frac{\partial \boldsymbol{S}}{\partial \rho_e}\overline{\boldsymbol{U}} \\ &= 2Re\left(\boldsymbol{\Upsilon_1}^T\frac{\partial \boldsymbol{S}}{\partial \rho_e}\boldsymbol{U}\right) \\ &= 2\mathrm{Re}(\boldsymbol{\Upsilon_1}^T\left(-\omega^2\frac{\partial \boldsymbol{M}}{\partial \rho_e} + i\omega\frac{\partial \boldsymbol{C}}{\partial \rho_e} + \frac{\partial \boldsymbol{K}}{\partial \rho_e}\right)\mathbf{U})\end{aligned} \tag{4.32}$$

Considering the expression of dynamic compliance

$$C_d = \sqrt{(\boldsymbol{F_R^T U_R} + \boldsymbol{F_I^T U_I})^2 + (\boldsymbol{F_I^T U_R} + \boldsymbol{F_R^T U_I})^2} \tag{4.33}$$

Assuming design load is real and independent, then $\boldsymbol{F = F_R = F^H}$. So the expression with respect to real part and imagine part of displacement is:

$$\frac{\partial C_d}{\partial \boldsymbol{U_R}} = \frac{\boldsymbol{F^T U_R}}{C_d}\boldsymbol{F^T}, \qquad \frac{\partial C_d}{\partial \boldsymbol{U_I}} = \frac{\boldsymbol{F^T U_I}}{C_d}\ \boldsymbol{F^T} \tag{4.34}$$

Substitute **Eq. (4.34)** into **Eq. (4.31)**

$$\boldsymbol{\Upsilon_1}^T \boldsymbol{S} = \frac{1}{2}\left(i\frac{\boldsymbol{F^T U_I}}{C_d} - \frac{\boldsymbol{F^T U_R}}{C_d}\right)\boldsymbol{F^T} = -\frac{1}{2C_d}\boldsymbol{F^T}\bar{\boldsymbol{U}}\boldsymbol{F^T} = -\frac{1}{2C_d}(\boldsymbol{U^T S}\bar{\boldsymbol{U}})\boldsymbol{F^T} \tag{4.35}$$

From **Eq. (4.27)**, we can obtain that $\boldsymbol{U^T S = F^T}$**,** then using **Eq. (4.35)**

$$\boldsymbol{\Upsilon_1}^T = -\frac{1}{2C_d}(\boldsymbol{U^T S}\bar{\boldsymbol{U}})\boldsymbol{U^T} \tag{4.36}$$

So **Eq. (4.32)** can be written as

$$\frac{d\Phi}{d\rho_e} = -Re(\frac{\boldsymbol{U^T S}\bar{\boldsymbol{U}}}{C_d}\boldsymbol{U^T}\left(-\omega^2\frac{\partial \boldsymbol{M}}{\partial \rho_e} + i\omega\frac{\partial \boldsymbol{C}}{\partial \rho_e} + \frac{\partial \boldsymbol{K}}{\partial \rho_e}\right)\boldsymbol{U}) \tag{4.37}$$

Substituting **Eq. (4.27)** into **Eq. (4.37)** then the sensitivity of dynamic compliance can be expressed as follow:

$$\frac{d\Phi}{d\rho_e} = -Re((\frac{\boldsymbol{U^T S}\bar{\boldsymbol{U}}}{|\boldsymbol{U^T SU}|})\boldsymbol{U}^T\left(-\omega^2\frac{\partial \boldsymbol{M}}{\partial \rho_e} + i\omega\frac{\partial \boldsymbol{C}}{\partial \rho_e} + \frac{\partial \boldsymbol{K}}{\partial \rho_e}\right)\boldsymbol{U}) \tag{4.38}$$

Similarly, a square plate with 4 edges simply supported and discretized with 400 uniform-sized square elements is built to verify the finite element model and sensitivity analysis. The result in **Fig** 4.9 shows that the sensitivity obtained by these two methods agrees well.

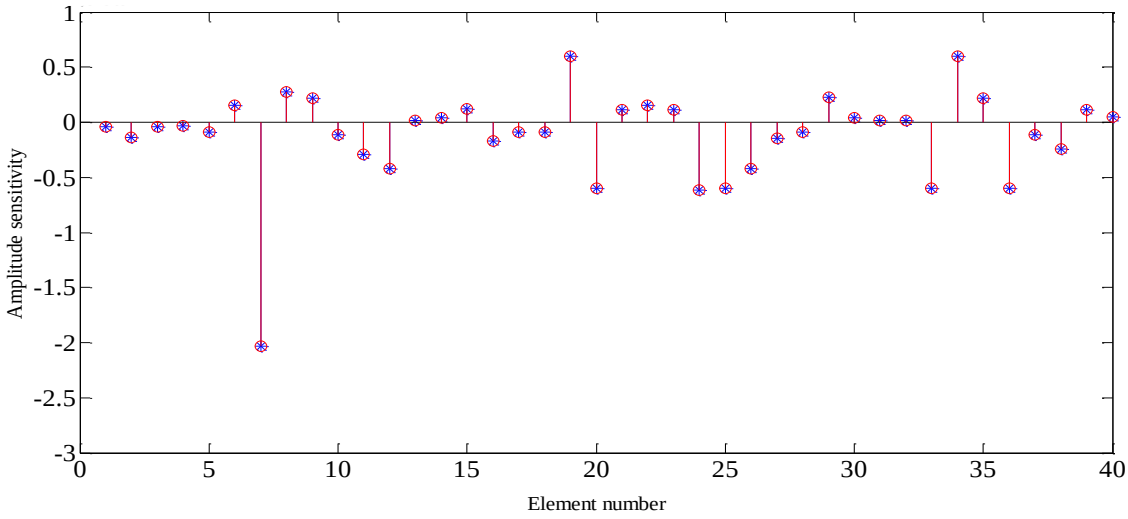

***Fig** 4.9 Sensitivity analysis results of vibration amplitude at the loading point with respect to the element relative density*

4.2.3 Numerical study

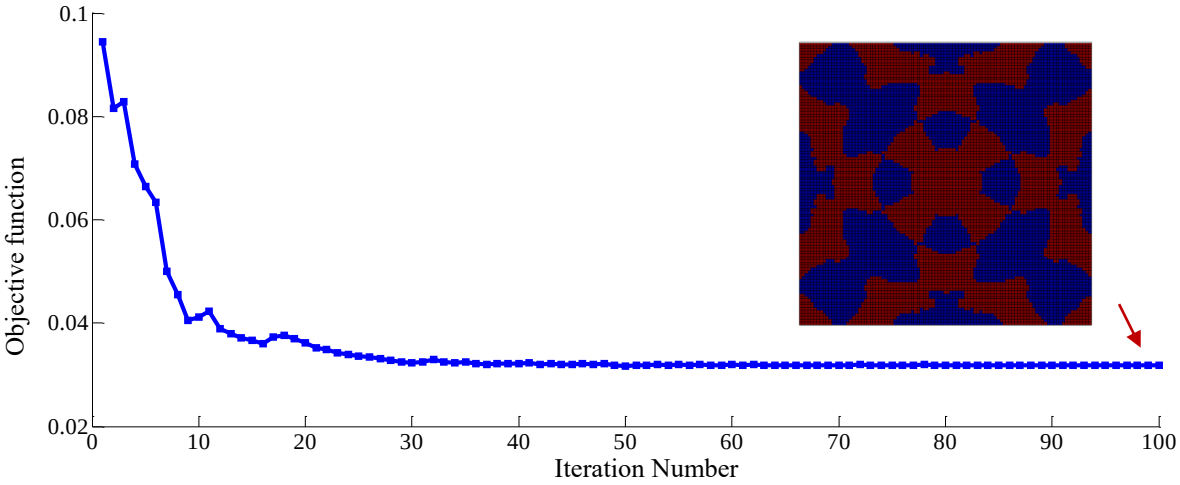

***Fig** 4.10 The optimal topology layout and iteration history of the design objective function for load frequency* $\omega = 693.0Hz$

In this section we show the example of plate optimized with the objective of minimizing the dynamic compliance given by **Eq. (4.27)**. The optimized model here is the same as that in **Section 4.1.4**, which has a geometrical dimension of $a = 0.5\ m$ and $t = 0.003\ m$. An external force $\boldsymbol{F}e^{i\omega t}$ is applied at centre point. Young's modulus, Poisson's ratio and the mass density of the strong material are $\mathrm{E}_s = 1.0 \times 10^{11}\ N/m^2$, $v_s = 0.3$ and $\rho_s = 7800$ Kg/m^3, respectively, while the properties of weak material are $\mathrm{E}_w = 1.0 \times 10^{10}\ N/m^2$, $\mu_w = 0.3$ and $\rho_w = 780\ Kg/m^3$, respectively. The damping coefficients of the damping material are given as $\alpha = 1 \times 10^{-4}, \beta = 1 \times 10^{-5}$. In order to ensure the accuracy of result by FE method at high frequency level, the FE model is meshed into 100×100. Same as the case study above,

the design variables $\rho_e(e = 1,2,\cdots,N_e)$ are initialized, usually by given uniform values 0.5. The dynamic compliance, as well as their derivatives with respect to the design variables, are then calculated. Using these data, the design variables are updated by the MMA optimizer. The optimization process repeats until the relative difference of the objective function values in two adjacent iteration steps $|(\Phi_{new} - \Phi_{old})/\Phi_{old}|$ is less than 0.001 or the iteration number >100. The iteration history and the optimal topology layout are shown in **Fig** 4.10**10.**

The steady-state amplitudes of the bi-material plate at the frequency ω=693.0Hz are shown in **Fig** 4.11. It is seen that the largest displacements are located around the plate centre where the load is applied for both initial layout and optimal layout. But the largest displacement amplitude of the optimized plate has been greatly decreased.

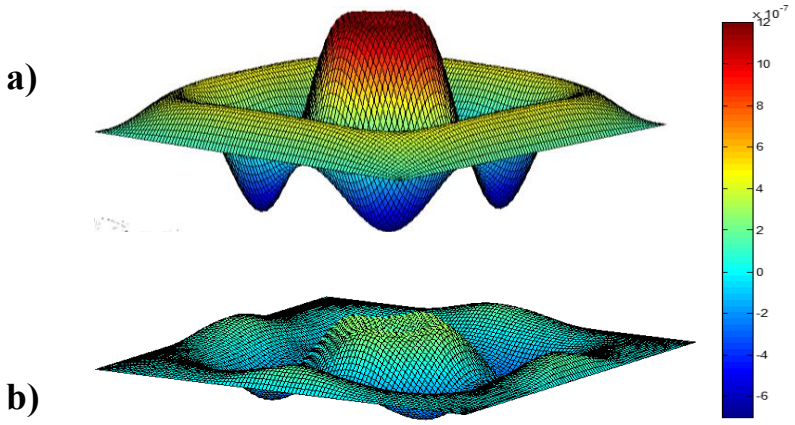

***Fig** 4.11 Steady displacement amplitudes subjected to a point load applied to the centre of plate with load frequency $\omega = 693.0Hz$ **a)** initial design **b)** optimal design*

To compare the topology layouts obtained by different objective function, it is seen from **Fig** 4.12 that the optimal topologies of two objective functions are slightly different for all five loading frequencies. Especially for the topology layouts with the first two optimization frequencies, they are almost indistinguishable (see **Fig** 4.12 a) and **Fig** 4.12 b). With the increasing of loading frequency, the difference of optimal topology layout between two objective functions becomes obvious (see **Fig** 4.12 c), d) and e)). These results provide numerical evidence that topology optimization with respect to minimum power flow response also has a great effect on the vibration suppression as well.

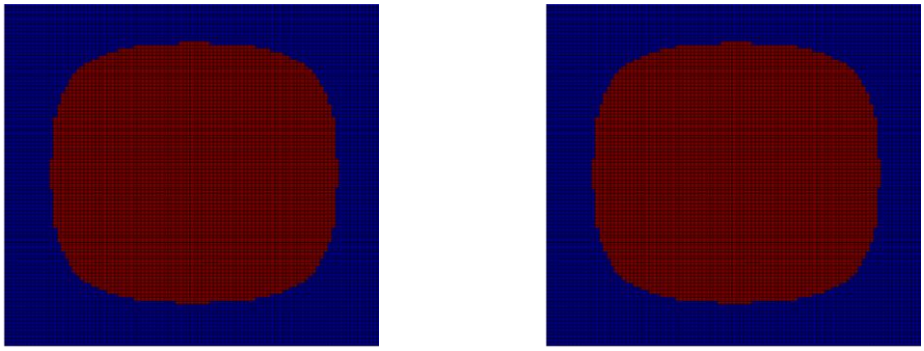

Powerflow response Dynamic compliance

Frequency ω=40.7 Hz

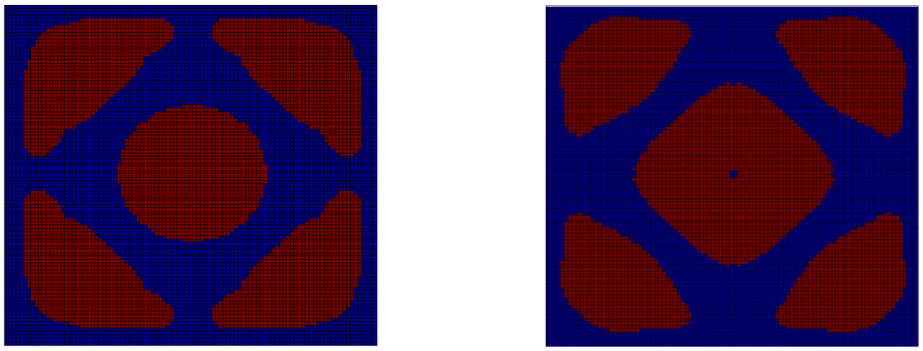

Powerflow response Dynamic compliance

Frequency ω=205.0Hz

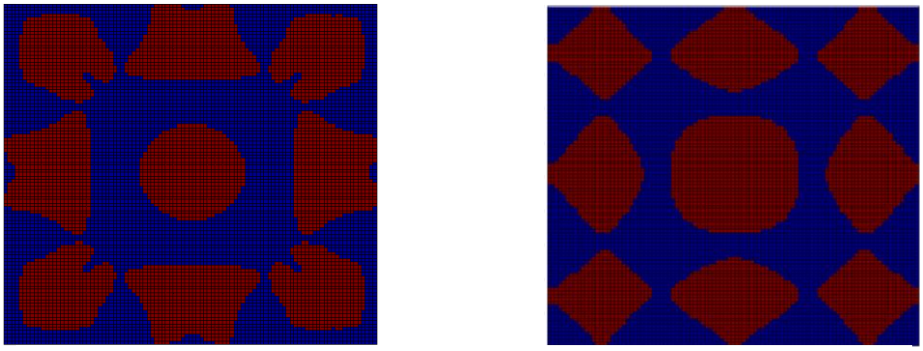

Powerflow response Dynamic compliance

Frequency ω=367.0Hz

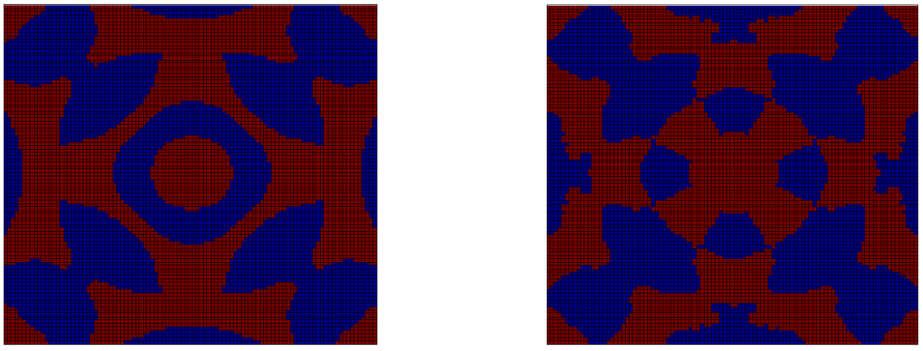

Powerflow response Dynamic compliance

Frequency ω=693.0Hz

***Fig** 4.12 Comparison of topology optimum layouts with two objective functions*

4.3 Summary

This chapter shows case studies on dynamic topology optimization of bi-material plate structure for vibration suppression. The mathematical formulation of topology optimization is established based on power flow response and bi-material solid isotropic material with SIMP model. The results of numerical examples and comparison of optimal results between two topological designs with minimum power flow response and minimum dynamic compliance verified the efficiency of this method. There is a common phenomenon in all numerical examples which obtained remarkable effect worth to notice. All these optimal designs have either driven the nearest resonance frequency as far away as possible from the prescribed excitation frequency, or has increased the gap between two neighbouring resonance frequencies as much as possible by redistributing material in space so that successfully avoid the resonance phenomenon occur. That is the reason why all these methods have great effect on vibration control.

Base on the investigation, the following conclusion can be drawn:

- Material distribution has a significant impact on structural vibration characteristic.
- Both the power flow response and dynamic compliance objective functions have great effect on vibration suppression.
- The effect of the Rayleigh damping ratio has a great impact on optimal topology pattern. In addition, the stiffness damping coefficient has more remarkable effect on the result of topology optimization than the mass damping coefficient.
- The reason for great effect on vibration suppression by redistributing material is that different material distribution will apply new dynamic characteristic on structure which drives the nearest resonance frequency as far away as possible from the prescribed excitation frequency, or has increased the gap between two neighbouring resonance frequencies as much as possible so that successfully avoid the resonance phenomenon occur.

Although the bi-material plate topology optimization model based on the two objective functions has achieved good results for vibration reduction, we have to admit the limitation of this bi-material model in application. In the previous examples, both materials are assumed to be ideally contacted, and not slip happened between the contact surfaces. So far, this model is too ideal to be manufactured in real world, therefore this Chapter is mainly to perform a complete topology optimization process with FE analysis and numerical optimization so that the feasibility of applying topology optimization method to passive structure vibration control can be verified. More models will be introduced in the following chapters.

Chapter 5 Application to free layer damping plate

Reducing vibration is often a major concern for structures subject to dynamic excitations. In particular, passive vibration control of flexible shell structures by incorporating damping materials has been used in many engineering fields, including vehicles, airplanes, automobiles, ships. This chapter investigates the optimal distribution of damping material in vibrating structures subject to harmonic excitations by using topology optimization method. An artificial damping material model that has a similar form as in the SIMP approach is suggested and the relative densities of the damping material are taken as design variables. In addition, different with most of the past research implemented the optimal damping layer design by their own finite element code, a Python package of commercial FE software Abaqus to implement topology optimization method is applied in this chapter. The optimal layouts obtained by topology optimization are discussed.

5.1 Governing equations

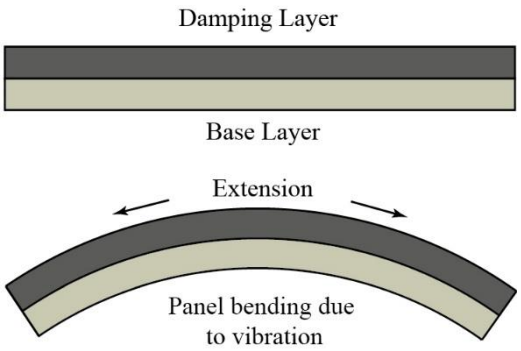

***Fig** 5.1 A plate structure with free damping layer treatments*

In this Chapter, the topology optimization problem for the layout design of the damping material surface layer with the aim to reduce the vibration amplitude is considered. Such a structure is schematically illustrated in **Fig** 5.1. It is assumed that the damping layer and the base structure is perfectly bonded. The governing equations of steady-state displacement are:

$$\left(-{\omega_p}^2\boldsymbol{M} + i\omega_p\boldsymbol{C} + \boldsymbol{K}\right)\boldsymbol{U} = \boldsymbol{F}, \tag{5.1}$$

Or

$$\boldsymbol{SU} = \boldsymbol{F}, \tag{5.2}$$

where symbols $\boldsymbol{K}$ and $\boldsymbol{M}$ represent the structural stiffness and mass matrix; $\boldsymbol{S} = -\omega_p{}^2\boldsymbol{M} + i\omega_p\boldsymbol{C} + \boldsymbol{K}$ is referred to as the dynamic stiffness matrix. $\boldsymbol{U}$ denotes the steady-state amplitude vector and $\boldsymbol{F}$ denotes the load magnitude vector. The steady state displacement amplitudes of each degree of freedom is given by

$$A_j = \sqrt{\left(U_j^R\right)^2 + \left(U_j^I\right)^2}, \qquad (j = 1, 2, \dots, n\ ) \tag{5.3}$$

where U_j^R and U_j^I $(j = 1, 2, \dots, n\ )$ are the real and imaginary parts of the complex amplitude A_j, respectively. Here n is the number of degree of freedom.

5.2 Topology optimization problem formulation

The aim of this Chapter is to find the optimal distribution of a given amount of damping material within a prescribed design domain for minimizing the vibration amplitudes at specified positions. The topology optimization problem is thus formulated as

$$\begin{aligned} \min_{\rho} \quad & \Pi = \sum_{j=1}^{m} A_j \\ s.t. \quad & \left(-\omega_p{}^2\boldsymbol{M} + i\omega_p\boldsymbol{C} + \boldsymbol{K}\right)\boldsymbol{U} = \boldsymbol{F} \\ & \sum_{e=1}^{N_e} \rho_e V_e^0 - f_v \sum_{e=1}^{N_e} \rho_e V_e^0 \le 0, \\ & 0 < \rho_{min} \le \rho_e \ \ (e = 1, \dots, N_e) \end{aligned} \tag{5.4}$$

where symbols $\boldsymbol{K}$ and $\boldsymbol{M}$ represent the structural stiffness and mass matrix; $\boldsymbol{\rho} = \{\rho_1, \rho_2, \rho_3, \dots, \rho_{N,}\}^T$ is the vector of the relative density design variables describing the damping material distribution. N_e denotes the total number of finite elements in the design domain; m is the number of specified degrees of freedom at which the displacement amplitudes $A_j (j = 1,2, \dots, m)$ are of interest. ω_p is excitation frequency in rad/s. Symbol f_v denotes the volume fraction ratio and V_e^0 is the damping material volume of the eth element when $\rho_e = 1$. As the spurious local eigenmodes will occur if the density of an element becomes extreme small, therefore the lower bound limit of the density variables ρ_{min} is prescribed as a small positive value, which is set to be 0.001 in this study. ω_p is the excitation frequency in rad/s. Since the system consists of a base-material load-bearing structure and a damping layer, the matrix $\boldsymbol{M}$ and $\boldsymbol{K}$ can be further expressed as

$$\begin{aligned} \boldsymbol{M} &= \boldsymbol{M}^b + \boldsymbol{M}^d \\ \boldsymbol{K} &= \boldsymbol{K}^b + \boldsymbol{K}^d \end{aligned} \tag{5.5}$$

where the superscript b denotes the quantities associated with the base material structure, while the superscript d denotes the contributions of the damping material. In general, the damping effect of the conventional base material is much smaller than that of the damping material. Therefore, damping properties of the base layer are neglected. The global mass matrix and the global stiffness matrix in the framework of the SIMP approach can be rewritten as

$$\begin{aligned} \boldsymbol{M} &= \sum_{e=1}^{N_e} \boldsymbol{M}_e^b + \rho_e \sum_{e=1}^{N_e} \boldsymbol{M}_e^d \\ \boldsymbol{K} &= \sum_{e=1}^{N_e} \boldsymbol{K}_e^b + \rho_e^p \sum_{e=1}^{N_e} \boldsymbol{K}_e^d \end{aligned} \tag{5.6}$$

where $\boldsymbol{K_e^b}$ and $\boldsymbol{M_e^b}$ denote the element stiffness matrix and element mass matrix of the base material, respectively, and they remain unchanged during the process of the optimization. The penalty p for element stiffness matrix is set to be 3. As mentioned, the damping effect of the base structural material is neglected. Therefore, the damping matrix in **Eq. (5.1)** becomes

$$\boldsymbol{C} = \sum_{e=1}^{N_e} \boldsymbol{C}_e^d \tag{5.7}$$

Where $\boldsymbol{C_e^d}$ is the element damping matrix, which is related to the density design variables. Analogously as in the elastic constant interpolation used in the SIMP model, an artificial damping model is suggested here for penalizing intermediate densities. Thus the elemental damping matrix in **Eq. (5.7)** is assumed as

$$\boldsymbol{C}_e^d = \alpha_0^d \rho_e^{q_1} \boldsymbol{M}_e^d + \beta_0^d \rho_e^{q_2} \boldsymbol{K}_e^d \tag{5.8}$$

Here, the constants α_0^d and β_0^d are Rayleigh damping coefficients of the fully solid damping material $\rho_e = 1$, real scalars $q_1 > 1$ and $q_2 > 1$ are penalty factors for the damping coefficients. In this section, both penalty factors for element damping matrix are set to be $q_1 = q_2 = 3$, which are suitable values for yielding a clear topology and a stable convergence from numerical experiences.

5.3 Design sensitivity analysis

As usual, the optimization problem **Eq. (5.4)** is solved by a gradient-based mathematical programming algorithm, which necessitates sensitivity analysis of the objective function with

respect to the design variables. The sensitivity analysis scheme for objective function Π is derived by using the adjoint variable method, which is more efficient than the direct variable method in the problems involving a large number of design variables[70]. Considering the vibration equation and its conjugate equation, we can rewrite the function Π as

$$\Phi = \Pi + \boldsymbol{\Upsilon_1^T}(\boldsymbol{SU} - \boldsymbol{F}) + \boldsymbol{\Upsilon_2^T}(\overline{\boldsymbol{S}}\,\overline{\boldsymbol{U}} - \overline{\boldsymbol{F}}) \tag{5.9}$$

Where $\overline{\boldsymbol{S}}$ and $\overline{\boldsymbol{F}}$ denote the conjugates of the dynamic stiffness matrix $\boldsymbol{S}$ and the force amplitude vector , respectively; $\boldsymbol{U}$ and $\overline{\boldsymbol{U}}$ denote the steady-state amplitude vector and its conjugate respectively; $\boldsymbol{\Upsilon_1}$ and $\boldsymbol{\Upsilon_2}$ are the adjoint vectors. Differentiating **Eq. (5.9)** with respect to the eth design variable leads to

$$\begin{aligned}\frac{d\Phi}{d\rho_e} &= \boldsymbol{\Upsilon_1^T}\frac{\partial \boldsymbol{S}}{\partial \rho_e}\boldsymbol{U} + \boldsymbol{\Upsilon_2^T}\frac{\partial \overline{\boldsymbol{S}}}{\partial \rho_e}\overline{\boldsymbol{U}} \\ &+ \frac{\partial \boldsymbol{U_R}}{\partial \rho_e}\left(\frac{\partial \Pi}{\partial \boldsymbol{U_R}} + \boldsymbol{\Upsilon_1^T U} + \boldsymbol{\Upsilon_2^T}\overline{\boldsymbol{U}}\right) \\ &+ \frac{\partial \boldsymbol{U_I}}{\partial \rho_e}\left(\frac{\partial \Pi}{\partial \boldsymbol{U_I}} + i\boldsymbol{\Upsilon_1^T U} - i\boldsymbol{\Upsilon_2^T}\overline{\boldsymbol{U}}\right)\end{aligned} \tag{5.10}$$

Let the adjoint variables satisfy the following equations

$$\begin{aligned}\boldsymbol{\Upsilon_1}^T\boldsymbol{S} &= \frac{1}{2}\left(-\frac{\partial \Pi}{\partial \boldsymbol{U_R}} + i\frac{\partial \Pi}{\partial \boldsymbol{U_I}}\right), \\ \boldsymbol{\Upsilon_2}^T\overline{\boldsymbol{S}} &= \frac{1}{2}\left(-\frac{\partial \Pi}{\partial \boldsymbol{U_R}} - i\frac{\partial \Pi}{\partial \boldsymbol{U_I}}\right).\end{aligned} \tag{5.11}$$

It can be seen from **Eq. (5.11)** that $\boldsymbol{\Upsilon_1} = \overline{\boldsymbol{\Upsilon_2}}$. Therefore, it is sufficient to solve **Eq. (5.11)** to determine the adjoint vectors in **Eq. (5.9)**. Then **Eq. (5.9)** becomes

$$\begin{aligned}\frac{d\Pi}{d\rho_e} &= 2Re(\boldsymbol{\Upsilon_1}^T\frac{\partial \boldsymbol{S}}{\partial \rho_e}\boldsymbol{U}) \\ &= 2Re(\boldsymbol{\Upsilon_1}^T(-\omega^2\frac{\partial \boldsymbol{M}}{\rho_e} + i\omega\frac{\partial \boldsymbol{C}}{\rho_e} + \frac{\partial \boldsymbol{K}}{\rho_e})\boldsymbol{U})\end{aligned} \tag{5.12}$$

where the derivatives of the mass matrix, the damping matrix and the stiffness matrix with respect to the design variables can be easily calculated as follow:

$$\begin{aligned}\frac{\partial \boldsymbol{M}}{\rho_e} &= \boldsymbol{M_e^d} \\ \frac{\partial \boldsymbol{K}}{\rho_e} &= p\rho_e^{p-1}\boldsymbol{K_e^d} \\ \frac{\partial \boldsymbol{C}}{\rho_e} &= q_1\rho_e^{q_1-1}\boldsymbol{K_e^d} + q_2\rho_e^{q_2-1}\boldsymbol{M_e^d}\end{aligned} \tag{5.13}$$

Take the sensitivity analysis of the vibration amplitude of the jth DOF A_j as an example. Position vector $\boldsymbol{p}_0 = \{0,0,1,\dots 0\}^T$ represents the position of the specified degrees of freedom in which the element equal 1 at the specified position and 0 elsewhere. The derivative of the objective function with respect to the real part of steady state vibration displacement response as follow:

$$\frac{dA_j}{d\boldsymbol{U_R}} = \frac{\partial\sqrt{\left(U_j^R\right)^2 + \left(U_j^I\right)^2}}{\partial \boldsymbol{U_R}} = \frac{\partial\sqrt{\left(U_j^R\right)^2 + \left(U_j^I\right)^2}}{\partial U_j^R}\boldsymbol{p}_0 = \frac{U_j^R}{A_j}\boldsymbol{p}_0 \tag{5.14}$$

$$\frac{dA_j}{d\boldsymbol{U_I}} = \frac{\partial\sqrt{\left(U_j^R\right)^2 + \left(U_j^I\right)^2}}{\partial \boldsymbol{U_I}} = \frac{\partial\sqrt{\left(U_j^R\right)^2 + \left(U_j^I\right)^2}}{\partial U_j^I}\boldsymbol{p}_0 = \frac{U_j^I}{A_j}\boldsymbol{p}_0 \tag{5.15}$$

Substituting **Eq. (5.14)** and **Eq. (5.15)** into **Eq. (5.11)**, then obtains the adjoint equations for this particular behaviour function:

$$\boldsymbol{\Upsilon}_1^T\boldsymbol{S} = \frac{1}{2A_j}\left(-U_j^R + iU_j^I\right)\boldsymbol{p}_0 = -\frac{\bar{U}_j}{2A_j}\boldsymbol{p}_0 \tag{5.16}$$

Once the adjoint vector is found by solving the adjoint equations, the derivative of the behaviour function Π can be obtained from **Eq. (5.16)**.

5.4 Numerical studies

In this section, two numerical examples: cantilever plate (see **Fig** 5.2) and simply supported plate (see **Fig** 5.11) are presented for illustrating the validity of the proposed sensitivity analysis and topology optimization formulation. In FE models, the base layer and damping layer are modelled with shell elements S4R in Abaqus with tie constraints at the contact faces and we assume there is no slip happened between the surfaces. Both layers has a geometrical dimension of $a = 3m$ and $t_b = t_d = 0.02m$. To define a more precise surface geometry for contact problems, the reference faces of base layer and damping layer are set to be top and bottom respectively. The design domain is discretized by a 60 × 60 mesh in the subsequent examples with total number of degrees of freedom equal 22326.

5.4.1 Implementation of topology optimization

The method of moving asymptotes is employed for solving the optimization problem **Eq. (5.4)**. At the beginning, the design variables are $\rho_e = 0.5$ $(e = 1,2,3,\dots,N_e)$. The volume fraction ratio of the damping material is restricted by $f_v = 0.5$. The well-known sensitivity filter technique proposed by Sigmund[119] with a filter radius of $r_{min} = 0.1m$ is employed for preventing checkerboard formation and mesh dependency of the optimal solution. The optimization procedure will be stopped when the relative difference of the objective function values between two adjacent iteration steps satisfies$|(f_{new} - f_{old})/f_{old}| < 0.005$.

5.4.2 Topology optimization of damping layer in a cantilever square plate

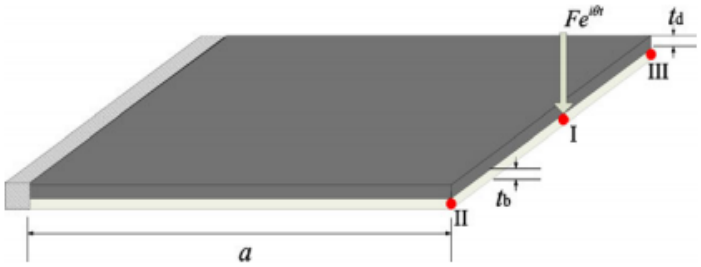

***Fig** 5.2 A cantilever square plate (a=3, t_d=t_b=0.02m) with a time-harmonic load applied at the mid-point of the free edge*

In the first example, the optimal layout design of the damping layer attached to a cantilever square plate as shown in **Fig** 5.2 is considered. External force $\boldsymbol{f}(t) = \boldsymbol{F}e^{i\omega t}$ is applied at point I (the mid-point of the free edge) with $F = 10^5 N$, $\omega = 2\pi f_p$ and $f_p = 30Hz$. Young's modulus, Poisson's ratio and the mass density of the base material (aluminium) are $E^b = 6.9 \times 10^{10} N/m^2$, $\mu^b = 0.3$ and $\rho^b = 2700Kg/m^3$, respectively, while the properties of the damping material (a rubber-like material) are $E^d = 2.2 \times 10^8 N/m^2$, $\mu^d = 0.49$ and $\rho^d = 980Kg/m^3$, respectively. Similar as the explanation in **Section 4.1.3**, Rayleigh damping model is adopted here for its mathematical convenience. Here, the damping coefficients of the damping material are given as $\alpha_0^d = 0.5, \beta_0^d = 1.0$. According to the **Eq. (4.10)** in Chapter 3, the damping layer is an over-damped structure since the overall damping ratio ξ is larger than 1.0. The Rayleigh damping coefficients adopted here is to magnify the damping effect. The objective of the design is to minimize the sum of vibration amplitudes at the loading point (point I) and two endpoints of the free edge (points II and III).

5.4.3 Results and discussions for cantilever square plate case

The iteration history of objective function value and volume fraction ratios are shown in **Fig** 5.3. It can be observed that the optimization procedure converged after 60 iterations and a stable decreasing of the objective function value during the optimization process. The objective function value has decreased from 1.21 for the initial design to 0.27 for the final optimal solution, a remarkable decreasing by 77.6% of the initial value. The volume fraction of damping material keeps stable at 0.5 during the whole optimization process except a slight downward at beginning. The damping material distribution and the deformation contour of the initial design and the optimal design are shown in **Fig** 5.4.

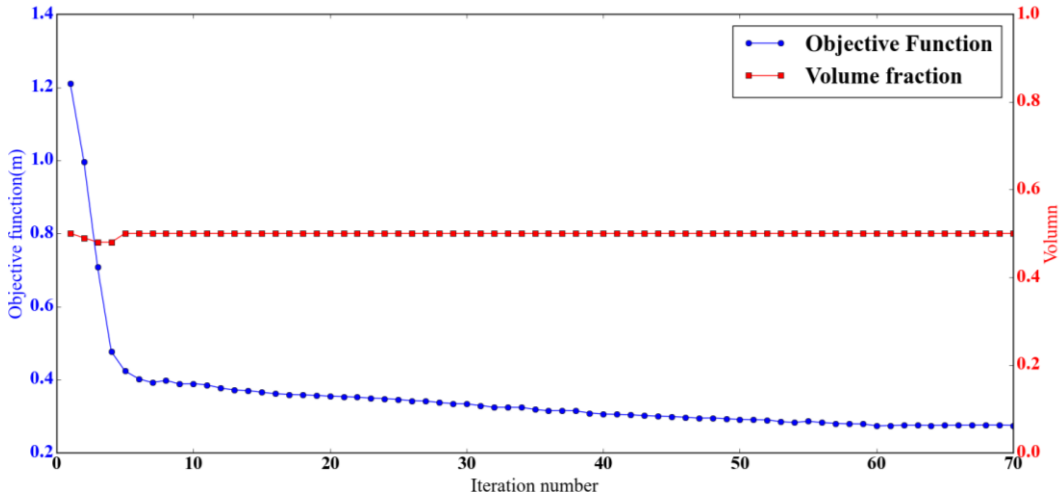

***Fig** 5.3 Iteration histories of objective function value and volume fraction ratio*

In **Fig** 5.4(a), the grey-scale indicates the relative density of the damping material in the initial design. It can be seen that there are still a few 'grey' elements with material densities neither 0 nor 1 in the final design (In **Fig** 5.4(b)). In fact, obtaining a clear 0-1 distribution is extremely difficult and quite time-consuming. Many factors such as filter radius, penal for stiffness and mass and sensitivities filter have significant effects on the final topology layout. A balance way to handle this problem is to stop the optimization process when the difference of two objective function values between adjacent iteration steps less than a prescribed value and then adopted a post-processing step proposed by Sigmund[61] to suppress the grey scale design. An adjustment of solid and void elements distribution according to the volume fraction limit set initially and material densities obtained by the optimization will be processed by this technique. The final clear distribution after post-processing step is shown in **Fig** 5.4(d) which indicates this technique is able to remove the 'grey elements' and keep the characteristic of original design at the same time.

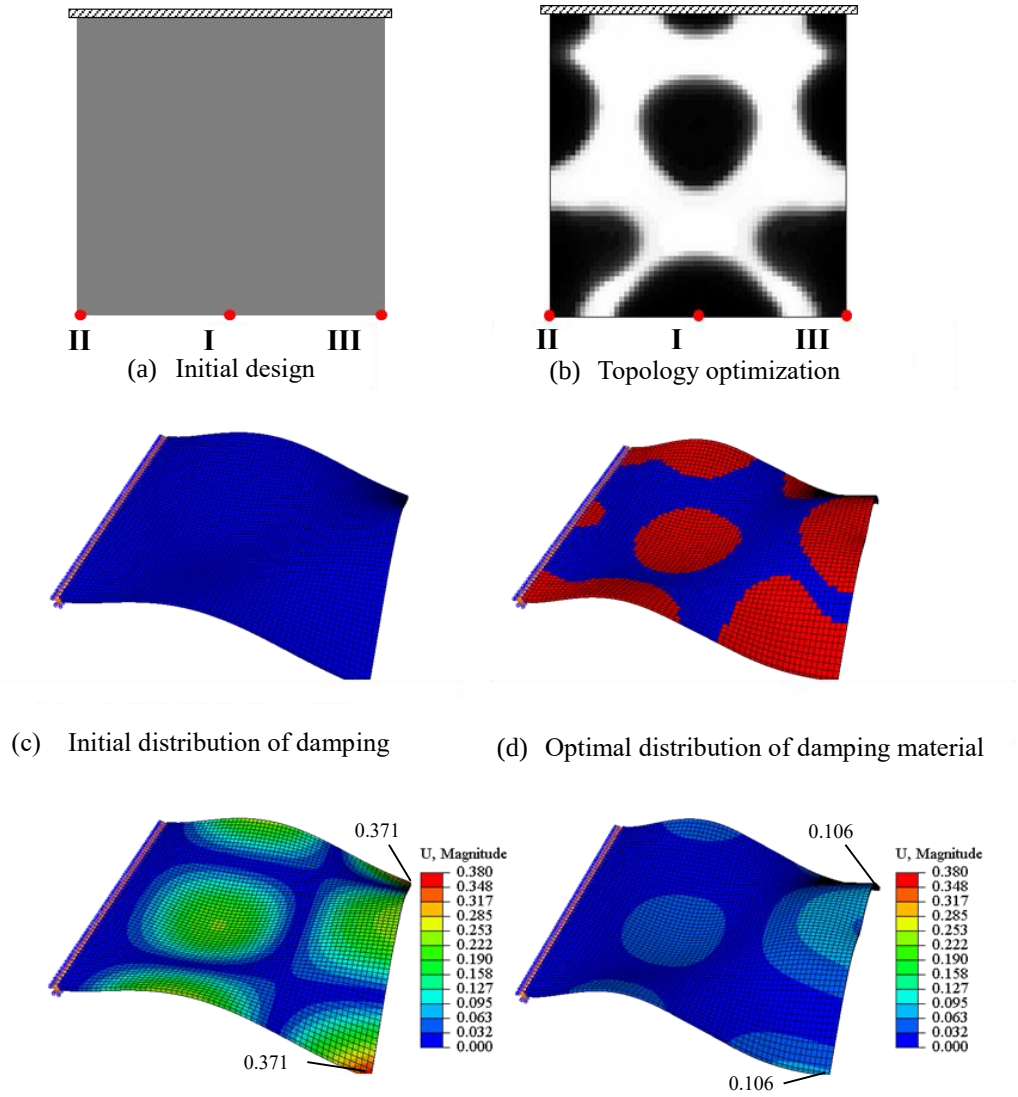

***Fig** 5.4 Comparison of initial design (a,c,e) and final topology optimization result (b,d,f). a,b Distribution of damping materal; c,d Deformed shape; e,f Deformation contour*

Fig 5.4(e) and **Fig** 5.4(f) are the vibration amplitudes comparisons between the initial design and optimal design. Since the model is a symmetrical plate with a point force at the middle of the edge, the displacements at point II and point III are exactly the same. It is also seen that not only the vibration amplitudes at the concerned positions, but also the overall vibration level of the constrained damping layer plate has been significantly reduced.

In order to investigate the effect of damping coefficients on reducing the vibration amplitude, the topology optimization cases with the damping coefficients $\alpha_0^d = 0$ and $\beta_0^d = 0$ are also be investigated. Both damping coefficients set to be 0 means the attached damping layer only contributes to the mass and the stiffness of the structure. Starting from the initial design $\rho_e = 0.5$ $(e = 1,2,\dots,3600)$, the optimization process converged to a final design as given in **Fig** 5.5(b).

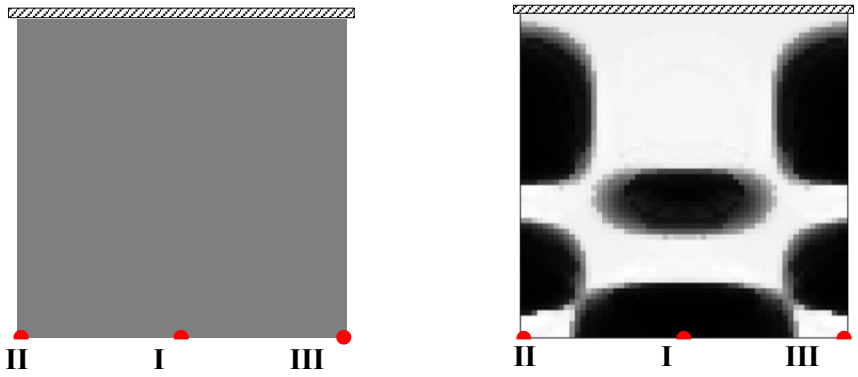

(a) Initial design (b) Topology optimization design

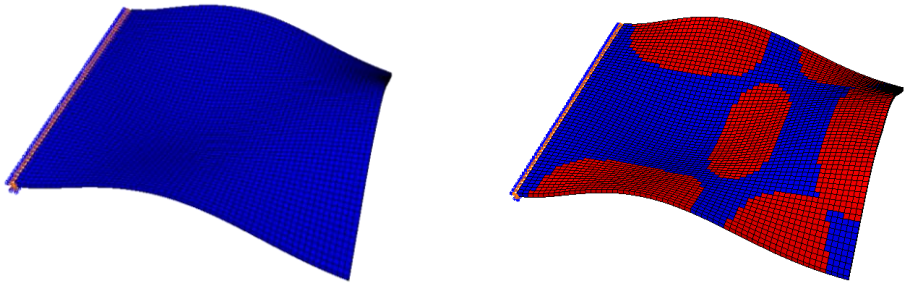

(c) Initial distribution of damping material (d) Optimal distribution of damping material

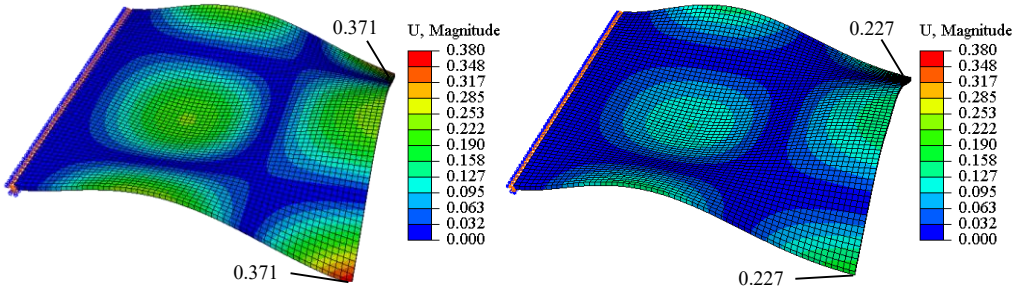

(e) Vibration amplitude of initial design (f) Vibration amplitude of optimal design

Fig *5.5 Initial design (a,c,e) and final topololgy optimization result (b,d,f) without damping effect. a,b Distribution of damping materal; c,d Deformed shape; e,f Deformation contour*

Although similar to last case, a different optimal layout of the attached damping layer is obtained without considering the damping effect. Similarly, the displacements at point II and point III are exactly the same. One conclusion drawn from the comparison is that the optimization case considering damping effect is much better than the one without considering the damping effect. This can be seen from that the maximal vibration amplitude of the optimized structure shown in **Fig** 5.5(f) which is much higher than that is shown in **Fig** 5.4(f). This result implies that the damping effect of the attached damping layer plays a significant role in optimal layout for vibration suppression. Based on this conclusion, the investigation of the damping effect on the optimal layout is performed.

All parameters of this case is kept the same but three more different values of the stiffness damping coefficients β_0^d =0.1, 0.5, 0.8 are considered. Based on the conclusion obtained from Chapter 4 that the effect of the stiffness damping coeifficent on the optimal topology is more remarkable than that of the mass damping coeifficent, thus only the effect of stiffness damping is investigated here. All optimal layouts with different damping coefficients from 0.0 to 1.0 are

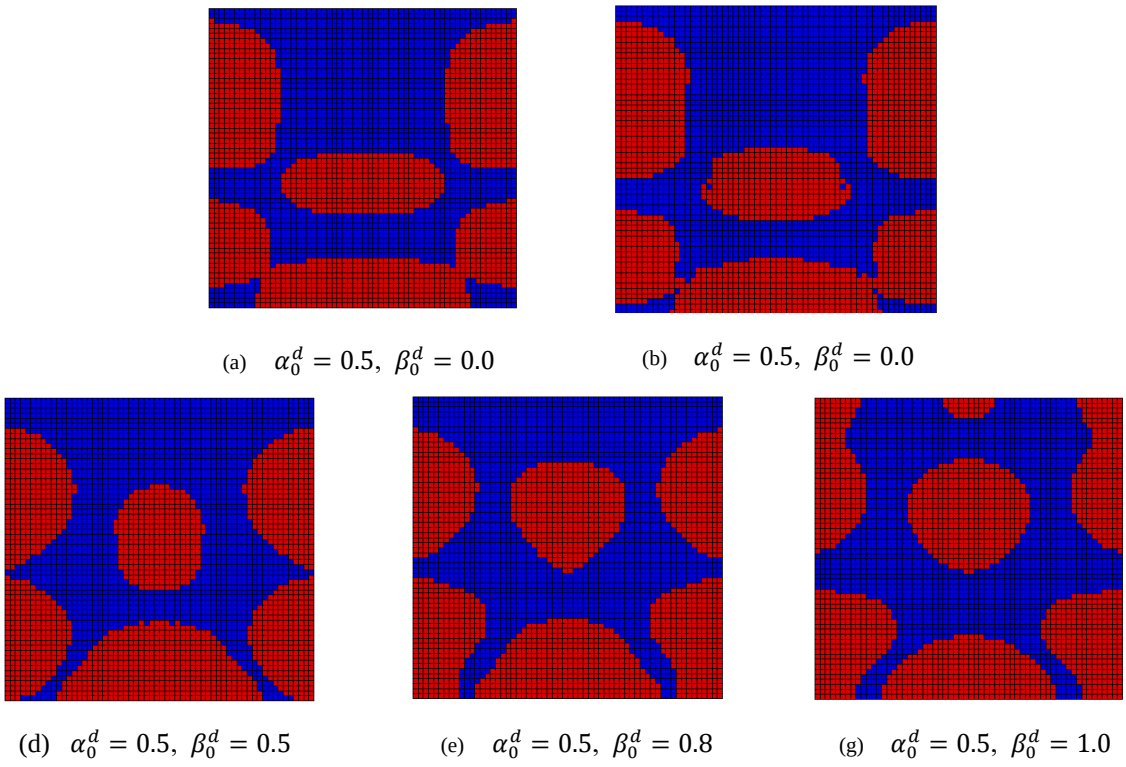

***Fig** 5.6 Optimal results under excitation frequency f_p=30Hz with different damping coefficients*

shown in **Fig** 5.6 We can see that the optimal distribution with $\beta_0^d = 0.1$ (**Fig** 5.6 (b)) is almost the same as the case with $\beta_0^d = 0.0$ (**Fig** 5.6 (a)) and objective values of these two cases are nearly the same at 30Hz in **Fig** 5.7. The reason is mainly because stiffness damping coefficient is not larger enough to reflect the suppression effect on vibration. As the stiffness damping coefficient increases, the optimal layout become different gradually and a remarkable reduction can be seen in **Fig** 5.7. A visible tendency is that the damping materials move from the free edge to the clamped edge. For example, the centre part of damping material in **Fig** 5.6 move from the place close to the free edge to the place with larger vibaration amplitude close to the clamped edge. An explanation for the significant reduction as the stiffness damping coefficient increases is that damping materials tend to distribute on the place with larger amplitude to increase energy comsumed by damping material. In addition, the damping materials attached on the base plate also change the dynamic characteristic of the whole structure which move the resonant peak away from the optimizaiton frequency.

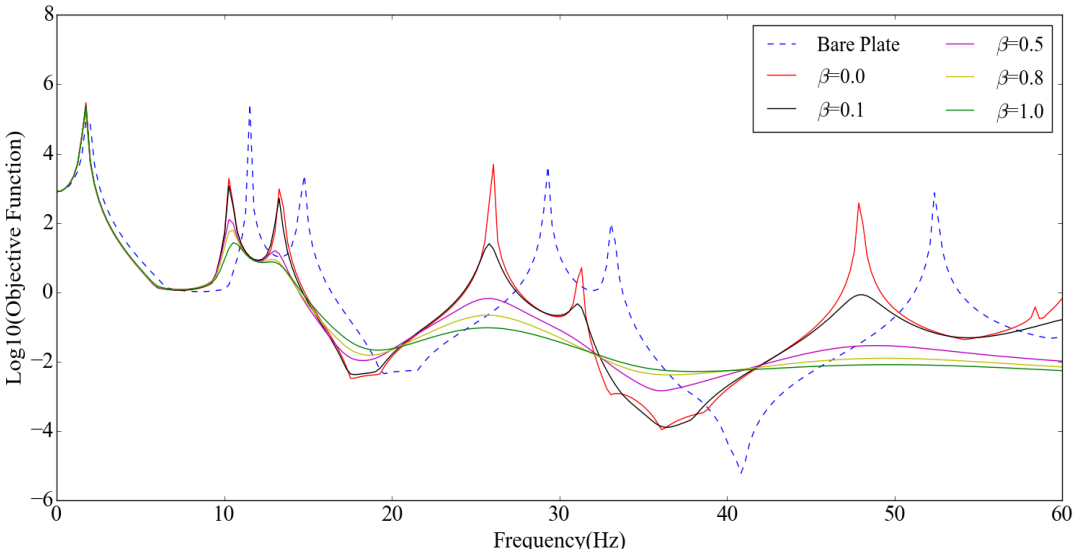

Fig 5.7 *Optimal objective values with different stiffness damping coefficient at range of 0Hz to 60Hz*

Another evidence can also be observed in **Fig** 5.7 as well. The red line in **Fig** 5.7 is the optimal layout with $\beta_0^d = 0.0$, which means no damping effect is considered in the case. But a remarkable reduction can be seen compared to the bare plate (blue dash line) at 30Hz. The reason to explain this reduction is the optimal distribution of damping layer change the natural frequency of original structure which benefit the effect of vibration suppression. The same reason has been discussed in Chapter 3.

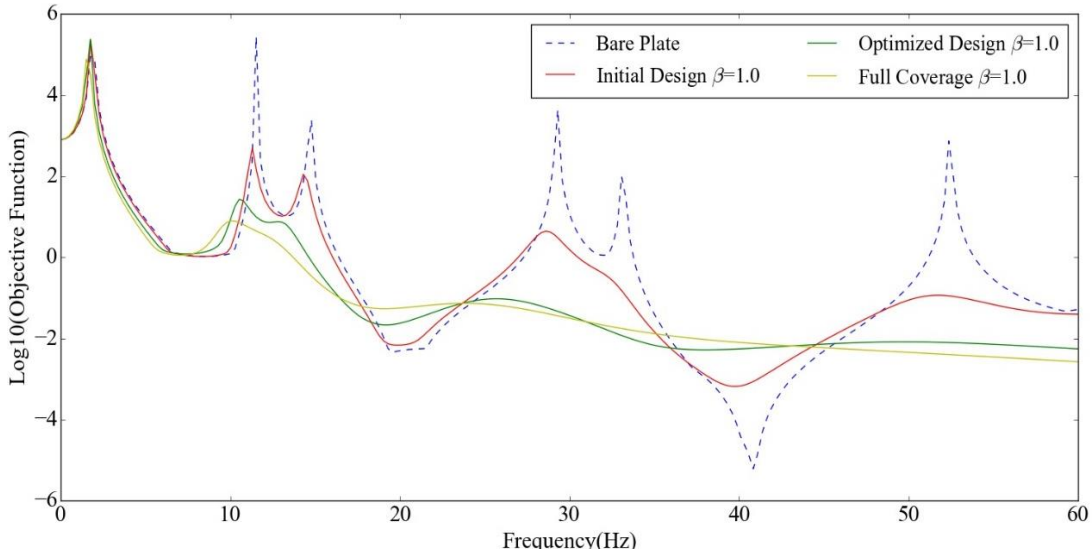

Fig *5.8 optimal objective values with Initial design, Optimized design and Full coverage design at range of 0Hz to 60Hz*

Fig 5.8 compares the initial, optimized and full coverage design when stiffness coefficient $\beta_0^d =$ 1.0. A remarkable reduction between initial design and optimized design can be seen and the

optimized design with only 50% volume of damping material has similar effect of vibration suppression with the design fully covered. The results illustrate significance of the damping material distribution optimization in vibration suppression, minimizing structure weight and saving materials.

The effect of elastic modulus of damping mateirals is investigated subsequently. The damping coefficients are chosen as $\alpha_0^d = 0$, $\beta_0^d = 0$. Four different elastic modulus values of damping mateirals: $E^d = 10\%E^b$, $E^d = 30\%E^b$, $E^d = 100\%E^b$ and $E^d = 200\%E^b$ are considered, see **Fig 5.9**. It can be observed that the optimal layouts in **Fig** 5.9(a), **Fig** 5.9(b) and **Fig** 5.9(c) are almost the same. The optimal objective values of these three cases are also very close at 30Hz in **Fig 5.10** even though the elastic modulus of the case in **Fig 5.9** (c) is 100 times larger than the case in **Fig** 5.9 (a). An explaination is that the elastic modulus of the case in **Fig 5.9** (c) is still too small compared to base plate to change the eigenfrequency effectively. When the elastic modulus of damping layer increases to the same level as the base plate (yellow line in **Fig** 5.10), a better optimized result can been obtained.

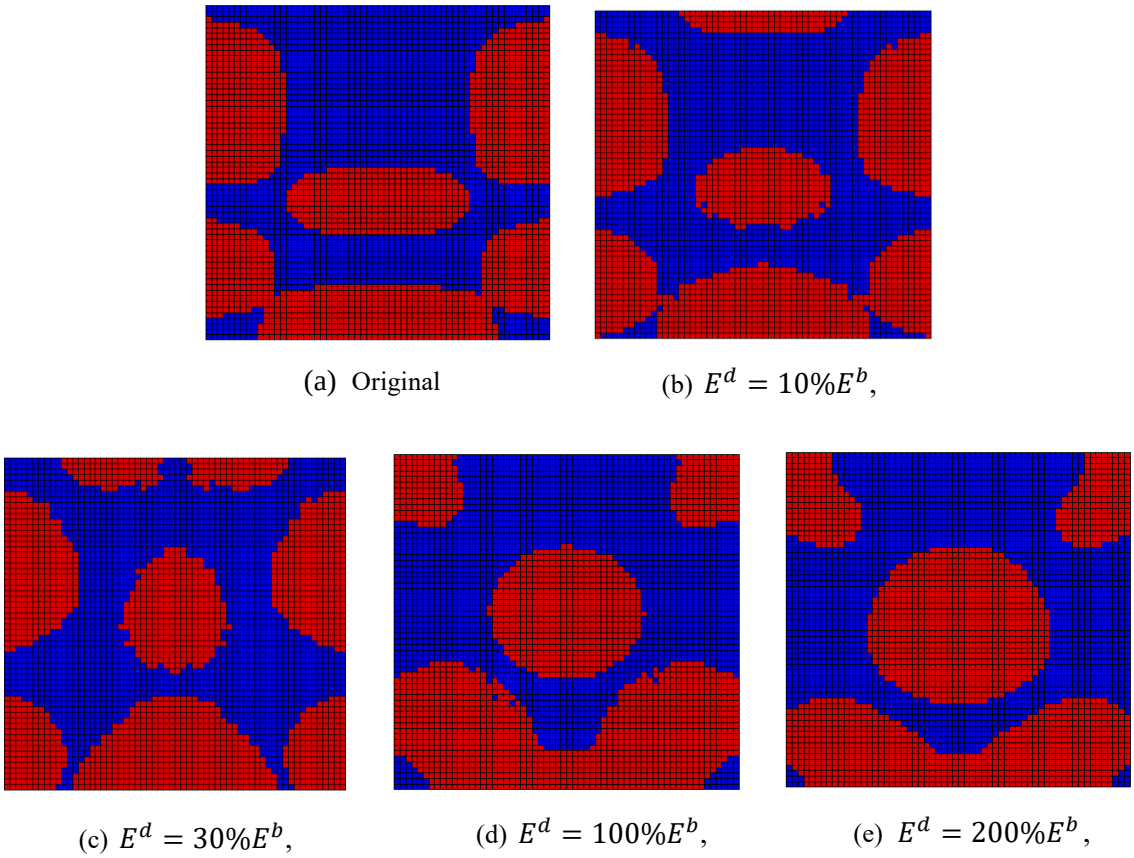

(a) Original (b) $E^d = 10\%E^b$, (c) $E^d = 30\%E^b$, (d) $E^d = 100\%E^b$, (e) $E^d = 200\%E^b$,

Fig 5.9 *Optimal damping layout under excitation frequency fp=30Hz with different elastic modulus (* $\alpha_0^d = 0$, $\beta_0^d = 0$ *)*

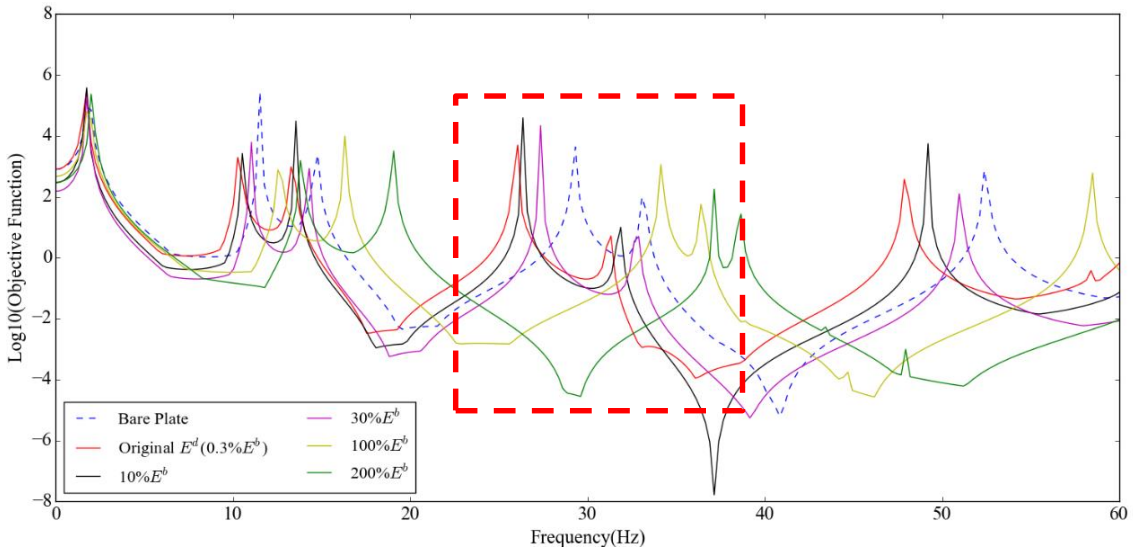

Fig 5.10 *Optimal objective values with different elastic modulus ($\alpha_0^d = 0.0$, $\beta_0^d = 0.0$)*

Further, when the elastic modulus of damping layer increases to 200% of elastic modulus of the base plate, a better topology layout has been achieved. We could see a large gap with the excitation frequency rested at the concave of the green line in **Fig 5.10**. The significant reduction of the objective value is because a stiff layer with larger elastic modulus has a greater impact on dynamic characteristic of the whole struture which leads to a shift of natural frequency to avoid optimized frequency. The same essence has been shown in bi-material plate case in Chapter 4. However, for some applications, the dynmaic characteristic of the structure ususlly require to keep unchanged. Thus, attaching a stiff layer is not a suitable solution for these cases. And what's more, as shown in **Fig** 5.7, reducing vibration by increasing damping coefficent has a remarkable suppression effect on overall vibration level compared to origial desin. Thus, enhancing damping effect of the damping material is a better way to suppress vibration for free damping layer case.

5.4.4 Topology optimization of FLD square plate

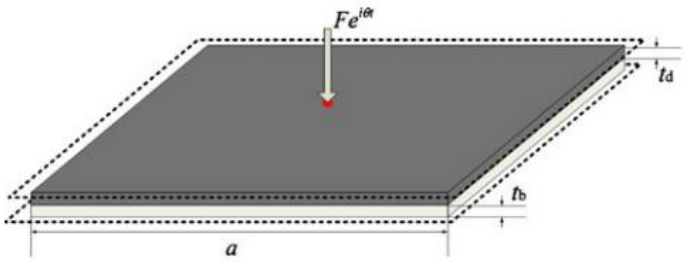

Fig 5.11 *A simply supported square plate (a=3, t_d=t_b=0.02m) with a time-harmonic load applied at centre*

In this example, topology optimization of a square plate under different excitation frequencies

and different damping coefficients are considered. The geometry of the plate, the elastic properties and mass densities of the damping and base materials are as the same as the previous example. All the edges are simply supported and a time-harmonic load $\boldsymbol{f}(t) = \boldsymbol{F}e^{i\omega t}$, with the amplitude $\boldsymbol{F} = 10^5 N$ is applied to the centre of the structure, as shown in **Fig 5.11**.

The different boundaries between the simply supported square plate and the cantilever plate lead to a different strategy to define objective function. In cantilever plate case, the displacement at the free edge is always dominant steady-state responses of the whole structure. So the sum of the amplitudes of the loading point and two endpoints on the free edge is chosen as objective in last case. However, it's a different case for simply supported plate. As the excitation frequency increases, the modes of structure become complex and the amplitude of the loading point is probably not the largest one of the whole structure. Therefore, it's not enough to achieve a good topology layout by just taking the amplitude of the loading point as the objective. So, the design objective chosen here is the sum of the vibration amplitudes of all nodes on plate. In what follows, the impacts of the excitation frequencies and the damping coefficients on the optimal layout of the damping layer will be explored.

5.4.5 Results and discussions for simply supported square plate case

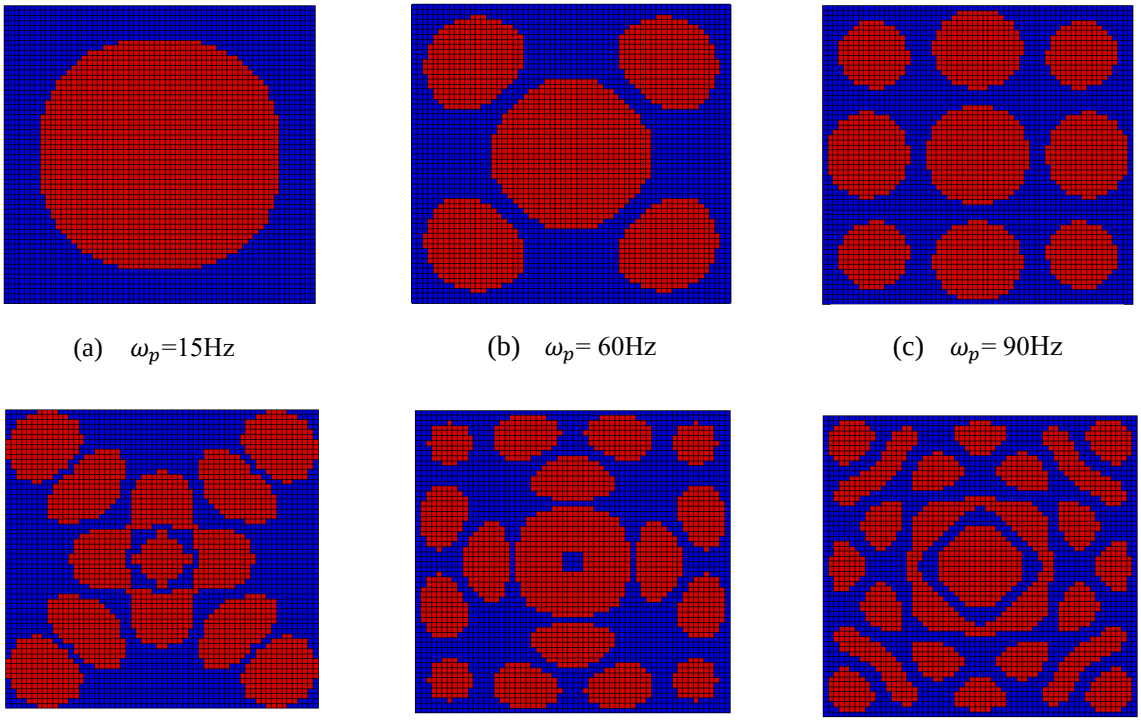

(a) ω_p=15Hz (b) ω_p= 60Hz (c) ω_p= 90Hz

(d) ω_p= 150Hz (e) ω_p= 200Hz (f) ω_p= 300Hz

Fig 5.12 *(a)-(f) Optimization results with different values of prescribed loading frequencies and small damping coefficients*

We first considered 6 different excitation frequencies, ω_p = 15, 60, 90, 150, 200 and 300 Hz. The damping coefficients of the damping material are given as $\alpha_0^d = 0.5$ and $\beta_0^d = 0.001$. The optimal distributions obtained under each loading frequency are shown in **Fig 5.12**. It is obvious that, as the loading frequency ω_p increases, the optimal layouts of the damping material become spatially more complex. This is natural since a higher loading frequency will excite higher order of eigenmodes, which typically have more localized features.

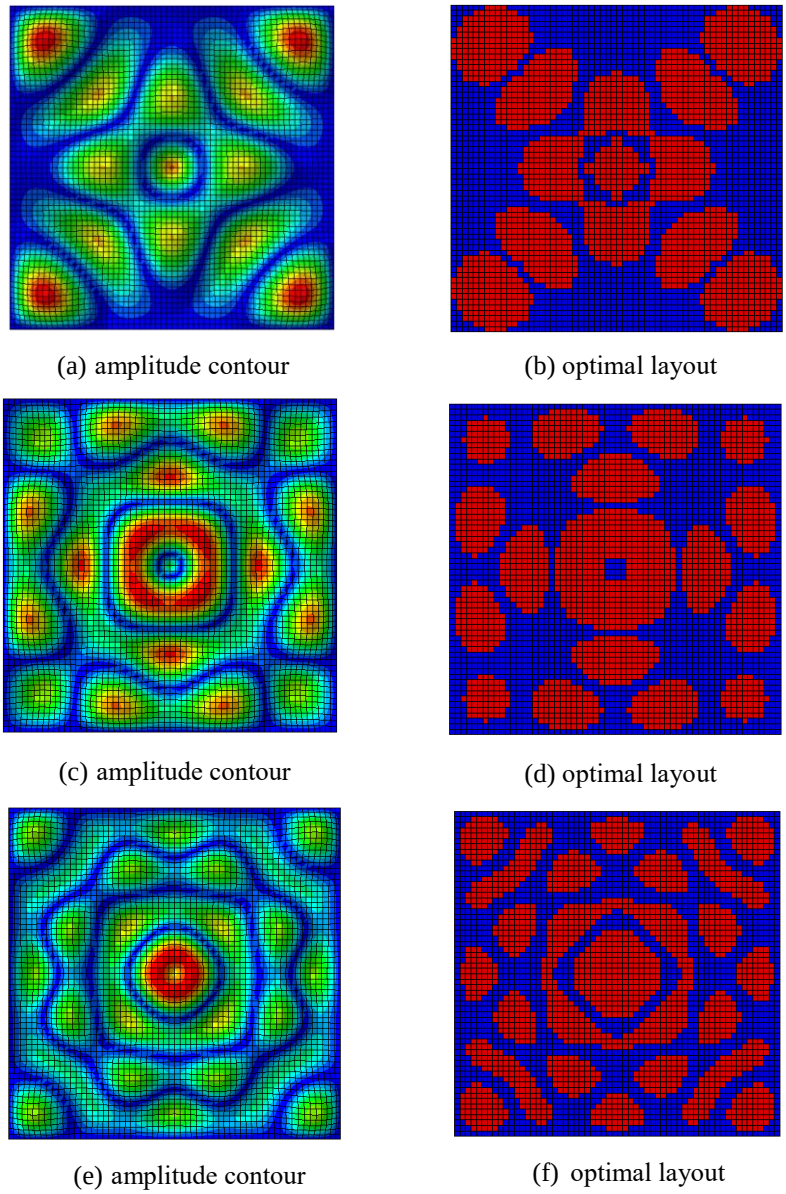

(a) amplitude contour (b) optimal layout

(c) amplitude contour (d) optimal layout

(e) amplitude contour (f) optimal layout

***Fig** 5.13 Comparison between the amplitude contour and according optimal layout under 150Hz, 200Hz and 300Hz*

Comparison between the amplitude contours and corresponding optimal layouts under 150Hz, 200Hz and 300Hz are shown in **Fig** 5.13. An interesting phenomenon can be observed is that the places which covered with damping material in the optimal layout are mostly the place with large amplitude. This phenomenon validates the conclusion achieved in **Section 5.4.4** that the

optimal damping materials are more likely to be distributed in the places with large amplitude which help to take advantage of damping material to dissipate vibration energy.

5.5 Optimization strategy for free layer damping plate

From the conclusion drawn above, a rapid material distribution strategy for obtaining the distribution of damping material is proposed. For the similarity of the optimal layouts and the steady-state amplitude contours, the damping material distribution can be achieved according to the steady-state responses from the initial structure by assigning the element to be solid if its amplitude are larger than a threshold and to be void if its amplitude are smaller than a threshold. The threshold is determined by material volume limit. According to this strategy, the material distributions can be obtained rapidly and the comparison between the optimal layouts and the layouts obtained by new strategy is shown in **Fig 5.14**.

***Table** 5.1 Comparison of the objective values in different cases*

Case	Frequency	Objective Value			
		Bare Plate	Optimal	New Strategy	Full Coverage
1	15Hz	2.7988	1.7014	1.7016	1.6506
2	60Hz	0.5952	0.2472	0.2446	0.2351
3	90 Hz	0.2962	0.1914	0.1923	0.1923
4	150Hz	0.1570	0.1348	0.1482	0.1750
5	200Hz	0.0715	0.0419	0.0429	0.0429
6	300Hz	0.0703	0.0257	0.0290	0.0271

New Strategy * represents the layout obtained by steady-state response of initial structure

As seen in **Table** 5.1, most of the optimization cases have remarkable reduction on the objective values and some of them are even better than full coverage cases which indicates the optimal layouts of damping materials have a better performance of energy dissipation. Besides that, the objective values of the layouts obtained from the steady-state responses of initial structure are very close to optimal objective values which indicates this strategy can be an alternative measure to achieve the optimal material distribution directly from the steady-state analysis of initial structure. In addition, Case 4 indicates another noticeable conclusion that the plate with

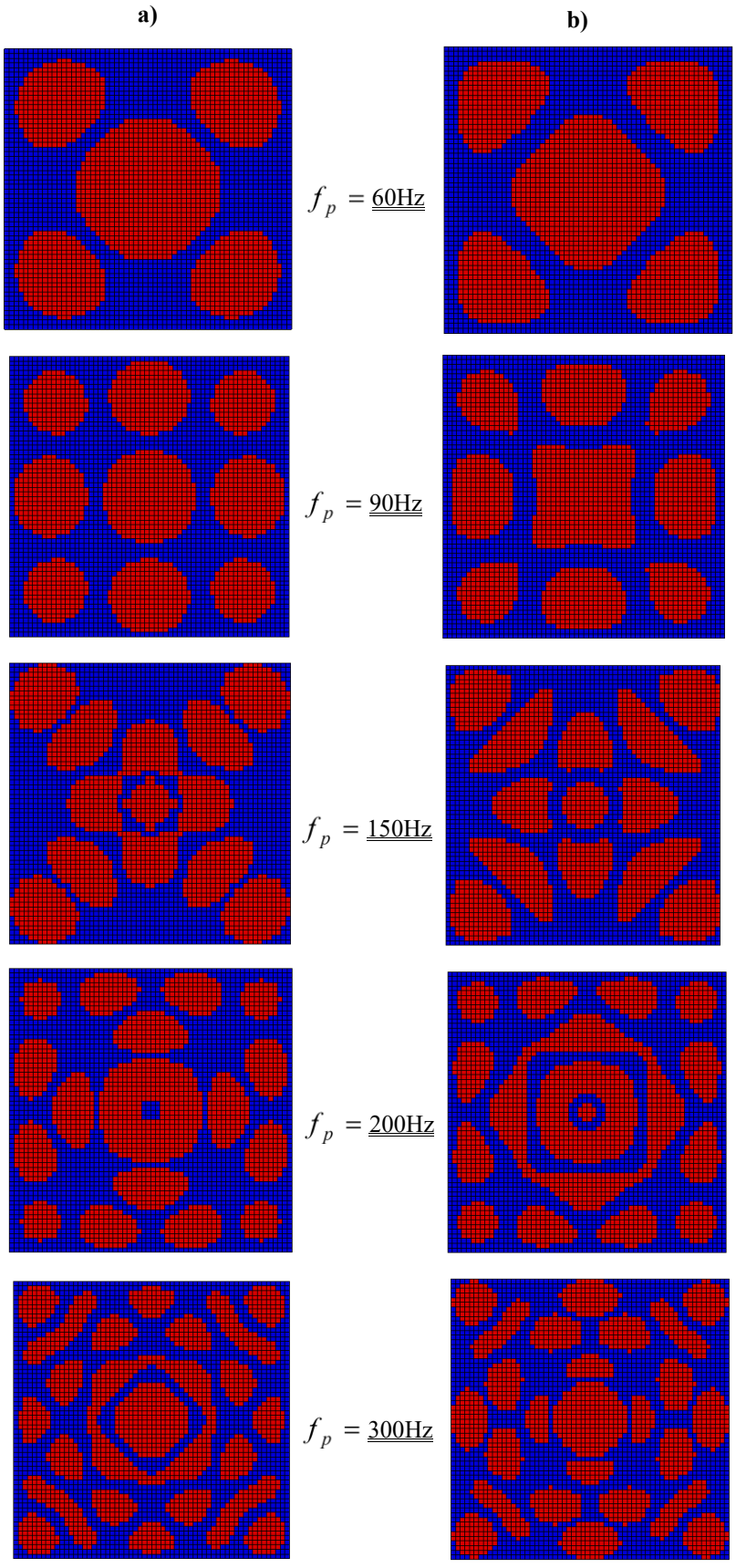

Fig 5.14 *Comparison between the optimal layouts and steady-state response layouts under 60Hz, 90Hz, 150Hz, 200Hz and 300Hz. Series* ***a)*** *represent optimal layouts and Series* ***b)*** *represent steady-state response layouts.*

fully covered damping material may not only cannot suppress vibration but also even strength the vibration behaviour in some cases. The result demonstrates the necessity of damping materials distribution optimization.

Although the new strategy is able to achieve a damping material layout which has similar performance as the optimal layout, there is a prerequisite for implying this strategy. That is the damping layer should have a small effect on the natural frequency of base plate. If the addition of damping layer has a remarkable effect on dynamic characteristics, it probably keeps changing the mode of the structure to completely different shapes during the optimization process. In this situation, the layout obtained from the steady-state response would not work. But if the condition satisfied, we can obtain a feasible layout from its steady-state response which could save a lot of time and computation sources.

5.6 Summary

This chapter investigates topology optimization of damping layers in a vibrating structure under harmonic excitations. An artificial damping material mode with penalization that has a similar form as in the SIMP approach is suggested. Numerical examples are given for illustrating the applicability and efficiency of the present approach. Optimal topologies obtained under different excitation frequencies and damping coefficients are also compared. Similar as many other formulations for optimization of structural dynamic behaviours, the considered topology optimization problem is in nature a highly non-convex one, characterized by multiple local optima. However, numerical experiences in this study confirm that the present approach is usually able to provide meaningful solutions for guiding the layout design of the damping layer at a reasonable computational cost. In addition, a rapid strategy to obtain a feasible damping material layout from the steady-state response analysis has been proposed. Based on the investigation, the following conclusion can be drawn:

- A free damping material layer plate with optimized material distribution could achieve a similar vibration reduction performance as the fully covered plate but with 50% less material volume. The results illustrate significance of the damping material distribution optimization in vibration suppression and minimizing structure;
- Material distribution of damping layer on a base plate has a significant impact on structural dynamic characteristic. A plate with fully covered damping material may not always guarantee a better performance of vibration suppression;
- The objective function should be sensitive to the distribution of damping material to ensure the success of the optimization process;

- The damping material tend to be distributed in the places with large amplitudes which help to dissipate vibration energy by taking advantage of the deformation of damping material.
- If the additional damping layer has only a slight effect on the natural frequency compared to the base plate, a feasible material distribution layout could be obtained from the steady-state responses of initial structure. The performance of the material distribution layout obtained by this strategy is close to the one obtained by topology optimization in some cases.

Compared with the bi-material topology optimization model in Chapter 4, the model proposed in this chapter has greatly improved the feasibility of topology optimization method. As long as there is a very tight contact between damping layer and base layer, free layer damping model is suitable for the vibration reduction design of plate structures. Usually strong adhesive could be used to manufacture the free layer damping plate. A possible application for FLD plate is to reduce car vibration during driving by laying damping materials inside, thus providing a more comfortable driving environment for car users. And at the same time, by using the model proposed in this Chapter, less damping materials are needed thereby reducing the cost to apply this strategy as well. In addition, the model can expand its application scope by building different finite element models.

Chapter 6 Application to passive constrained layer damping plate

From the conclusion obtained in Chapter 5, an additional damping layer on a base plate has a significant impact on vibration characteristic of the whole structure and a proper material distribution of damping layer usually lead to a better performance of vibration suppression. In order to enhance the energy dissipated by the damping material, it's natural to consider adding an extra stiff layer on the top of the damping layer to enlarge the shear deformation of the damping material so that increase vibration energy dissipation. In decades, after the first studies of constrained damping treatments, this area has been regarded as an effective way to suppress structural vibrations and sound radiation. In this Chapter, a topology optimization model has been proposed to obtain the optimal layout of constrained damping material treatments to enhance energy dissipation and suppress structural vibration in an economical and effective way.

6.1 Analytical solutions for passive constrained layer damping plate

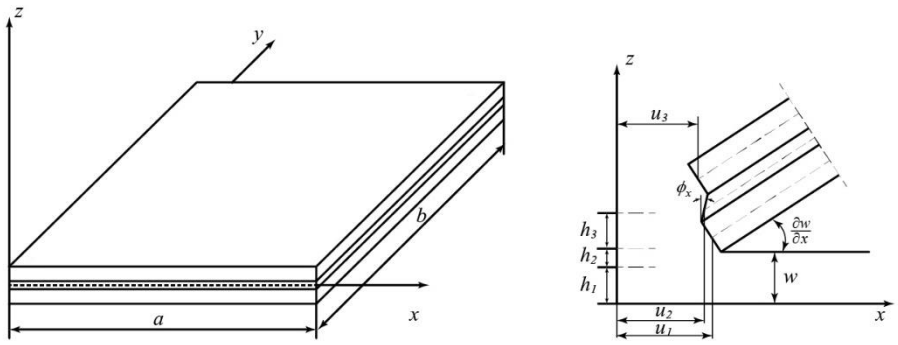

Fig 6.1 *The dimensions and displacements of the sandwich plate*

The three-layered plate under consideration and layer displacements are shown in **Fig 6.1** where h_1, h_2, and h_3 are the thicknesses of the base plate, viscoelastic layer and constrained layer, respectively; a, b are geometrical dimension of three-layered plate; w is the longitudinal displacements in the mid-plane; ϕ_x is the rotation of the normal to the mid-lane of the viscoelastic core layer. ϕ_x given in the **Fig 6.1** are positive. Before deriving the analytical solution for sandwich plate, some assumptions are made:

1) no transverse shear deformation happens in face-layers;

2) no slip between the core and face-layers

3) only consider the transverse inertia effects of the plate

4) the core only carries transverse shear, no in-plane

6.1.1 The relations of displacements

Based on the classical laminate theory, the relations of between the displacements and strains in face layers can be expressed to be as follows:

$$\begin{Bmatrix} \varepsilon_x^{(i)} \\ \varepsilon_y^{(i)} \\ \gamma_{xy}^{(i)} \end{Bmatrix} = \begin{Bmatrix} \partial u_i/\partial x \\ \partial v_i/\partial y \\ \partial u_i/\partial y + \partial v_i/\partial x \end{Bmatrix} = \begin{Bmatrix} \partial u_{0i}/\partial x \\ \partial v_{0i}/\partial y \\ \partial u_{0i}/\partial y + \partial v_{0i}/\partial x \end{Bmatrix} - z \begin{Bmatrix} \partial^2 w/\partial x^2 \\ \partial^2 w/\partial y^2 \\ 2\partial^2 w/\partial x \partial y \end{Bmatrix} \quad i = 1,3 \qquad (6.1)$$

Where $\varepsilon_x, \varepsilon_y$ and γ_{xy} are the strain components in three directions. u, v are the displacement in x- and y- direction. w is the longitudinal displacements in the mid-plane. And $i = 1$ stands for base layer and $i = 3$ for cover layer. The shear strains $\gamma_{xz}^{(2)}$ and $\gamma_{yz}^{(2)}$ of viscoelastic core layer as follow:

$$\begin{aligned} \gamma_{xz}^{(2)} &= \phi_x + \frac{\partial w}{\partial x} \\ \gamma_{yz}^{(2)} &= \phi_y + \frac{\partial w}{\partial y} \end{aligned} \qquad (6.2)$$

Where ϕ_x and ϕ_y are the rotations along y- and x-axis. As shown in **Fig 6.1**, The continuity of displacements at the interfaces between the core and the face layers requires that the following relations hold:

$$\begin{aligned} u_1 - \frac{h_1}{2}\frac{\partial w}{\partial x} &= u_2 - \frac{h_2}{2}\phi_x \\ u_3 + \frac{h_3}{2}\frac{\partial w}{\partial x} &= u_2 + \frac{h_2}{2}\phi_x \end{aligned} \qquad (6.3)$$

Where h_1, h_2, and h_3 are the thicknesses of the base plate, viscoelastic layer and constrained layer, respectively. similar equations are true in the y direction and **Eq.(6.3)** are used, then :

$$\begin{aligned} \gamma_{xz}^{(2)} &= (u_3 - u_1 + h\frac{\partial w}{\partial x})/h_2 \\ \gamma_{yz}^{(2)} &= (v_3 - v_1 + h\frac{\partial w}{\partial y})/h_2 \end{aligned} \qquad (6.4)$$

where $h = \frac{(h_1+2h_2+h_3)}{2}$

6.1.2 The governing equations of free vibration

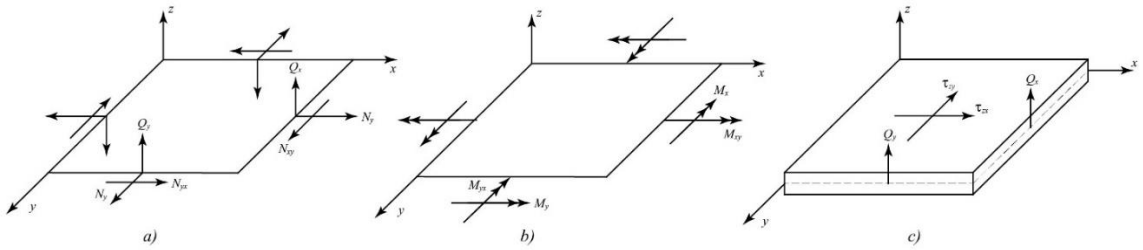

Fig 6.2 *a) and b) Free body diagram of the constrained layer and base layer; c) Free body diagram of viscoelastic layer*

Fig 6.2 shows the positive direction of the axial forces, moments and shear forces for each layer. The axial forces and moments of the constrained layer and base layer can be represented as follow:

$$\begin{bmatrix} N_x^{(i)} \\ N_y^{(i)} \\ N_{xy}^{(i)} \end{bmatrix} = \frac{E_i h_i}{1-\mu_i} \begin{bmatrix} 1 & \mu_i & 0 \\ \mu_i & 1 & 0 \\ 0 & 0 & \frac{1-\mu_i}{2} \end{bmatrix} \begin{bmatrix} \partial u_{0i}/\partial x \\ \partial v_{0i}/\partial y \\ \partial u_{0i}/\partial y + \partial v_{0i}/\partial x \end{bmatrix}$$
$$\begin{bmatrix} M_x^{(i)} \\ M_y^{(i)} \\ M_{xy}^{(i)} \end{bmatrix} = \frac{E_i h_i^3}{12\left(1-\mu_i^{\,2}\right)} \begin{bmatrix} 1 & \mu_i & 0 \\ \mu_i & 1 & 0 \\ 0 & 0 & \frac{1-\mu_i}{2} \end{bmatrix} \begin{bmatrix} \partial^2 w/\partial x^2 \\ \partial^2 w/\partial y^2 \\ 2\partial^2 w/\partial x \partial y \end{bmatrix} \tag{6.5}$$

Where N_x , N_y , N_{xy} are the axis forces and M_x , M_y , M_{xy} are the moments. μ is Poissons' ratio and E is Young's modulus. u, v are the displacement in x- and y- direction. w is the longitudinal displacements in the mid-plane. For the viscoelastic core layer, which carries only shear stress, the constitutive equations are

$$\tau_{xz} = G_2^* \gamma_{xz}, \tau_{yz} = G_2^* \gamma_{yz} \tag{6.6}$$

Where G_2^* is a complex shear modulus, $G_2^* = G_2(1 + i\eta_v)$, G_2 is the real shear modulus and η_v is material loss factor in this expression. For the base layer, the force equilibrium in x, y and z directions yields

$$\begin{aligned} \frac{\partial N_x^{(1)}}{\partial x} + \frac{\partial N_{yx}^{(1)}}{\partial y} + \tau_{zx}^{(2)} &= 0 \\ \frac{\partial N_{xy}^{(1)}}{\partial x} + \frac{\partial N_y^{(1)}}{\partial y} + \tau_{zy}^{(2)} &= 0 \\ \frac{\partial Q_x^{(1)}}{\partial x} + \frac{\partial Q_y^{(1)}}{\partial y} &= \rho_1 h_1 \frac{\partial^2 w}{\partial t^2} \end{aligned} \tag{6.7}$$

Based on the moment equilibrium, the following equations hold

$$\begin{aligned}\frac{\partial M_x^{(1)}}{\partial x}+\frac{\partial M_{xy}^{(1)}}{\partial y}-Q_x^{(1)}-\frac{h_1}{2}\tau_{zx}^{(2)}=0\\ \frac{\partial M_{xy}^{(1)}}{\partial x}+\frac{\partial M_y^{(1)}}{\partial y}-Q_y^{(1)}-\frac{h_1}{2}\tau_{zy}^{(2)}=0\end{aligned} \tag{6.8}$$

Substitute the **Eq.(6.7)** into **Eq.(6.8)** to eliminate $Q_x^{(1)}$ and $Q_y^{(1)}$ to obtain

$$\frac{\partial^2 M_x^{(1)}}{\partial x^2}+\frac{\partial^2 M_y^{(1)}}{\partial y^2}-2\frac{\partial^2 M_{xy}^{(1)}}{\partial x\partial y}-\frac{h_1}{2}\left(\frac{\partial \tau_{xz}^{(2)}}{\partial x}+\frac{\partial \tau_{yz}^{(2)}}{\partial y}\right)=\rho_1 h_1\frac{\partial^2 w}{\partial t^2} \tag{6.9}$$

For the constrained layer, similar to the base layer, only the directions of are opposite. The following equations are obtained following the same rules.

$$\begin{aligned}&\frac{\partial N_x^{(3)}}{\partial x}+\frac{\partial N_{yx}^{(3)}}{\partial y}-\tau_{zx}^{(2)}=0,\\ &\frac{\partial N_{xy}^{(3)}}{\partial x}+\frac{\partial N_y^{(3)}}{\partial y}-\tau_{zy}^{(2)}=0,\\ &\frac{\partial^2 M_x^{(3)}}{\partial x^2}+\frac{\partial^2 M_y^{(3)}}{\partial y^2}-2\frac{\partial^2 M_{xy}^{(3)}}{\partial x\partial y}-\frac{h_3}{2}\left(\frac{\partial \tau_{xz}^{(2)}}{\partial x}+\frac{\partial \tau_{yz}^{(2)}}{\partial y}\right)=\rho_3 h_3\frac{\partial^2 w}{\partial t^2}\end{aligned} \tag{6.10}$$

Applied the same to the z direction of viscoelastic layer results in:

$$\frac{\partial Q_x^{(2)}}{\partial x}+\frac{\partial Q_y^{(2)}}{\partial y}+\rho_2 h_2\frac{\partial^2 w}{\partial t^2}=0 \tag{6.11}$$

Where $Q_x^{(2)}=h_2\tau_{xz}^{(2)}$ and $Q_y^{(2)}=h_2\tau_{yz}^{(2)}$. According to the principle of virtual work, in which **Eq.** (6.8)-**Eq.** (6.11) are used, the governing equations of motion for sandwich plate with constrained damping layer are as follows:

$$\begin{aligned}&\frac{\partial N_x^{(1)}}{\partial x}+\frac{\partial N_{yx}^{(1)}}{\partial y}+\tau_{zx}^{(2)}=0,\frac{\partial N_{xy}^{(1)}}{\partial x}+\frac{\partial N_y^{(1)}}{\partial y}+\tau_{zy}^{(2)}=0,\\ &\frac{\partial N_x^{(3)}}{\partial x}+\frac{\partial N_{yx}^{(3)}}{\partial y}-\tau_{zx}^{(2)}=0,\frac{\partial N_{xy}^{(3)}}{\partial x}+\frac{\partial N_y^{(3)}}{\partial y}-\tau_{zy}^{(2)}=0,\\ &\frac{\partial^2 M_x^{(1)}}{\partial x^2}+\frac{\partial^2 M_y^{(1)}}{\partial y^2}+\frac{\partial^2 M_x^{(3)}}{\partial x^2}+\frac{\partial^2 M_y^{(3)}}{\partial y^2}+2\left(\frac{\partial^2 M_{xy}^{(1)}}{\partial x\partial y}+\frac{\partial^2 M_{xy}^{(3)}}{\partial x\partial y}\right)-h\left(\frac{\partial \tau_{xz}^{(2)}}{\partial x}+\frac{\partial \tau_{yz}^{(2)}}{\partial y}\right)=\rho\frac{\partial^2 \mathrm{w}}{\partial t^2}\end{aligned} \tag{6.12}$$

where$\rho=\rho_1 h_1+\rho_2 h_2+\rho_3 h_3$, these five equations include four in-plane equilibrium equations, two for shell and two for constrained layer and on transverse dynamic equation. Then substitute **Eq.** (6.5) into **Eq.** (6.12) to represent the results by displacements (101)

6.1.3 Analytical solution for free vibration

Simply supported boundary conditions are adopted in this thesis, which are

i. at $x = 0, a$: $v_1 = v_3 = 0,\ w = 0$

ii. at $y = 0, b$: $u_1 = u_3 = 0,\ w = 0$

For these boundary conditions the displacements and electric potential have the forms:

$$\begin{aligned} u_i(x,y,t) &= U_i \cos\frac{m\pi x}{a}\sin\frac{n\pi y}{b}e^{i\omega^* t} \\ v_i(x,y,t) &= V_i \sin\frac{m\pi x}{a}\cos\frac{n\pi y}{b}e^{i\omega^* t} \qquad i = 1,3 \\ w(x,y,t) &= W \sin\frac{m\pi x}{a}\sin\frac{n\pi y}{b}e^{i\omega^* t} \end{aligned} \tag{6.13}$$

where ω^* is complex frequency, $(\omega^*)^2 = \omega^2(1 + \eta_v i)$ where η_v is the loss factor of structure. U_1, V_1, U_3, V_3, W are the coefficients of the natural mode shapes. Substituting **Eq**. (6.13) into **Eq**. (6.12) and rewrite the equations in matrix form as follow

$$\boldsymbol{M\ddot{X}} + \boldsymbol{KX} = 0 \tag{6.14}$$

where $\boldsymbol{X} = \{u_1, v_1, u_3, v_3, w\}^T$, $\boldsymbol{M}$ is the mass matrix and $\boldsymbol{K}$ is the matrix differential operator of stiffness. The substitution of solutions into **Eq.** (6.14) results in an eigenvalue problem, from which the eigenfrequencies and the vectors of eigenfunctions can be found. Rao D.K. [120] proposed the formulate to calculate circular frequency and loss factor of the plate from the complex eigenfrequencies for a given mode of vibration

$$\omega = \sqrt{Re((\omega^*)^2)},\ \eta_v = Im((\omega^*)^2)/Re((\omega^*)^2) \tag{6.15}$$

In order to validate the equation derived as well as numerical procedures used in the paper, the natural frequencies and modal loss factors have been calculated for plates analysed in Johnson C.D.[121]. The plate is an isotropic symmetric plate with constrained damping layer a=0.3048 m, b= 0.348 m, h_1=h_3=0.762 mm, h_2=0.254 mm, and v_1=v_3=0.3, E_1=E_3=6.89×10^{10} N/m^2 ρ_1=ρ_3=2.74×10^3 kg/m^3, ρ_2=0.999×10^3 kg/m^3, η_v=0.5, G_2=0.896×10^6 N/m^2.

***Table** 6.1 The natural frequencies and modal loss factors of a plate with PCLD*

Mode m , n	Analytical solution[3]		NASTRAN/MSE[3]		Present solution	
	Frequency (Hz)	Loss factor	Frequency (Hz)	Loss factor	Frequency (Hz)	Loss factor
1 , 1	60.3	0.190	57.4	0.176	60.2	0.190
1 , 2	115.4	0.203	113.2	0.188	115.2	0.203
2 , 1	130.6	0.199	129.3	0.188	130.4	0.199
2 , 2	178.7	0.181	179.3	0.153	178.5	0.181
1 , 3	195.7	0.174	196.0	0.153	195.4	0.174

The predicted modal frequencies and the corresponding modal loss factors are tabulated against the exact solution in **Table** 6.1. A very well agreement with the closed form analytical solution can be found in the table above.

6.1.4 Analytical solution of forced vibration

To solve the equation of the forced vibration, the mode superposition method is often used. For the continued plate structure, there are infinite number of natural frequencies and associated vibration modes. We express the dynamic deflections of the plate separable in space and time and in terms of all vibration modes:

$$\begin{aligned} u_i(x,y,t) &= \sum_{m,n=1}^{\infty} U_{mn}^{(i)} \cos\frac{m\pi x}{a}\sin\frac{n\pi y}{b}e^{i\omega t} \\ v_i(x,y,t) &= \sum_{m,n=1}^{\infty} V_{mn}^{(i)} \sin\frac{m\pi x}{a}\cos\frac{n\pi y}{b}e^{i\omega t} \quad i = 1,3 \\ w(x,y,t) &= \sum_{m,n=1}^{\infty} W_{mn} \sin\frac{m\pi x}{a}\sin\frac{n\pi y}{b}e^{i\omega t} \end{aligned} \tag{6.16}$$

Where $U_{mn}^{(i)}$, $V_{mn}^{(i)}$, W_{mn} are the unknown (m,n) order normal coordinates to be determin ed. Assume load $f(x,y)^{i\omega t}$ applied at the centre of the plate in z direction. Then the ge neralized force can be obtained as follow:

$$P_{mn}(t) = \int_0^a \int_0^b W_{mn} \sin\frac{m\pi x}{a}\sin\frac{n\pi y}{b} p(x,y)e^{i\omega t}dxdy \tag{6.17}$$

Then the force vector $\boldsymbol{F} = \{0,0,0,0,P_{mn}(t)\}^T$ is applied at the right side of the **Eq**. (6.14). The maximum amplitude of steady state response can be solved after the normal natural modes and according normal coordinates are obtained.

$$w(x,y,t) = \sum_{m,n=1}^{\infty} W_{mn} \sin\frac{m\pi x}{a}\sin\frac{n\pi y}{b}e^{i\omega t} \tag{6.18}$$

A same example as in section 6.1.3 is taken here to validate the performance of the constrained damping layer model. A unit transverse harmonic point load of 1N at the centre of the plate. **Fig** 6.3 shows the transverse frequency response function, calculated from **Eq. (6.18)** by using $m = 1\sim10$ and $n = 1\sim10$ of the loading point.

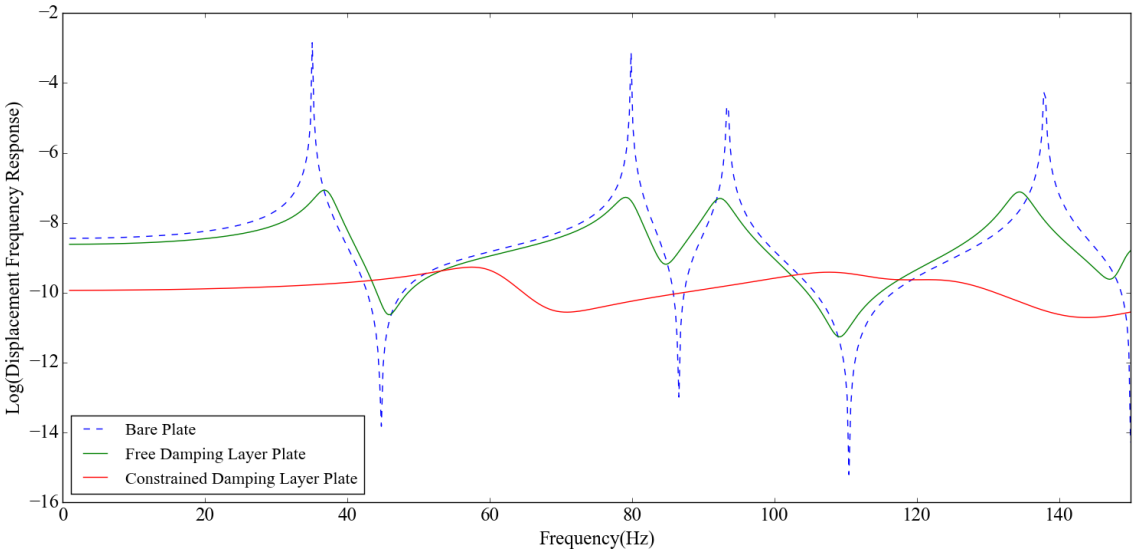

***Fig** 6.3 Displacement frequency response of base plate, free damping layer plate and constrained damping layer plate*

As seen in **Fig** 6.3, dash blue curve and green curve represents the frequency response of the bare plate and free damping layer plate respectively which obtained from the finite element method represented in Chapter 3 and Chapter 4. The red curve represents the constrained damping layer plate. As expected, significant damping effects appeared in the constrained damping layer plate case. The answer can be found in **Eq**. (6.4). For the vibration energy dissipation is mostly due to the shear deformation of the viscoelastic core, the difference of in-plane displacements between the constrained damping layer and base layer in **Eq**. (6.4) contributes to the extra shear strain which lead to more energy dissipation. In addition, the constrained layer also makes the whole model stiffer which help to reduce the vibration amplitude.

For the free damping layer plate, an obvious reduction of the displacement amplitude can also be seen in **Fig** 6.3. That is because the additional damping materials are attached to the bare plate which has been explained in Chapter 5. It is also seen that as the shear modulus of viscoelastic material is quite small compared to the elastic modulus of the bare plate, the peaks of the frequency responses of the free damping layer plate is very close to that of the bare plate. However, in constrained damping layer model case, as the presence of the constrained layer, frequency shift phenomenon occurred. Overall, one conclusion can be drawn that the plate model with constrained damping layer has a better performance of vibration reduction than the bare plate and the free damping layer model.

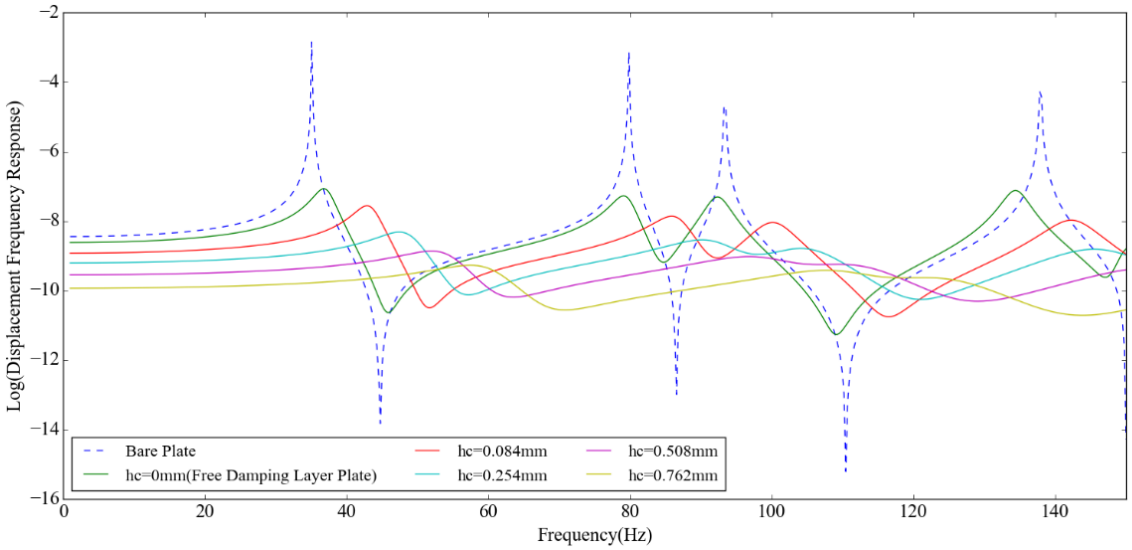

***Fig** 6.4 Displacement frequency responses with different constrained layer thicknesses*

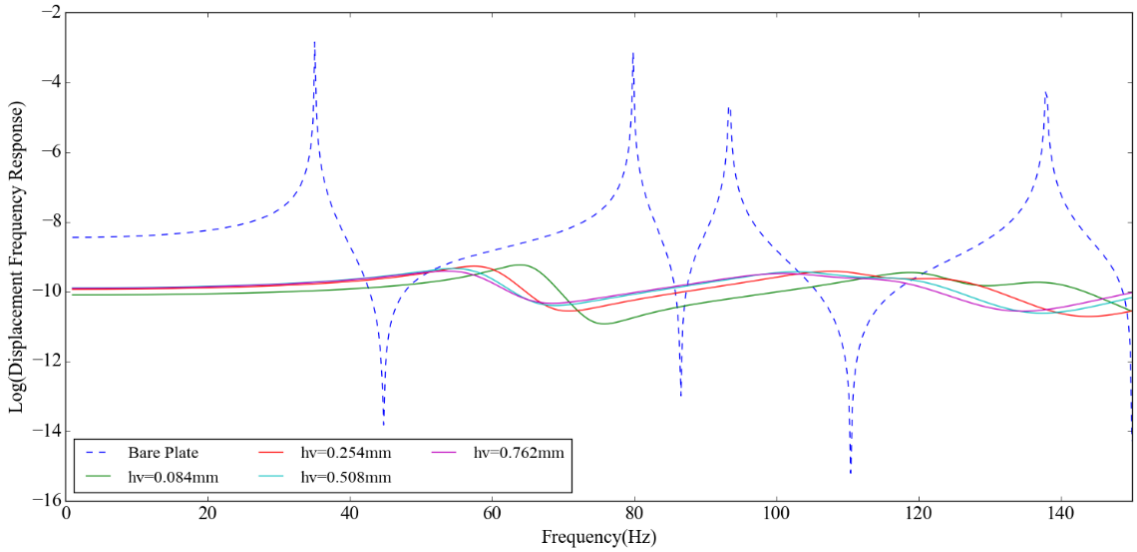

***Fig** 6.5 Displacement frequency responses with different viscoelastic layer thicknesses*

Fig 6.4 and **Fig** 6.5 show the comparison of viscoelastic core layer and constrained layer with different thicknesses. In **Fig** 6.4, the thickness of the viscoelastic core layer is kept as 0.254mm and the thicknesses of the constrained layer varies from 0.084mm to 0.762mm. In **Fig** 6.5, the thickness of the constrained layer is kept as 0.762mm while the viscoelastic layer varies from 0.084mm to 0.762mm. It is seen that increasing the thickness of both two layers respectively resulted in a better performance of vibration suppression. However, the increasing of constrained layer has a continuous decreasing effect on the vibration amplitude while the same phenomenon is not that obvious for viscoelastic layer. When the thickness of viscoelastic layer reaches 0.254mm (red line in **Fig** 6.5), there is no obvious decreasing of the vibration amplitude when the thickness of the viscoelastic core layer continues to increase.

6.2 Modal loss factor definition

For viscoelastic material, hysteretic damping is adopted instead of Rayleigh damping in FE modelling. Hysteretic damping is a type of dissipation that is a function of friction within a material. This form of damping is observed to not increase with frequency. Therefore more suitable for describing the behaviour of viscoelastic material.

Shearing is assumed to be the only significant energy storage mechanism in the viscoelastic core, and dissipation under harmonic loading is introduced by taking the core shear modulus to be complex. In a certain frequency range, the shear modulus can be described approximately by a linear and viscoelastic, frequency-independent, complex constant shear modulus as Nakra B.C. et al.[122]

$$G_v^* = G_v(1 + i\eta_v) \tag{6.19}$$

The main objective in vibration damping is to dissipate the vibration energy, which can be achieved by maximizing the modal loss factors. Based on our FE model, the dynamic equations for free vibration of the structure with viscoelastic materials has the form as

$$\boldsymbol{M\ddot{X}} + (\boldsymbol{K_R} + j\boldsymbol{K_I})\boldsymbol{X} = 0 \tag{6.20}$$

where $\boldsymbol{M}$ is the global mass matrix, $\boldsymbol{K_R}$ is the real part of the global stiffness matrix, $\boldsymbol{K_I}$ is the imaginary part of the global stiffness matrix, and $\boldsymbol{X}$ is the displacement vector. Then, the *r*th modal loss factor can be found using FE-MSE method[121]

$$\eta_r = \frac{\boldsymbol{\Phi}_r^T \boldsymbol{K_I} \boldsymbol{\Phi}_\mathbf{r}}{\boldsymbol{\Phi}_r^T \boldsymbol{K_R} \boldsymbol{\Phi}_\mathbf{r}} \tag{6.21}$$

Where $\boldsymbol{\Phi}_\mathbf{r}$ is the **r**th mode shape vector of the associated undamped system.

6.3 MAC tracking technique in topology optimization problem

Pseudo modes is an inevitable problem when the objective function is highly related to the eigenvalues and eigenvectors eg. Modal damping ratio in this case. Pseudo modes may lead to erroneous results and evoke instability in optimization process. The desired solutions can be obtained by removing the elements from the finite element model when they become void. However, this is not feasible in topology optimization based on SIMP model because once the element has been removed it is not possible for it to come back. In this Chapter, two measures have been taken to avoid the pseudo modes problem. The first one is to increase the eigenvalues of the local low density area by penalizing the mass matrix more than stiffness matrix. As low

order modes of the structure are mainly concerned in this case, the mass of void elements will be small compared with their stiffness, low order pseudo modes will vanish. Secondly, the MAC[102] tracking technique is introduced as constraint in optimization problem. The modal assurance criterion (MAC) defined as follows:

$$MAC = \frac{(\boldsymbol{\Phi}_0^T \boldsymbol{\Phi}_r)^2}{(\boldsymbol{\Phi}_0^T \boldsymbol{\Phi}_0)(\boldsymbol{\Phi}_r^T \boldsymbol{\Phi}_r)} \tag{6.22}$$

Where $\boldsymbol{\Phi_0}$ and $\boldsymbol{\Phi_r}$ are column vectors respectively describing the targeted and objective mode shapes. MAC represents the degree of correlation between the two vectors. Its value varies between 0 and 1, and it defines the degree of resemblance between vectors $\boldsymbol{\Phi_0}$ and $\boldsymbol{\Phi_r}$, where a higher value indicates a greater degree of similarity. To synthesize the objective eigenmodes, MAC is added in the optimization as a new constraint:

$$\delta - \frac{(\boldsymbol{\Phi}_0^T \boldsymbol{\Phi}_r)^2}{(\boldsymbol{\Phi}_0^T \boldsymbol{\Phi}_0)(\boldsymbol{\Phi}_r^T \boldsymbol{\Phi}_r)} \leq \ 0 \tag{6.23}$$

Where δ is a bound value, or a threshold which defines the minimal degree in similarity between the rth target and objective modes.

6.4 Topology optimization of PCLD plate

The same as before, the SIMP is used as interpolation schemes of variable density methods. Define the relative densities as the design variable vector $\boldsymbol{\rho} = \{\rho_1,\ \rho_2, \ldots\ \ \rho_{N_e}\}$, N_e denotes the total number of the elements. The design domain contains not only viscoelastic layer but also its corresponding constraining layer. Then, the SIMP model can be expressed as

$$\begin{aligned} \boldsymbol{K} &= \boldsymbol{K}^{(1)} + \sum_{e=1}^{N_e} \rho_e^p (\boldsymbol{K}^{(1)} + j\eta_v \boldsymbol{K}^{(2)} + \boldsymbol{K}^{(3)}) \\ \boldsymbol{M} &= \boldsymbol{M}^{(1)} + \sum_{e=1}^{N_e} \rho_e^q (\boldsymbol{M}^{(2)} + \boldsymbol{M}^{(3)}) \end{aligned} \tag{6.24}$$

Where $\boldsymbol{K}^{(1)}$ and $\boldsymbol{M}^{(1)}$ are the stiffnessmatrix and mass matrix of the base layer, $\boldsymbol{K}^{(2)}$ and $\boldsymbol{M}^{(2)}$ are the real part of the stiffness matrix and mass matrix of the xth element of viscoelastic layer, respectively, and $\boldsymbol{K}^{(3)}$ and $\boldsymbol{M}^{(3)}$ are the real part of the stiffness matrix and mass matrix of the xth element of constraining layer, respectively. p and q are the penalization factors. These penalty factors are used to accelerate the convergence of iteration results and obtain a clear pattern of the constrained damping layer treatments on the plate. In this Chapter, $p = q$ =3 are applied in the topology optimization problem.

For convenience, the objective function is selected as the inverse of the modal loss factor, which

transforms the maximum problem to a minimum problem. Furthermore, in order to get an averaged effect over multi-mode, we define the final objective function Π as

$$\Pi = \sum_r \frac{a_r}{\eta_r} \tag{6.25}$$

Where a_r is the associated weighting factor and satisfies $\sum_r a_r = 1$. The mathematical formulation of the optimization problem is defined as

$$\begin{aligned} Min: \quad & \Pi = \sum_r \frac{a_r}{\eta_r} \\ s.t. \quad & \sum_{e=1}^{N_e} \rho_e V_e - \alpha V_0 \\ & \phi_r^T (\boldsymbol{K}_r - \lambda_r \boldsymbol{M}) \phi_r = 0 \\ & \delta - \frac{(\boldsymbol{\Phi}_0^T \boldsymbol{\Phi}_r)^2}{(\boldsymbol{\Phi}_0^T \boldsymbol{\Phi}_0)(\boldsymbol{\Phi}_r^T \boldsymbol{\Phi}_r)} \leq 0 \\ & 0 \leq \rho_{min} \leq \rho_e \leq 1, \quad e = 1,2,\dots,N_e \end{aligned} \tag{6.26}$$

Where $\boldsymbol{\Phi_0}$ and $\boldsymbol{\Phi_r}$ are column vectors respectively describing the targeted and objective mode shapes. $\boldsymbol{K}_r$ is the real part of stiffness matrix, $\boldsymbol{M}$ is the mass matrix and λ_r is the rth eigenvalue. η_r is the rth modal loss factor. Symbol α denotes the volume fraction ratio and V_e is the damping material volume of the eth element when $\rho_e = 1$. V_0 is the volume limit for damping material. δ is a bound value for MAC tracking.

6.5 Sensitivity analysis of MDR

The sensitivity of the objective function with respect to the design variables can be expressed from **Eq.** (6.26)

$$\frac{\partial \Pi}{\partial \rho_e} = \sum_r a_r \frac{\partial}{\partial \rho_e}\left(\frac{1}{\eta_r}\right) \tag{6.27}$$

Where

$$\frac{\partial}{\partial \rho_e}\left(\frac{1}{\eta_r}\right) = \frac{\frac{\partial(\boldsymbol{\Phi}_k^T \boldsymbol{K_R} \boldsymbol{\Phi}_k)}{\partial \rho_e}(\boldsymbol{\Phi}_k^T \boldsymbol{K_I} \boldsymbol{\Phi}_k) - \frac{\partial(\boldsymbol{\Phi}_k^T \boldsymbol{K_I} \boldsymbol{\Phi}_k)}{\partial \rho_e}(\boldsymbol{\Phi}_k^T \boldsymbol{K_R} \boldsymbol{\Phi}_k)}{(\boldsymbol{\Phi}_k^T \boldsymbol{K_I} \boldsymbol{\Phi}_k)^2} \tag{6.28}$$

Here, for convenience, orthonormal modes are used. That is

$$\boldsymbol{\Phi}_k^T \boldsymbol{M} \boldsymbol{\Phi}_k = 1, \qquad \boldsymbol{\Phi}_k^T \boldsymbol{K} \boldsymbol{\Phi}_k = \lambda_k \tag{6.29}$$

Then, the **Eq. (6.28)** can be rewritten as

$$\frac{\partial}{\partial \rho_e}\left(\frac{1}{\eta_r}\right) = \frac{\frac{\partial \lambda_k}{\partial \rho_e}(\boldsymbol{\Phi}_k^T \boldsymbol{K_I} \boldsymbol{\Phi}_k) - \lambda_k \left(2\left(\frac{\partial \boldsymbol{\Phi}_k}{\partial \rho_e}\right)^T \boldsymbol{K_I} \boldsymbol{\Phi}_k\right) + \boldsymbol{\Phi}_k^T \frac{\boldsymbol{K_I}}{\partial \rho_e} \boldsymbol{\Phi}_k}{(\boldsymbol{\Phi}_k^T \boldsymbol{K_I} \boldsymbol{\Phi}_k)^2} \tag{6.30}$$

Based upon the work by Lee and Jung[124], the sensitivities of eigenvalue and eigenvector are

found as

$$\begin{Bmatrix} \frac{\partial \boldsymbol{\Phi}_k}{\partial \rho_e} \\ \frac{\partial \boldsymbol{\lambda}_k}{\partial \rho_e} \end{Bmatrix} = \begin{bmatrix} \boldsymbol{K}_R - \lambda_k \boldsymbol{M} & -\boldsymbol{M}\boldsymbol{\Phi}_k \\ -\boldsymbol{\phi}_k^T \boldsymbol{M} & 0 \end{bmatrix} \begin{Bmatrix} -\left(\frac{\partial \boldsymbol{K}_R}{\partial \rho_e} - \lambda_k \frac{\partial \boldsymbol{M}}{\partial \rho_e}\right) \boldsymbol{\Phi}_k \\ 0.5 \boldsymbol{\phi}_k^T \frac{\partial \boldsymbol{M}}{\partial \rho_e} \boldsymbol{\Phi}_k \end{Bmatrix} \tag{6.31}$$

6.6 Numerical studies

A simply supported sandwich plate is considered in this section. It has the same dimensions as the validation case except the constrained layer with thickness of 0.254 mm. The base plate and constrained layer are made of aluminium and treated with viscoelastic sheets of DYAD606 from SOUNDCOAT Company (Ling Z. et al.[111]). Physical parameters of viscoelastic core sheet are G_v= 20MPa, v_v= 0.48, ρ_v= 1140 kg/m^3 and η_v= 0.5. The aluminium plate has the constant properties of E_I=69.0GPa, v_I= 0.33, and ρ_I = 2700 kg/m^3. The boundary conditions are taken as simply supported at edges of base plate with unrestrained core and constrained layer on the top. 20 × 20 mesh and 400 elements in total are used in the FE model.

Fig 6.6 shows the optimal layouts of the constrained damping layer when the first, second and third modal damping ratios are maximized. We could find that when the boundary conditions are symmetric, the optimal layouts are symmetrical as well. **Fig** 6.6 d), **Fig** 6.6 e) and **Fig** 6.6 f) show the corresponding mode of the constrained damping layer model. As seen in the **Fig** 6.6, the optimal layouts are related to the corresponding mode shapes. **Fig** 6.6 c) is similar to **Fig** 6.6 b) rotated by 90 degrees. The same difference can be seen between the mode shapes shown in **Fig** 6.6 e) and **Fig** 6.6 f).

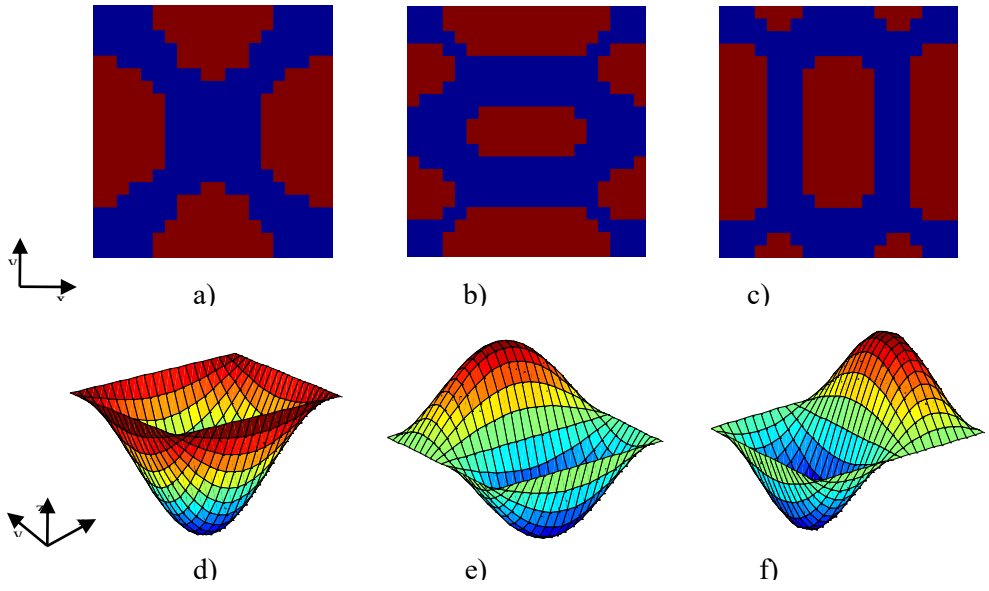

***Fig** 6.6 The optimal topology layouts and corresponding mode for the first, second and third modal damping ratio case*

Fig 6.7-**Fig** 6.9 reflect the evaluation process of the first three modal damping ratios when iteration numbers increase. It can be seen that these modal damping ratios increase with iteration numbers gradually until the maximums are achieved. Especially in **Fig** 6.9 and **Fig** 6.9, both objective modal damping ratios become the largest ones after about 40 iterations while the other two modal damping ratios almost keep the same as the initial value. The results indicate the optimization algorithm is capable of achieving a material distribution with a higher modal damping ratio. However, because the modal damping ratio is very sensitive to the material distribution, the optimization process is not stable enough, a slight fluctuant can be found in all three figures **Fig** 6.7-**Fig** 6.9.

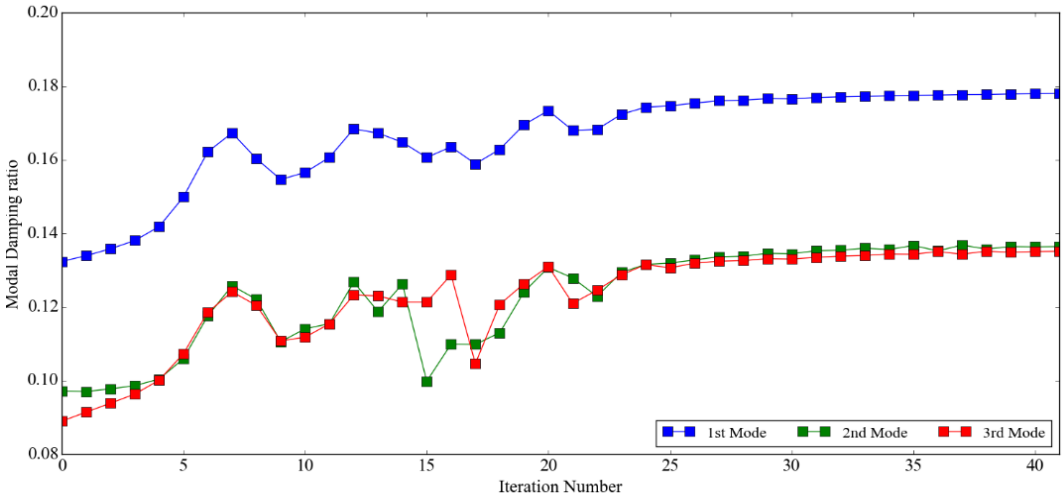

Fig 6.7 *Iteration histories for different modes when objective function is the 1st modal damping ratio*

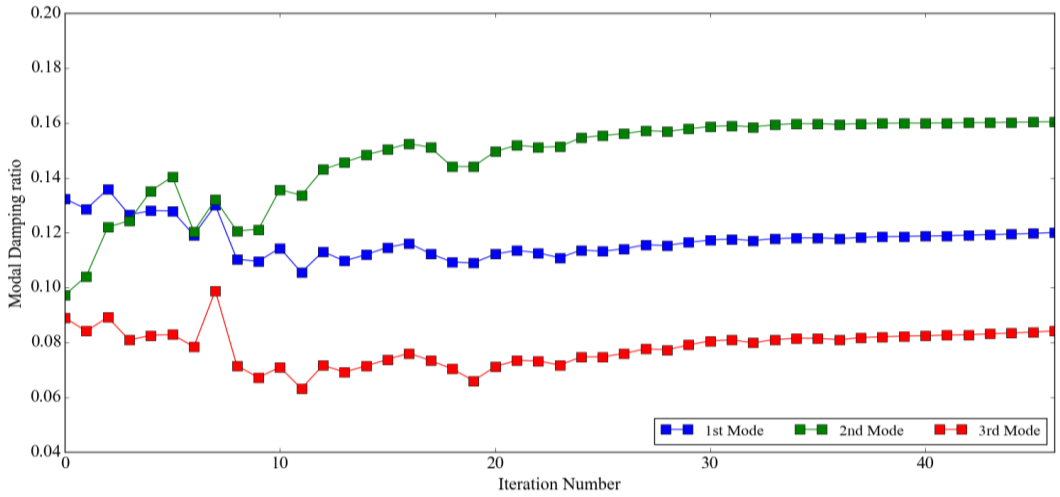

Fig *6.8 Iteration histories for different modes when objective function is the 2nd modal damping ratio*

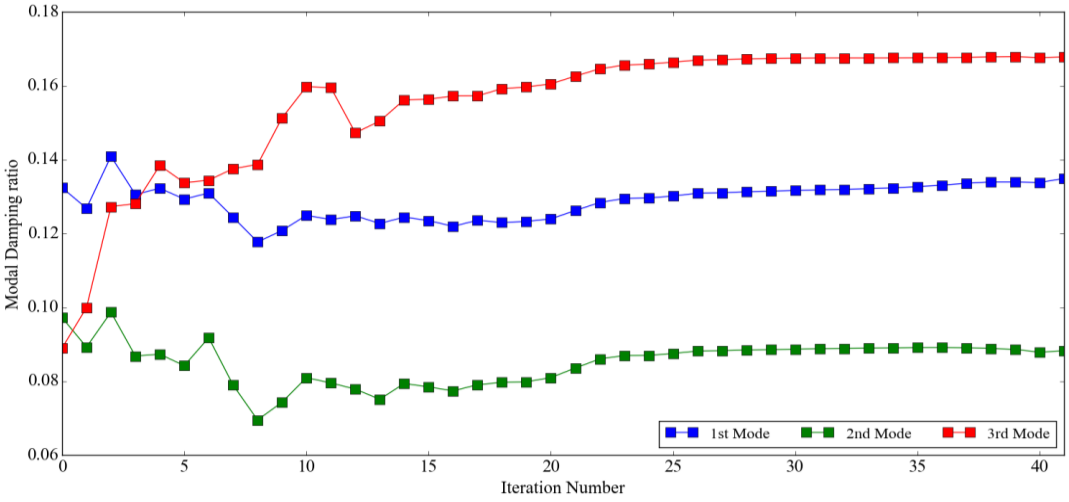

***Fig** 6.9 Iteration histories for different modes when objective function is the 3rd modal damping ratio*

Another phenomenon is worth to investigate. As shown in **Fig** 6.6, the void elements are concentrated in the centre of plate which is exactly opposite to results obtained in Chapter 5 (see **Fig 5.12**(a)). The same results can be found in **Fig** 6.6 (b)&(e) and **Fig** 6.6 (c)&(f) as well. Usually, the places with the maximum amplitudes are void while the edges of the plate are distributed with solid elements.

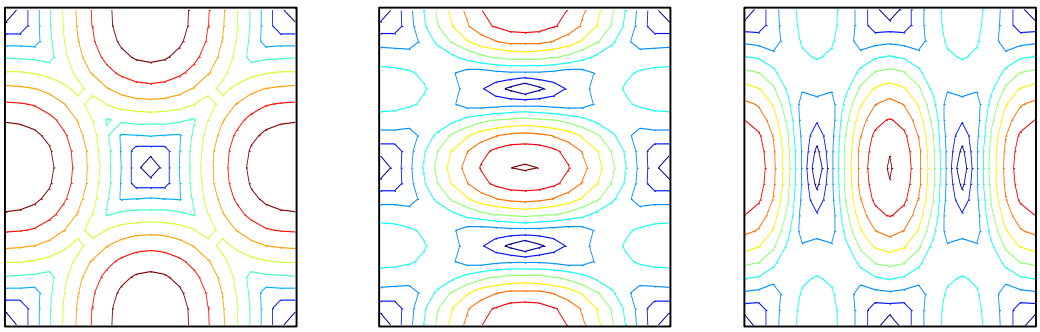

***Fig 6.10** The gradient contours of first three mode shapes*

In order to explain this phenomenon, the gradient contours of mode shapes are shown in **Fig 6.10** a), b) and c) which represents the gradient contours of first, second and third mode respectively. The red lines represent the region with large deformation gradient, the blue lines indicate the deformation of that region is flatter than red ones. From this figure, we could find a good match with the optimal layouts in **Fig** 6.6. The viscoelastic material and constrained layer always distribute in the region with large deformation gradient. An explanation for this is that the large gradient will lead to large relative deformation between viscoelastic material and stiff face layer which increase the energy dissipation in corresponding mode. It's a different

optimization logic when the modal damping ratio is chosen as the objective function.

Usually, by using mode superposition method, good approximate steady-state amplitude solutions can be obtained via superposition with only first few mode shapes. Thus we can choose the objective function as the combination of several modal damping ratios to achieve a boarder range of vibration suppression. In next case, we consider the rectangular plate with first three modes as objective and the weighting factors in the objective function are $a_1 = 0.3, a_2 = 0.4$ and $a_3 = 0.3$. **Fig** 6.11 shows the optimal layout of constrained damping layer. Compared to the optimal layouts in **Fig** 6.6, it looks like the combination of the three layouts in **Fig** 6.6. **Fig** 6.12 shows the evaluation of the modal damping ratio when the iteration increase. As we expected, all three modal damping ratios increase gradually. The frequency responses at the centre point of the rectangle plate with three different material distributions are illustrated in **Fig** 6.13. It can be seen that, although the results of the partial coverage case are not as good as that of the full coverage case, they still achieve significant improvement comparing with the results of the bare plate, and have 50% weight of the constrained damping patch saved comparing with the full covered case.

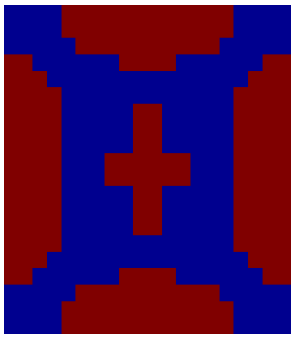

***Fig** 6.11 The optimal layout of constrained damping layer when first three modal damping ratios are objective function*

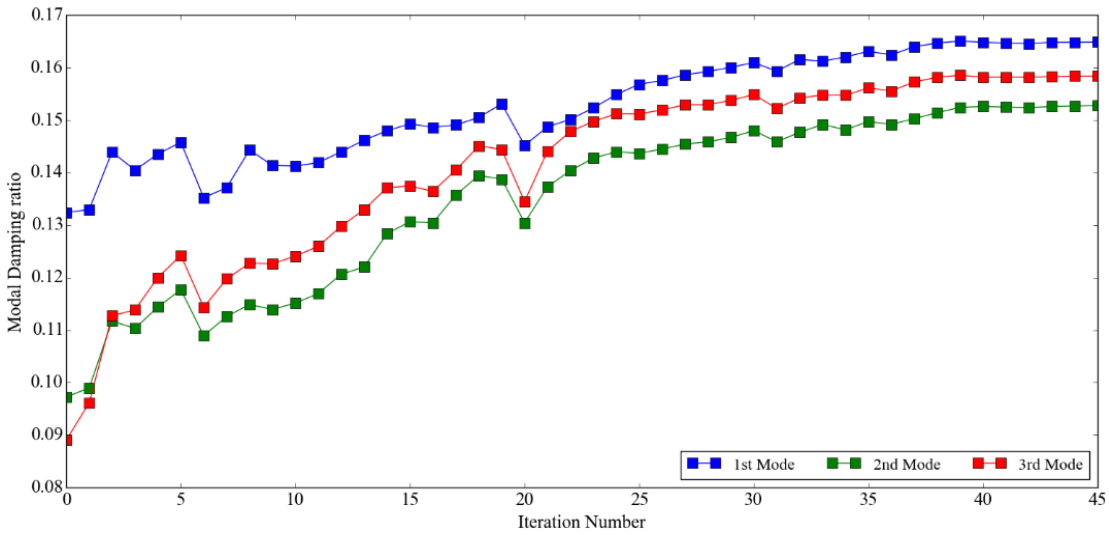

***Fig** 6.12 Iteration histories for different modes when objective function is first three modal damping ratios*

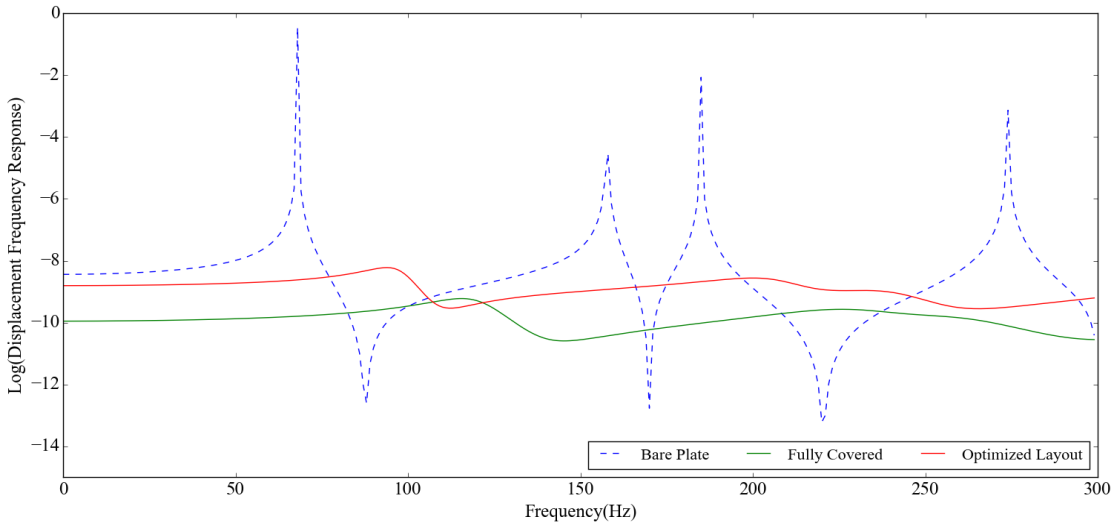

***Fig** 6.13tFrequency responses of base plate, fully covered plate and optimal layout plate*

6.7 Summary

The analytical solution of constrained damping layer plate model has been obtained in this Chapter and vibration reduction effects of this sandwich structure has also been discussed. The results indicate that constrained damping layer model could achieve a better performance of vibration energy dissipation than the free damping layer model. Then a topology optimization approach was proposed to design of the constrained damping layer treatments on flat base plates. In the proposed approach, an interface finite element is introduced to modelling the viscoelastic layer of constrained damping layer treatment to simplify the FE model in the optimization procedure. The SIMP interpolation scheme is applied to generate the mass and stiffness matrices of the structure. The optimal layout obtained in optimization achieve a remarkable effect on vibration suppression with 50% reduction of weight. Base on the investigation, the following conclusion can be drawn:

- A stiff layer on a free damping layer treatments plate could increase the shear deformation of the viscoelastic core which would help to dissipate vibration energy.
- The optimal layout based on maximum the modal damping ratio is related to the mode shapes and the constrained damping patches are more likely distributed in regions of mode shape with large deformation gradient.
- As the modal damping ratio is sensitive to the material distribution, the optimization process is not stable enough, slight fluctuant can be found during the optimization process. But usually, an expected optimal result can be obtained after optimization.

The performance of vibration reduction of the constrained damping layer plate is better than that of the plate with free damping layer, but the former is not as convenient as the latter in practical application considering that the addition of the constrained layer may have influence on the dynamic characteristics of the whole structure. A possible application of constrained layer damping plates is to achieve better properties as composite materials or as building materials to reduce vibration and achieve sound insulation. Since sandwich plate has been widely used in our life, its mature manufacturing process may be helpful for the application of the PCLD plate model proposed in this thesis.

It is worth to point out that the work presented in this Chapter is limited to the case where the property of viscoelastic material is frequency-independent. It is, therefore, meaningful to carry out further study targeting to other frequency- dependent objective functions. Furthermore, the base structure is limited to the flat plat and also we assume there is no slip happened between cover layer and viscoelastic layer.

Chapter 7 Conclusion and recommendation for future work

7.1 Conclusions

This thesis has investigated the optimal distribution of damping material in vibrating structures subject to harmonic excitations by using topology optimization method. Objective functions for vibration suppression such as power flow response, dynamic compliance, steady-state vibration amplitude and modal damping ratio have been applied to topology optimization. The optimized topology layouts of three optimization models: bi-material, free damping layer plate and constrained damping layer plate also have been discussed. Advice of optimization strategy are given at the end of each chapter. The main conclusions are categorized into three parts:

1) Bi-material topology optimization model:

   A Bi-material topology optimization model has been built for comparison between two topological designs with minimum power flow response and minimum dynamic compliance. The effect of Rayleigh damping ratio is discussed. Bi-material topology optimization model provides a general material mapping model which can be applied to almost all the SIMP models though it is a case study without clear engineering background. Conclusions are drawn as below:

   - The effect of the Rayleigh damping ratio has a great impact on optimal topology pattern. In addition, the stiffness damping coefficient has more remarkable effect on the result of topology optimization than the mass damping coefficient.
   - The reason for great effect on vibration suppression by redistributing material is that different material distribution will apply new dynamic characteristic on structure which drives the nearest resonance frequency as far away as possible from the prescribed excitation frequency, or has increased the gap between two neighbouring resonance frequencies as much as possible so that successfully avoid the resonance phenomenon occur.

2) Free damping layer model:

   Based on the material interpolation method in bi-material optimization model, both simple supported and cantilever plate with free damping layer model under harmonic excitation are investigated. Different with the bi-material model, free damping layer model has been applied to the engineering problem for vibration suppression and noise reduction.

Conclusions are drawn as below:

- A free damping material layer plate with optimized material distribution could achieve a similar vibration reduction performance as the fully covered plate but with 50% less material volume. The results illustrate significance of the damping material distribution optimization in vibration suppression and minimizing structure;
- Material distribution of damping layer on a base plate has a significant impact on structural dynamic characteristic. A plate with fully covered damping material may not always guarantee a better performance of vibration suppression;
- The damping material tend to be distributed in the places with large amplitudes which help to dissipate vibration energy by taking advantage of the deformation of damping material.
- If the additional damping layer has only a slight effect on the natural frequency compared to the base plate, a feasible material distribution layout could be obtained from the steady-state responses of initial structure. The performance of the material distribution layout obtained by this strategy is close to the one obtained by topology optimization in some cases.

3) Constrained damping layer model:

Constrained damping layer structure is the most common structure in the real world among all three models. This kind of structure stem from the natural idea to add an extra stiff layer on the top of the damping layer to enlarge the shear deformation of the damping material so that increase vibration energy dissipation. Conclusions are drawn as below:

- Increasing the thickness of viscoelastic layer and constrained layer respectively both resulted in a better performance of vibration suppression. However, the increasing of constrained layer has a continuous decreasing effect on the vibration amplitude while the same phenomenon is not that obvious for viscoelastic layer.
- The optimal layout based on maximum the modal damping ratio is related to the mode shapes and the constrained damping patches are more likely distributed in regions of mode shape with large deformation gradient.
- As the modal damping ratio is sensitive to the material distribution, the optimization process is not stable enough, slight fluctuant can be found during the optimization process. But usually, an expected optimal result can be obtained after optimization.

7.2 Recommendations for future work

The outcomes of the previous work demonstrate the importance of applying topology optimization method to structural design for vibration reduction. To further dig the potential of

this method, the following points summarize part of the future directions worth to work on:

1) waves propagate along the periodic cells only within specific frequency bands called the pass bands, while these waves are completely blocked within other frequency bands called the stop bands. The band gap properties of metamaterials, such as Phononic crystals, has been widely concerned by many researchers, however, most of the applications in this area are related to acoustic and optical fields, the applications to the vibration control by topology optimization method are very limited.

2) In this thesis, the current research is limited to optimization theory and numerical research work. In the future, the experimental platform of vibration active and passive control is established, and the experimental verification method related to structural vibration optimization is essential for further research on structural vibration topology optimization.

3) The time spending on solving finite element model in topology optimization process is considerable. This situation is getting worse when solving large-scale finite element model with a great amount of degrees of freedom. While commercial finite element software is really good at solving large-scale liner equations. Thus a deeper integrating with mature finite element solver is always necessary.

Reference

[1] J. Ro and A. Baz, Optimum placement and control of active constrained layer damping using modal strain energy approach. J. Vib. Control 8:861–876. (2002)

[2] Y.P. Xiong, J.T. Xing and W.G. Price, A power flow mode theory based on a system's damping distribution and power flow design approaches, Proc. R. Soc. A 461, 3381-3411. (2005)

[3] T.T. Soong, M.C. Costantinou, Passive and Active Structural Vibration Control in Civil Engineering. Springer. (1994)

[4] P. Jorge, I. Arenas, N. Ravi and A.N. Margasahayam, NOISE AND VIBRATION OF SPACECRAFT STRUCTURES RUIDO Y VIBRACIÓN DE ESTRUCTURAS DE VEHÍCULOS ESPACIALES Ingeniare. Revista chilena de ingeniería, vol. 14 Nº 3, 2006, pp. 251-264 (2005)

[5] P. Ambrosio, G. Cazzulani, et al. An optimal vibration control logic for minimizing fatigue damage in flexible structures. J. Sound Vib. 333(2014)1269–1280. (2014)

[6] A.K. Nandy and C.S. Jog, Optimization of vibrating structures to reduce radiated noise. Struct. Multidisc. Optim. 45:717-728. (2012)

[7] M.D. Rao and S. He, Recent applications of viscoelastic damping for noise control in automobiles and commercial airplanes. (2003)

[8] M.P. Bendsøe and N. Kikuchi, Generating optimal topologies in structural design using a homogenization method. Comput. Methods Appl. Mech. Eng. 71, 197–224. (1988)

[9] M.P. Bendsøe and O. Sigmund, Topology optimization: theory, methods and applications, 2nd edn. Springer, Berlin. (2003)

[10] A. Michell and M. Melbourne, The limits of economy of material in frame-structures [J] Philosophical Magazine. 1904, 8(47): 589-597.(1904)

[11] K.T. Cheng and N. Olhoff, An investigation concerning optimal design of solid elastic plates International [J]. Journal of Solids and Structures, 1981, 17 (3): 305-323.(1981)

[12] X.P. Zhang and Z. Kang, Topology optimization of damping layers for minimizing sound radiation of shell structures. J. Sound Vib. 332:2500-2519. (2013)

[13] H. Zheng, C. Cai, G. Pau and G.R. Liu, Minimizing vibration response of cylindrical shells through layout optimization of passive constrained layer damping treatments. J. Sound Vib. 279:739–756. (2005)

[14] M. Zhou and G.I.N. Rozvany, On the validity of ESO type methods in topology optimization. Struct. Multidisc. Optim. 21:80–83. (2001)

[15] U. Kirsch Structural optimization[M]. Springer, Berlin, 1993.

[16] GIN Rozvany, M. Zhou The coc algorithm, part i: cross section optimization or sizing[J]. Comp Meth Appl Mech, 89:281-308.（1991）

[17] K. Svanberg. The method of moving asymptotes--a new method for structural optimization[J]. International Journal for Numerical Methods in Engineering, 24:359-373., 1987

[18] K. Suzuki and N. Kikuchi, A homogenization method for shape and topology optimization, In Computer Methods in Applied Mechanics and Engineering, 93(3):291-318., 1991,

[19] X.Y. Yan, Energy finite element analysis developments for high frequency vibration analysis of composite structures. Naval Architecture and Marine Engineering, University of Michigan. Ph.D. Dissertation. (2008)

[20] G.H. Yoon, Maximizing the fundamental eigenfrequency of geometrically nonlinear structures by topology optimization based on element connectivity parameterization. Comput. Struct. 88(1–2):120–133. (2010a)

[21] V. Young, O.M. Querin, G.P. Steven and Y.M. Xie, 3D and multiple load case bi-directional evolutionary structural optimization (BESO). Struct. Optim. 18(2–3):183–192. (1999)

[22] L.H. Tenek and L. Hagiwara, Static and vibrational shape and topology optimization using homogenization and mathematical programming [J]. Computer Methods in Applied Mechanics and Engineering, 1993, 109(1-2):143-154. (1993)

[23] Hassani and E. Hinton, Homogenization and Structural Topology Optimization [M]·London: Springer-Verlag Limited. (1999)

[24] M.P. Bendsøe, Optimal shape design as a material distribution problem. Struct. Optim. 1, 193–202. (1989)

[25] M. Zhou and G.I.N. Rozvany, The COC algorithm, Part II: Topological, geometrical and generalized shape optimization. Compute. Methods Appl. Mech. Eng. 89, 309–336. (1991)

[26] M. P. Bendsøe, O. Sigmund, Material interpolation schemes in topology optimization [J]. Archive of Applied Mechanics, 69(9), 635-654. 1999

[27] O. Sigmund A 99 line topology optimization code written in Matlab. Struct. Multidisc. Optim. 21 (2):120-127.2001

[28] D, Tcherniak and O. Sigmund. A web-based topology optimization program[J]. Struct Multidisc Optim , 22:179-187. 2001

[29] O. Sigmund, On the design of compliant mechanisms using topology optimization [J]. Mech Struct Mach, 1997, 25:493–524. (1997)

[30] T. Buhl, C.B.W. Pedersen, O. Sigmund, Stiffness design of geometrically nonlinear structures in topology optimization [J]. Struct Multidisc Optim, 2000 19:93-104.(2000)

[31] J.S. Jensen and O. Sigmund, Systematic design of photonic crystal structures using topology optimization: low-loss waveguide bends [J]. Appl Phys Lett, 2004, 84:2022-2024 (2004)

[32] J.S. Jensen and O. Sigmund, Topology optimization of photonic crystal structures: a high-bandwidth low-loss T-junction waveguide [J]. J Opt Soc Am B Opt Phys, 2005, 22:1191-1198. (2005)

[33] O. Sigmund and J.S. Jensen, Systematic design of phononic band gap materials and structures by topology optimization [J]. Philos Trans R Soc A Math Phys Eng Sci, 2003, 361:1001-1019. (2003)

[34] G. Kharmanda and N. Olhoff, Reliability based topology optimization [J]. Struct Multidisc Optim, 2004, 26:295-307.(2004)

[35] J. Du, N. Olhoff, Topological design of freely vibrating continuum structures for maximum values of simple and multiple eigenfrequencies and frequency gaps [J]. Structural and Multidisciplinary Optimization, 2007, 34(2), 91-110. (2007)

[36] J.B. Du, N. Olhoff, Minimization of sound radiation from vibrating bi-material structures using topology optimization [J]. Struct Multidisc Optim, 2007, 33: 305-321.(2007)

[37] J. Du and N. Olhoff, Topological optimization of continuum structures with design-ependent surface loading-Part I: new computational approach for 2D problems [J]. Structural and Multidisciplinary Optimization, 2004, 27(3):151-165.(2004)

[38] Y.M. Xie, G.P. Steven A simple evolutionary procedure for structural optimization. Comp. & Struct. 49, 885–896, 1993

[39] D. Manickarajah, Y.M. Xie, G.P. Steven. An evolutionary method for optimization of plate buckling resistance [J]. Finite Elements in Analysis and Design, 1998, 29 (3-4):205-230.(1998)

[40] Q. Li, G.P. Steven and Y.M. Xie, Displacement minimization of thermoelastic structures by evolutionary thickness design [J]. Computer Methods in Applied Mechanics and Engineering, 1999, 179(3-4):361-378.(1999)

[41] Q. Li, G.P. Steven, Y.M. Xie, et al., Evolutionary topology optimization for temperature reduction of heat conducting fields [J]. International Journal of Heat and Mass Transfer, 2004, 47(23):5071-5083.(2004)

[42] X.Y. Yang, Y.M. Xie, G.P. Steven and O.M. Querin, Bi-directional evolutionary structural Optimization [C]// Proceedings of the 7th AIAA/USAF/NASA/ISSMO Symposium Multidisc Anal. Optim (St. Louis), pp 1449-1457.(1998)

[43] X. Huang, Y.M. Xie and M.C. Burry, Advantages of Bi-Directional Evolutionary Structural Optimization (BESO) Over Evolutionary Structural gptimization (ESO) [J].

Advances in Structural Engineering, 2007, 10:727-737.(2007)

[44] J.D.Deaton, & R.V. Grandhi, A survey of structural and multidisciplinary continuum topology optimization: post 2000 Struct Multidisc Optim 49: 1 (2014)

[45] X.Y. Yang, Y. Xie, J.S. Liu, G.T. Parks and P.J. Clarkson, Perimeter control in the bi-directional evolutionary optimization method. Struct. Multidisc. Optim. 24(6):430–440. (2003)

[46] S.J. Osher, F. Samosa, Level Set Methods for Optimization Problems Involving Geometry and Constraints: I. Frequencies of a Two-Density Inhomogeneous Drum [J]. Journal of Computational Physics, 2001, 171(1):272-288.(2001)

[47] Allaire G, Jouve F, Toader A-M. Structural optimization using sensitivity analysis and a level-set method [J]. Journal of Computational Physics, 2004, 194(1):363-393. (2004)

[48] Allaire G, Gournay F, Jouve F, et al. Structural optimization using topological and shape sensitivity via a level set method [J]. Control and Cybernetics, 2005, 34(1):59-81. (2005)

[49] Allaire G, Jouve F. A level-set method for vibration and multiple loads structural optimization [J]. Computer Methods in Applied Mechanics and Engineering, 2005, 194 (30-33): 3269-3290. (2005)

[50] M.Y. Wang, X. Wang and D. Guo, A level set method for structural topology optimization. Comput. Methods Appl. Mech. Eng. 192(1–2):227–246. (2003)

[51] M.Y. Wang and X. Wang, PDE-driven level sets, shape sensitivity and curvature flow for structural topology optimization. Comput. Model Eng. Sci. 6(4):373–395. (2004b)

[52] M.Y. Wang, S. Chen, X. Wang and Y. Mei, Design of multimaterial compliant mechanisms using level-set methods. J. Mech. Des. 127:941–956. (2005)

[53] G. Allaire, F. Gournay, F. Jouve and A.M. Toader, Structural optimization using topological and shape sensitivity via a level set method. Control Cybern 34(1):59–80. (2005)

[54] G.I.N. Rozvany, Book: Topology optimization in structure mechanic (2014)

[55] G. Allaire, F. Jouve and A.M. Toader, Structural optimization using sensitivity analysis and a level-set method. J. Comput. Phys. 194(1):363–393. (2004)

[56] Y.M. Xie and G.P. Steven, Evolutionary structural optimization. Springer. (1997)

[57] M. Nouh, O. Aldraihem and A. Baz, Wave propagation in metamaterial plates with periodic local resonances. J. Sound Vib. 341(2015):53-73. (2015)

[58] K. Svanberg, A class of globally convergent optimization methods based on conservative convex separable approximations. SIAM J. Optim. 12(2):555–573. (2002)

[59] P. Gill P, W. Murray and M.A. Saunders, SNOPT: an SQP algorithm for large-scale constrained optimization. SIAM Rev 47(1):99–131. (2005)

[60] A. Wächter and L. Biegler, On the implementation of an interior point filter line-search

algorithm for large-scale nonlinear programming. Math Program 106(1):25–57. (2006)

[61] O. Sigmund and M. Kurt, Topology optimization approaches. Struct. Multidisc. Optim. 48: 1031–1055. (2013)

[62] R. Yang and J. Du, Microstructural topology optimization with respect to sound power radiation. Struct. Multidisc. Optim. 47:191-206. (2013)

[63] R.J. Yang and A.I. Chahande, Automotive applications of topology optimization Struct. Multidisc. Optim. 9(3):245-249. (1995)

[64] X.Y. Yang, Y. Xie, G.P. Steven and O.M. Querin, Bidirectional evolutionary method for stiffness optimization. AIAA J 37(11):1483–1488. (1999)

[65] R. Balamurugan, C. Ramakrishnan and N. Singh, Performance evaluation of a two stage adaptive genetic algorithm (TSAGA) in structural topology optimization. Appl Soft Comput. 8(4):1607–1624. doi:10.1016/j.asoc.2007.10.022. (2008)

[66] R. Balamurugan, C. Ramakrishnan and N. Swaminathan, A two phase approach based on skeleton convergence and geometric variables for topology optimization using genetic algorithm. Struct. Multidisc. Optim. doi:10.1007/s00158-010-0560-4. (2011)

[67] H. Zhou, Topology optimization of compliant mechanisms using hybrid discretization model. J. Mech. Des. 132(11):111003. doi:10.1115/1.4002663. (2010)

[68] G. C. Luh and C.H. Chueh, Multi-objective optimal design of truss structure with immune algorithm. Computers and Structures, 82(11-12), 829-844. (2004)

[69] Y.M. Tseng and T.Y. Wu, Analysis and Improvement on a Contributory Group Key Exchange Protocol Based on the Diffie–Hellman Technique. Computer & Communication Sciences Volume 21, Number 2 / 2010 247-258. (2010)

[70] O. Sigmund, On the usefulness of non-gradient approaches in topology optimization. Struct. Multidisc. Optim. 43:589-596. (2011)

[71] M.P. Bendsee, Optimization of structural topology, shape and material [M]. Berlin, Heidelberg, New York: Springer. (1995)

[72] M.P. Bendsoe, N. Kikuchi, A.R. Diaz，Topology and generalized layout optimization of elastic structures [M]. In: Bends Oe, M.P.; Mota Soares, C.A. (eds.) Topology design of structures, Dordrecht: Kluwer, 1993, 159-205. (1993)

[73] O. Sigmund, J. Petersson. Numerical instabilities in topology optimization: A survey on procedures dealing with checkerboards, mesh-dependencies and local minima [J].Structural and Multidisciplinary Optimization, 1998, 16 (1):68-75. (1998)

[74] Y.P. Xiong, Novel approach for structural dynamic topology optimizations based on power flow mode theory. Vibration Engineering and Technology of Machinery Mechanisms and Machine Science Volume 23, pp 1065-1076. (2015)

[75] S.L. Xu, Y.W. Cai and G.D. Cheng, Volume preserving nonlinear density filter based on Heaviside functions. Struct. Multidisc. Optim. 41, 495–505. (2010)

[76] X.G. Xue, G.X. Li, Y.P. Xiong and J.Z. Gong, Power Flow Response Based Dynamic Topology Optimization of Bi-material Plate Structures. Chinese Journal of Mechanical engineering 26(3):620-628. (2013)

[77] N. Olhoff, M.P. Bendsoe, J. Rasmussen, On CAD-integrated structural topology and design optimization [J]. Computer Methods in Applied Mechanics and Engineering, 1991, 89(1-3):259-279. (1991)

[78] M.P. Bendsoe, J. Rasmussen. On CAD-integrated structural topology optimization [J]. Computer Methods in Applied Mechanics and Engineering, 1991, 89(1-3):259-279. (1991)

[79] O. Sigmund, Design of material structures using topology optimization[D]. Ph.D. Thesis, Department of Solid Mechanics, Technical University of Denmark, 1994. (1994)

[80] O. Sigmund, On the design of compliant mechanisms using topology optimization [J]. Mech. Struct. Mach. 1997, 25:495-526. (1997)

[81] J. Andkjær, N.A. Mortensen and O. Sigmund. Towards all-dielectric, polarization-independent optical cloaks[J]. Appl. Phys. Lett, 2012, 100:101-106. (2012)

[82] A. Diaz, O. Sigmund. Checkerboard patterns in layout optimization [J]. Structural Optimization, 1995, 10 (1):40-45. (1995)

[83] M. Zhou, Y.K. Shyy, H.L. Thomas, Checkerboard and minimum member size control in topology optimization[J]. Structural and Multidisciplinary Optimization, 2001, 21 (2):152-158. (2001)

[84] Allaire G., Jouve F. and Toader A.M. A level-set method for shape optimization. C. R.Math 334(12):1125 1130. doi:10.1016 /S1631-073X(02)02412-3. (2002)

[85] J. Du and N. Olhoff, Topology optimization of continuum structures with respect to simple and multiple eigenfrequencies. 6th World Congresses of Structural and Multidisciplinary Optimization, Rio de Janeiro, 30 May - 03 June 2005, Brazil. (2006a)

[86] J. Du and N. Olhoff, Topological design of freely vibrating continuum structures for maximum values of simple and multiple eigenfrequencies and frequency gaps. Struct. Multidiscip. Optim. 34(2):91–110. (2007b)

[87] X. Huang and Y.M. Xie, Evolutionary topology optimization of continuum structures: methods & applications. Wiley, New York. (2010b)

[88] J.F. Madeira, H.L. Pina, H.C. Rodrigues, GA topology optimization using random keys for tree encoding of structures. Struct. Multidisc. Optim. 40:227-240. (2010)

[89] C.S. Jog, Topology design of structures subjected to periodic loading. J. Sound. Vib. 253(3):687–709. (2002)

[90] Y.M. Xie and G.P. Steven, A simple evolutionary procedure for structural optimization. Comput. Struct. 49:885–896. (1993)

[91] Y.P. Xiong, J.T. Xing and W.G. Price, Power flow analysis of complex coupled systems by progressive approaches, J. Sound Vib. 239 (2) 275-295. (2001)

[92] Y.P. Xiong, J.T. Xing and W.G. Price, A general linear mathematical model of power flow analysis and control for integrated structure–control systems, J. Sound Vib. 267 (2) 301-334. (2003)

[93] J. Du and N. Olhoff, Topological design of continuum structures subjected to forced vibration. 6th World Congresses of Structural and Multidisciplinary Optimization, Rio de Janeiro, 30 May - 03 June 2005, Brazil. (2006b)

[94] J. Dahl, J.S. Jensen, O. Sigmund, Topology optimization for transient wave propagation problems in one dimension. Struct. Multidisc. Optim. 36(6):585-595. (2007)

[95] Lei Shu, Michael Yu Wang, Zongde Fang, Zhengdong Ma, Peng Wei, Level set based structural topology optimization for minimizing frequency response, In Journal of Sound and Vibration, Volume 330, Issue 24, Pages 5820-5834(2011)

[96] J.A. Sethian and A. Wiegmann, Structural boundary design via level set and immersed interface methods. J. Comput. Phys. 163(2):489–528. (2000)

[97] L. Shu, Y.M. Wang and Z.D. Ma, Level set based topology optimization of vibrating structures for coupled acoustic-structural dynamics. Computers and Structures. Volume 132 Pages 34-42. (2014)

[98] W.M. Vicente, Z.H. Zuo, et al., Concurrent topology optimization for minimizing frequency responses of two-level hierarchical structures. Comput. Methods Appl. Mech. Engrg. 301 (2016) 116–136. (2016)

[99] A. Mohammed, Al-Ajmi, Homogenization and structural topology optimization of constrained layer damping treatments. Ph.D Dissertation, University of Maryland, 2004.

[100] M. Alvelid. Optimal position and shape of applied damping material. J. ound Vib. 310:947 965.81. (2008)

O. Sigmund, A 99 line topology optimization code written in Matlab. Struct. Multidisc. Optim. 21 (2):120-127. (2001)

[101] D.J. Thompson, A continuous damped vibration absorber to reduce broad-band wave propagation in beams. J. Sound. Vib 311 (3-5) 824-842. (2008)

[102] M.Y. Wang and X. Wang, “Color” level sets: a multi-phase method for structural topology optimization with multiple materials. Comput. Methods Appl. Mech. Eng. 193(6–8):469–496. (2004a)

[103] M.Y. Wang and L. Li, Shape equilibrium constraint: a strategy for stress-constrained

structural topology optimization. Struct. Multidisc. Optim. 47:335–352. (2013)

[104] L. Xia, P. Breitkopf. Design of materials using topology optimization and energy-based homogenization approach in Matlab. Struct. Multidisc. Optim. 52(6):1229-1241. (2015)

[105] X. Huang and Y.M. Xie, A further review of ESO type methods for topology optimization. Struct. Multidisc. Optim. 41(5):671–683. (2010c)

[106] Andreassen, E., Clausen, A., Schevenels, M. et al. Efficient topology optimization in MATLAB using 88 lines of code Struct Multidisc Optim (2011)

[107] V.J. Challis, A discrete level-set topology optimization code written in matlab. Struct. Multidisc. Optim. 41(3):453–464. doi:10.1007/s00158-009-0430-0. (2010)

[108] K. Liu and A. Tovar, An efficient 3D topology optimization code written in Matlab. Struct. Multidisc. Optim. 50(6):1175-1196. (2014)

[109] N. Aage, B.S. Lazarov, Parallel framework for topology optimization using the method of moving asymptotes. Struct. Multidisc. Optim. 47(4):493–505. (2013)

[110] Z.H. Zuo, Y.M. Xie, A simple and compact Python code for complex 3D topology optimization. Advances in Engineering Software 85 (2015) 1–11. (2015)

[111] Z. Ling, R. Xie, W. Yi and A. El-Sabbagh, Topology optimization of constrained layer damping on plates using Method of Moving Asymptote (MMA) approach. Shock. Vib. 18:221–244. (2011)

[112] C.D. Johnson and D. Kienholz Finite element prediction of damping in structures with constrained viscoelastic layers, AIAA Journal 20 1284-1290 (1981)

[113] M.P. Bendsøe and O. Sigmund, Material interpolation schemes in topology optimization. Arch. Appl. Mech. 69(9–10):635–654. (1999)

[114] N.L. Pedersen, Maximization of eigenvalues using topology optimization. Struct. Multidisc. Optim. 20(1):2–11. (2000)

[115] J.S. Jensen and N.L. Pedersen, On maximal eigenfrequency separation in two-material structures: the 1D and 2D scalar cases. J. Sound Vib. 289(4–5):667–686. (2006)

[116] T.K. Caughey and M.E.J. O'Kelly, "Classical normal modes in damped linear dynamic systems." Transactions of ASME, Journal of Applied Mechanics, 32, 583–588. (1965)

[117] J. Du and N. Olhoff, Topological design of vibrating structures with respect to optimum sound pressure characteristics in a surrounding acoustic medium. Struct. Multidisc. Optim. 42:43-54. (2010)

[118] 95. K. Svanberg, The method of moving asymptotes-a new method for structural optimization. Int. J. Numer. Methods Eng. 24:359–373. (1987)

[119] O. Sigmund, On the design of compliant mechanisms using topology optimization. Mech. Struct. Mach. 25, 495–526. (1997)

[120] M.D. Rao, Frequency and loss factor of sandwich beams under various boundary conditions. Journal of Mechanical Engineering Science 20, 271-282. (1978)

[121] C.D. Johnson and D. Kienholz, Finite element prediction of damping in structures with constrained viscoelastic layers, AIAA Journal 20(1981), 1284-1290. (1981)

[122] B.C. Nakra, Vibration control in machines and structures using viscoelastic damping, J. Sound. Vib 211 (1998), 449-465. (1998)

[123] T.D. Tsai, C.C. Cheng, Structural design for desired eigenfrequencies and mode shapes using topology optimization. Struct. Multidisc. Optim. 47(5):673-686. (2012)

[124] I.W. Lee, G.H. Jung, An efficient algebraic method for the computation of natural frequency and mode shape sensitivities. Comput Struct 62(3):429-435. (1997)

[125] V. D. Belov, S. A. Rybak, B. D. Tartakovskii, Propagation of vibrational energy in absorbing structures[J]. Journal of Soviet Physics Acoustics, 1977, 23(2): 115–119.

[126] H. G. D. Goyder, R. G. White, Vibrational power flow from machines into built-up structures. I. Introduction and approximate analysis of beam and plate-like foundations[J]. Journal of Sound and Vibration, 1980, 68: 59–75.

[127] H. G. D. Goyder, R. G. White, Vibrational power flow from machines into built-up structures. II. Wave propagation and power flow in beam-stiffened plates[J]. Journal of Sound and Vibration, 1980, 68: 77–96.

[128] R. S. Langley, Analysis of power flow in beams and frameworks using the direct-dynamic stiffness method[J]. Journal of Sound and Vibration, 1990, 136: 439–452.

[129] J. T. Xing, W. G. Price, A power flow analysis based on continuum dynamics[J]. Proc. R. Soc. A, 1999, 455: 401–436.

[130] Y.P. Xiong, J. T. Xing, W. G. Price, A power flow mode theory based on a system's damping distribution and power flow design approaches[J]. Proc. R. Soc. A, 2005, 461: 3 381–3 411.

[131] S. P. Timoshenko and S Woinowsky-Krieger, Theory of Plates and Shells. McGraw-Hill. (1959).

Appendices

Appendix I Analytical solutions for PCLD plate

The governing equations of free vibration of sandwich represented by displacements

$$\begin{cases} \frac{E_1 h_1}{1-\mu_1^2}\left(\frac{\partial^2 u_1}{\partial x^2}+\frac{1+\mu_1}{2}\frac{\partial^2 u_1}{\partial x \partial y}+\frac{1-\mu_1}{2}\frac{\partial^2 u_1}{\partial y^2}\right)+\frac{G_2^*}{h_2}\left(u_3-u_1-h\frac{\partial w}{\partial x}\right)=0, \\ \frac{E_1 h_1}{1-\mu_1^2}\left(\frac{\partial^2 v_1}{\partial y^2}+\frac{1+\mu_1}{2}\frac{\partial^2 v_1}{\partial x \partial y}+\frac{1-\mu_1}{2}\frac{\partial^2 v_1}{\partial x^2}\right)+\frac{G_2^*}{h_2}\left(v_3-v_1-h\frac{\partial w}{\partial y}\right)=0, \\ \frac{E_3 h_3}{1-\mu_3^2}\left(\frac{\partial^2 u_3}{\partial x^2}+\frac{1+\mu_3}{2}\frac{\partial^2 u_1}{\partial x \partial y}+\frac{1-\mu_3}{2}\frac{\partial^2 u_3}{\partial y^2}\right)+\frac{G_2^*}{h_2}\left(u_3-u_1-h\frac{\partial w}{\partial x}\right)=0, \\ \frac{E_3 h_3}{1-\mu_3^2}\left(\frac{\partial^2 v_3}{\partial y^2}+\frac{1+\mu_3}{2}\frac{\partial^2 v_3}{\partial x \partial y}+\frac{1-\mu_3}{2}\frac{\partial^2 v_3}{\partial x^2}\right)+\frac{G_2^*}{h_2}\left(v_3-v_1-h\frac{\partial w}{\partial y}\right)=0, \\ h\frac{G_2^*}{h_2}\left(\frac{\partial u_3}{\partial x}-\frac{\partial u_1}{\partial x}+\frac{\partial v_3}{\partial y}-\frac{\partial v_1}{\partial y}\right)+\left[\frac{E_1 h_1^3}{12(1-\mu_1^2)}+\frac{E_3 h_3^3}{12(1-\mu_3^2)}\right]\left(\frac{\partial^4 w}{\partial x^4}+\frac{\partial^4 w}{\partial y^4}+2\frac{\partial^4 w}{\partial x^2 y^2}\right) \\ -\frac{h^2}{h_2}G_2^*\left(\frac{\partial^2 w}{\partial x^2}+\frac{\partial^2 w}{\partial y^2}\right)=\rho\frac{\partial^2 w}{\partial t^2}, \end{cases} \quad \text{(II-1)}$$

Appendix II Part of the Python code for ABAQUS package

```
# Verison 1.2
# Add Read_ESM function used to read STIFFNESS and MASS matrices from files.
# Stop obtaining Element Elastic Energy from ABAQUS, Calculate Objective by external function
# Delete Resubmit Function for it's useless. The reason, which is not sure enough, why ABAQUS
collapse is MemoryError
# Adopt SIMP model which means OC algorithm and sensitivity filter were introduced in this
version
# Add some help functions: Modify INP, Pre_Matrix, Result_Plot_SIMP
#Version 1.3
# SIMP Bi-Mateiral Model Static Optimization
# Add Dynamic Optimization
# Modify Obj_Cal for complex calculation
# Fix a bug for Read_ESM function. It can't read MASS matrix before.
# Fix a bug in preFlt function. distance of two elements should be sqrt of the sum of the
squares of coordinates.
# Add Self-define excitation frequency of load
# Modify OC algorithm for Non-Negative in sqrt function
#Version 1.4
# Add Power-flow Objective function and redesign code structure which enable the code more
compatible for different Objective function.
# Fix excitation frequency. Should be natural(radian) frequency NOT cycles frequency
# Add MMA Algorithm
# Add Structural Intensity Function
# Fix Structural Intensity Function under Global Coordinate System
#Version 1.5
# Add Restore Mechanism
# Add Post-process
# Revise the programming structure. Add global parameters setting
# Add Final Run
# Revise restore mechanism by global variables
#Version 1.6
# Add Displacement Objective
# Add Free Damping Layer Model
# Change the FEA run mode by command line
# Add GROSS MATRIX READ function
# Read Node Index as well as the Element Matrix
# Add a function to change Node Number to DOF Number
#Version 1.7
# Add MDR Objective
# Add Constrained Damping Layer Model
# Add a function to construct gross stiffness/mass matrix for laminated plate
```

```
#Version 1.8
# Rewrite the sensitivity of MDR by FORTRAN to improve the efficiency, now "mdr.dll" is used
to solve the sensitivities of MDR.

import os
import time
import pickle
import numpy as np
import numpy.linalg
from numpy.ctypeslib import load_library,ndpointer
from ctypes import c_int,c_double
from caeModules import *
import math, customKernel
from AbaqusConstants import *
from odbAccess import openOdb

def Read_ESM(ESM_Name, STIF, MASS, NODENUM, NODESUM, DOFNUM, N, l1, l2, l3 , Slave, Master):
    f=open(ESM_Name,'r')
    E_line='Start'
    E_NUM=0
    while E_line<>'':
        E_line = f.readline()
        if E_line[3:17]=='ELEMENT NUMBER':
            E_NUM=E_NUM+1
        elif E_line[1:13]=='USER ELEMENT':
            NODESUM=int(E_line[21:31].strip())
        elif E_line[3:16]=='ELEMENT NODES':
            E_line = f.readline()
            NODE_T=np.array(E_line[2:-1].strip().split(','),dtype=int)
            E_line = f.readline()
            DOFNUM=len(E_line.strip().split(','))
        Head=E_line[8:len(E_line)-1].strip()
        if Head=='TYPE=STIFFNESS' and E_NUM<>0:
            STIF[E_NUM-1],MASS[E_NUM-1]=Read_Matrices(f,N,Head[5:len(Head)],E_NUM)
            if Slave<>[]:
                # Construct DOF Index
                NODE_T=list(np.kron(Node2DOF(NODE_T,l1,l2,l3),np.ones(DOFNUM,dtype=int))+np.kr
on(np.ones(NODESUM,dtype=int),range(DOFNUM)))
                # Replace Constrained DOF
                for i in range(len(Slave)):
                    if Slave[i] in NODE_T:
                        m=NODE_T.index(Slave[i])
                        NODE_T[m]=Master[i]
                NODENUM[E_NUM-1]=NODE_T
```

```
    f.close()

def Read_Matrices(f,N,Type,Enum):
    Line_Matrix=[];K=np.zeros([N,N]);M=np.zeros([N,N])
    data_line = f.readline()
    data_line=data_line.strip().split(',');data_line.pop()
    while data_line[0]<>'**':
        Line_Matrix.extend(data_line)
        data_line = f.readline()
        if data_line=='':break
        data_line=data_line.strip().split(',')
        if data_line[-1]=='': data_line.pop()
    Line_Matrix.reverse()
    for i in range(1,1+N):
        for j in range(1,1+i):
            K[i-1,j-1]=Line_Matrix.pop()
            if i<>j:K[j-1,i-1]=K[i-1,j-1]
    Line_Matrix.pop();Line_Matrix.pop()
    for i in range(1,1+N):
        for j in range(1,1+i):
            M[i-1,j-1]=Line_Matrix.pop()
            if i<>j:M[j-1,i-1]=M[i-1,j-1]
    return K,M

def Modify_INP(INP_name):
    # Open *.INP
    try:
        f=open(INP_name+'.inp','r+')
    except ValueError:
        print 'Can\'t open {0}.inp'.format(INP_name)
    E_line='Start'
    while E_line<>'':
        E_line = f.readline()
        E_line=E_line.strip()
        if E_line=='*End Step':
            f.seek(-11,2)
            f.write("*FILE FORMAT, ASCII\n*ELEMENT MATRIX OUTPUT, ELSET=LAYER-1.whole, FILE
NAME=ESMLAYER3600-2, STIFFNESS=YES, MASS=YES, OUTPUT FILE=USER DEFINED\n*ELEMENT MATRIX
OUTPUT, ELSET=BASE-1.whole, FILE NAME=ESMBASE3600, STIFFNESS=YES, MASS=YES, OUTPUT FILE=USER
DEFINED\n*End Step\n")
            E_line=''
    f.close()

def preFlt(Rmin,Elmts,Nds):
```

```
    Fm={}
    # Calculate element centre coordinates
    elm, c0 = np.zeros(len(Elmts)), np.zeros((len(Elmts),3))
    for i in range(len(elm)):
        elm[i] = Elmts[i].label
        nds = Elmts[i].connectivity
        for nd in nds: c0[i] = np.add(c0[i],np.divide(Nds[nd].coordinates,len(nds)))
    # Weighting factors
    for i in range(len(elm)):
        Fm[elm[i]] = [[],[]]
        for j in range(len(elm)):
            dis = np.sqrt(np.sum(np.power(np.subtract(c0[i],c0[j]),2)))
            if dis<Rmin:
                Fm[elm[i]][0].append(elm[j])
                Fm[elm[i]][1].append(Rmin - dis)
        Fm[elm[i]][1] = np.divide(Fm[elm[i]][1],np.sum(Fm[elm[i]][1]))
    return Fm

def fltAe(Ae,Fm,Xe):
    raw = Ae.copy()
    for el in Fm.keys():
        Ae[el-1] = 0.0
        for i in range(len(Fm[el][0])): Ae[el-1]+=raw[Fm[el][0][i]-
1]*Fm[el][1][i]*Xe[Fm[el][0][i]-1]/Xe[el-1]
    return Ae

def OC(Vf,Xe,Ae,Ele_NUM):
    lo, hi, move = 0, 1e9, 0.1
    tv = Vf*Ele_NUM
    while (hi-lo)/(hi+lo) > 1.0e-3:
        lmid = (lo+hi)/2.0
        xnew=np.maximum(0.001,np.maximum(Xe-
move,np.minimum(1,np.minimum(Xe+move,Xe*np.sqrt(np.maximum(0,-Ae/lmid))))))
        if sum(xnew)-tv>0:
            lo = lmid
        else:
            hi = lmid
    return xnew

def FE_Mdb(mdb,Mats,N,w):
    # Params Define
    mdl = mdb.models['Model-1']
    #-------First Model-------------#
    PN=Part_Name[0]
```

```
    part = mdl.parts[PN]
    # Build sections and assign solid section
    # Define materials and element sets
    # Updating Material Parameters
    #-------Part1 Update-------------#
    E0=Mats[PN]['E0'];E1=Mats[PN]['E1'];D0=Mats[PN]['D0'];D1=Mats[PN]['D1']
    alpha=Mats[PN]['alpha'];beta=Mats[PN]['beta'];th=Mats[PN]['th'];possion=Mats[PN]['possion'
]
    E=Xe**penal*E1+(1-Xe**penal)*E0
    D=Xe**penal*D1+(1-Xe**penal)*D0
    for i in range(1,N+1):
        mdl.Material('Material'+PN+str(i)).Elastic(((E[i-1], possion),))
        mdl.materials['Material'+PN+str(i)].Density(((D[i-1],),))
        mdl.materials['Material'+PN+str(i)].Damping(alpha=alpha, beta=beta)
        mdl.HomogeneousSolidSection(name='Sec'+PN+str(i),material='Material'+PN+str(i),thickne
ss=None)
        part.SectionAssignment(part.Set('Set'+PN+str(i),part.elements[i-1:i]),'Sec'+PN+str(i))
    #-------Part2 Update-------------#
    PN=Part_Name[1]
    part = mdl.parts[PN]
    E0=Mats[PN]['E0'];E1=Mats[PN]['E1'];D0=Mats[PN]['D0'];D1=Mats[PN]['D1']
    alpha=Mats[PN]['alpha'];beta=Mats[PN]['beta'];th=Mats[PN]['th'];possion=Mats[PN]['possion'
]
    E=Xe**penal*E1+(1-Xe**penal)*E0
    D=Xe**penal*D1+(1-Xe**penal)*D0
    for i in range(1,N+1):
        mdl.Material('Material'+PN+str(i)).Elastic(((E[i-1], possion),))
        mdl.materials['Material'+PN+str(i)].Density(((D[i-1],),))
        mdl.materials['Material'+PN+str(i)].Damping(alpha=alpha, beta=beta)
        mdl.HomogeneousShellSection(name='Sec'+PN+str(i),material='Material'+PN+str(i),thickne
ss=th)
        part.SectionAssignment(part.Set('Set'+PN+str(i),part.elements[i-
1:i]),'Sec'+PN+str(i),offsetType=BOTTOM_SURFACE)
    #mdl.steps['Step-1'].setValues(frequencyRange=((w, w, 2, 1.0), ))

def Run_FEA(mdb,Iter):
    # Job Submit
    mdb.Job(name='Design_Job'+str(Iter), model='Model-1')
    a=os.system('del Design_Job'+str(Iter)+'*')
    mdb.jobs['Design_Job'+str(Iter)].writeInput(consistencyChecking=OFF)
    # Modify INP for Gross Matrix
    f=open('Design_Job'+str(Iter)+'.inp','r+')
    E_line='Start'
    while E_line<>'':
```

```
        E_line = f.readline()
        E_line=E_line.strip()
        if E_line=='*End Step':
            f.seek(-11,2)
            f.write("*END STEP\n*STEP, NAME=MATRIX\n*MATRIX GENERATE, STIFFNESS, MASS, VISCOUS
DAMPING\n*Boundary\nBase-1.b, PINNED\n*Boundary\nBase-1.all, 6, 6\n*Boundary\nTop-1.all, 6,
6\n*MATRIX OUTPUT, STIFFNESS, MASS, VISCOUS DAMPING\n*END STEP")
            E_line=''
    f.close()
    # Submit and wait for finishing
    os.system(u'Abaqus job='+'Design_Job'+str(Iter))
    FILE='Design_Job'+str(Iter)+'.lck'
    while not os.path.exists(FILE):
        time.sleep(1)
    while os.path.exists(FILE):
        time.sleep(1)
    return 'Design_Job'+str(Iter)

def Obj_Cal_DISP_READ(U,w,Name):
    K=np.zeros([441*6,441*6]);M=np.zeros([441*6,441*6]);C=np.zeros([441*6,441*6]);L=np.zeros([
441*6,1],dtype=complex)
    Obj=0
    #Reading Gross Matrix--------------------------------------#
    #Reading STIFFNESS MATRIX
    f=open(Name+'_STIF2.mtx','r')
    data_line = f.readline()
    while data_line<>'':
        data_line=data_line.strip().split(',')
        m=(int(data_line[0])-1)*6+int(data_line[1])-1
        n=(int(data_line[2])-1)*6+int(data_line[3])-1
        K[m,n]=float(data_line[4])
        K[n,m]=float(data_line[4])
        data_line = f.readline()
    f.close()
    #Reading MASS MATRIX
    f=open(Name+'_MASS2.mtx','r')
    data_line = f.readline()
    while data_line<>'':
        data_line=data_line.strip().split(',')
        m=(int(data_line[0])-1)*6+int(data_line[1])-1
        n=(int(data_line[2])-1)*6+int(data_line[3])-1
        M[m,n]=float(data_line[4])
        M[n,m]=float(data_line[4])
        data_line = f.readline()
```

```
    f.close()
    #Reading DAMPING MATRIX
    f=open(Name+'_DMPV2.mtx','r')
    data_line = f.readline()
    while data_line<>'':
        data_line=data_line.strip().split(',')
        m=(int(data_line[0])-1)*6+int(data_line[1])-1
        n=(int(data_line[2])-1)*6+int(data_line[3])-1
        C[m,n]=float(data_line[4])
        C[n,m]=float(data_line[4])
        data_line = f.readline()
    f.close()
    #-----------------------------------------------------------------#
    W=K+1j*w*C-w**2*M
    #Reading LOADING MATRIX
    f=open(Name+'_LOAD2.mtx','r')
    #=======================#
    data_line = f.readline()
    data_line = f.readline()
    #=======================#
    data_line = f.readline()
    while data_line<>'':
        data_line=data_line.strip().split(',')
        nm=int(data_line[0])-1
        nn=int(data_line[1])-1
        nU=U[nm].data[nn]+complex(0,U[nm].conjugateData[nn])
        L[nm*6+nn]=-np.conj(nU)/2.0/np.abs(nU)
        Obj+=np.abs(nU)
        data_line = f.readline()
    f.close()
    mu=np.linalg.solve(W,L)
    return mu.T,Obj

def Obj_Cal_MDR_READ(l1,l2,l3,GROSS_DOF,Name):
    K=np.zeros([GROSS_DOF,GROSS_DOF],dtype='f8',order='f');M=np.zeros([GROSS_DOF,GROSS_DOF],dt
ype='f8',order='f');C=np.zeros([GROSS_DOF,GROSS_DOF],dtype='f8',order='f')
    #Reading Gross Matrix--------------------------------------#
    #Reading STIFFNESS MATRIX
    f=open(Name+'_STIF2.mtx','r')
    data_line = f.readline()
    while data_line<>'':
        data_line=data_line.strip().split(',')
        data_line[0]=int(data_line[0])
        data_line[1]=int(data_line[1])
```

```
    data_line[2]=int(data_line[2])
    data_line[3]=int(data_line[3])
    data_line[4]=float(data_line[4])
    if data_line[0] <= l1:
        m=((data_line[0])-1)*6+data_line[1]-1
    elif l1< data_line[0] <= l2:
        m=l1*6+((data_line[0])-l1-1)*3+data_line[1]-1
    elif l2< data_line[0] <= l3:
        m=l1*6+(l2-l1)*3+((data_line[0])-l2-1)*6+data_line[1]-1
    if data_line[2] <= l1:
        n=((data_line[2])-1)*6+data_line[3]-1
    elif l1< data_line[2] <= l2:
        n=l1*6+((data_line[2])-l1-1)*3+data_line[3]-1
    elif l2< data_line[2] <= l3:
        n=l1*6+(l2-l1)*3+((data_line[2])-l2-1)*6+data_line[3]-1
    K[m,n]=data_line[4]
    K[n,m]=data_line[4]
    data_line = f.readline()
f.close()
#Reading MASS MATRIX
f=open(Name+'_MASS2.mtx','r')
data_line = f.readline()
while data_line<>'':
    data_line=data_line.strip().split(',')
    data_line[0]=int(data_line[0])
    data_line[1]=int(data_line[1])
    data_line[2]=int(data_line[2])
    data_line[3]=int(data_line[3])
    data_line[4]=float(data_line[4])
    if data_line[0] <= l1:
        m=((data_line[0])-1)*6+data_line[1]-1
    elif l1< data_line[0] <= l2:
        m=l1*6+((data_line[0])-l1-1)*3+data_line[1]-1
    elif l2< data_line[0] <= l3:
        m=l1*6+(l2-l1)*3+((data_line[0])-l2-1)*6+data_line[1]-1
    if data_line[2] <= l1:
        n=((data_line[2])-1)*6+data_line[3]-1
    elif l1< data_line[2] <= l2:
        n=l1*6+((data_line[2])-l1-1)*3+data_line[3]-1
    elif l2< data_line[2] <= l3:
        n=l1*6+(l2-l1)*3+((data_line[2])-l2-1)*6+data_line[3]-1
    M[m,n]=data_line[4]
    M[n,m]=data_line[4]
    data_line = f.readline()
```

```
    f.close()
    #Reading DAMPING MATRIX
    f=open(Name+'_DMPV2.mtx','r')
    data_line = f.readline()
    while data_line<>'':
        data_line=data_line.strip().split(',')
        data_line[0]=int(data_line[0])
        data_line[1]=int(data_line[1])
        data_line[2]=int(data_line[2])
        data_line[3]=int(data_line[3])
        data_line[4]=float(data_line[4])
        if data_line[0] <= l1:
            m=((data_line[0])-1)*6+data_line[1]-1
        elif l1< data_line[0] <= l2:
            m=l1*6+((data_line[0])-l1-1)*3+data_line[1]-1
        elif l2< data_line[0] <= l3:
            m=l1*6+(l2-l1)*3+((data_line[0])-l2-1)*6+data_line[1]-1
        if data_line[2] <= l1:
            n=((data_line[2])-1)*6+data_line[3]-1
        elif l1< data_line[2] <= l2:
            n=l1*6+((data_line[2])-l1-1)*3+data_line[3]-1
        elif l2< data_line[2] <= l3:
            n=l1*6+(l2-l1)*3+((data_line[2])-l2-1)*6+data_line[3]-1
        C[m,n]=data_line[4]
        C[n,m]=data_line[4]
        data_line = f.readline()
    f.close()
    #----SETTING BOUNDARY CONDITION----------------------------#
    N=[];N0=range(GROSS_DOF);
    for i in N0:
        if (K[i,i]==1.0e36) or (K[i,i]==0.0):
            N.append(i)
    dN=list(set(N0)-set(N));Ld=len(dN)
    K=K[np.ix_(dN,dN)];M=M[np.ix_(dN,dN)];C=C[np.ix_(dN,dN)]
    return K, M, C, np.array(dN,dtype='int'),Ld

def Obj_Cal_DC(Elmts,Nds,STIF,MASS,w,alpha,beta,Odb_name,Xe,penal,E1,E0,D1,D0):
    w=w*2*np.pi # Hz to Rad/s
    opdb=openOdb(Odb_name+'.odb')
    U=opdb.steps['Step-1'].frames[-1].fieldOutputs['U'].values
    UR=opdb.steps['Step-1'].frames[-1].fieldOutputs['UR'].values
    U_Obj_K=np.zeros(len(Elmts),dtype=complex);U_Obj_K_C=np.zeros(len(Elmts),dtype=complex)
    U_Obj_M=np.zeros(len(Elmts),dtype=complex);U_Obj_M_C=np.zeros(len(Elmts),dtype=complex)
    Obj_Layer=np.zeros(len(Elmts),dtype=complex)
```

```
Obj_Base=np.zeros(len(Elmts),dtype=complex)
Obj=np.zeros(len(Elmts),dtype=complex)
for i in range(len(Elmts)):
    Ue=[]
    for ec in Elmts[i].connectivity:
        j=Nds[ec].label-1
        Ue.extend(U[j].data+1j*U[j].conjugateData)
        Ue.extend(UR[j].data+1j*UR[j].conjugateData)
    Ue=np.array([Ue],dtype=complex)
    S_K=(1+1j*w*beta)*STIF[i+1]
    U_Obj_K[i]=(np.dot(np.dot(Ue,S_K),Ue.T))[0][0]
    U_Obj_K_C[i]=(np.dot(np.dot(Ue,S_K),np.conj(Ue.T)))[0][0]
    S_M=(1j*w*alpha-w**2)*MASS[i+1]
    U_Obj_M[i]=(np.dot(np.dot(Ue,S_M),Ue.T))[0][0]
    U_Obj_M_C[i]=(np.dot(np.dot(Ue,S_M),np.conj(Ue.T)))[0][0]
# Calculate Objective
Obj_K=U_Obj_K*(Xe**penal*E1+(1-Xe**penal)*E0)
Obj_M=U_Obj_M*(Xe**penal*D1+(1-Xe**penal)*D0)
Obj_Layer=np.sum(Obj_K+Obj_M)
# Process sensitivities
Obj_K_C=U_Obj_K_C*(Xe**penal*E1+(1-Xe**penal)*E0)
Obj_M_C=U_Obj_M_C*(Xe**penal*D1+(1-Xe**penal)*D0)
Ae=(np.sum(Obj_K_C+Obj_M_C))
Ae=-np.real(Ae*penal*Xe**(penal-1)*(U_Obj_M*(D1-D0)+U_Obj_K*(E1-E0)))
#--------------------------------------------------------------------#
# Elmts=mdb.models['Model-1'].parts['Base'].elements
# Nds =mdb.models['Model-1'].parts['Base'].nodes
# alpha=0;beta=0
# STIF={};MASS={};Read_ESM('ESMBASE400.mtx',STIF,MASS,24)
# for i in range(len(Elmts)):
    # Ue=[]
    # for ec in Elmts[i].connectivity:
        # j=Nds[ec].label-1
        # for k in range(len(U[j].data)):
            # Ue.append(U[j].data[k]+complex(0,U[j].conjugateData[k]))
        # for k in range(len(UR[j].data)):
            # Ue.append(UR[j].data[k]+complex(0,UR[j].conjugateData[k]))
    # Ue=np.array([Ue],dtype=complex)
    # S_K=(1+1j*w*beta)*STIF[i+1]
    # U_Obj_K[i]=(np.dot(np.dot(Ue,S_K),Ue.T))[0][0]
    # S_M=(1j*w*alpha-w**2)*MASS[i+1]
    # U_Obj_M[i]=(np.dot(np.dot(Ue,S_M),Ue.T))[0][0]
# Obj_Base=np.sum(U_Obj_K+U_Obj_M)
opdb.close()
```

```
    Obj=np.abs(Obj_Layer)#+Obj_Base)
    Ae=Ae/Obj
    return Obj,Ae

def Obj_Cal_DISP(Elmts,Nds,STIF,MASS,w,alpha,beta,Odb_name,Xe,penal,E1,E0,D1,D0):
    w=w*2*np.pi # Hz to Rad/s
    opdb=openOdb(Odb_name+'.odb')
    U=opdb.steps['Step-1'].frames[-1].fieldOutputs['U'].values
    UR=opdb.steps['Step-1'].frames[-1].fieldOutputs['UR'].values
    Mu,Obj=Obj_Cal_DISP_READ(U,w,Odb_name)
    U_Obj_K=np.zeros(len(Elmts),dtype=complex)
    U_Obj_M=np.zeros(len(Elmts),dtype=complex)
    for i in range(len(Elmts)):
        Ue=[];Mue=[]
        for ec in Elmts[i].connectivity:
            j=Nds[ec].label-1
            for k in range(len(U[j].data)):
                Ue.append(U[j].data[k]+complex(0,U[j].conjugateData[k]))
            for k in range(len(UR[j].data)):
                Ue.append(UR[j].data[k]+complex(0,UR[j].conjugateData[k]))
            Mue.extend(Mu[0,ec*6:ec*6+6])
        Ue=np.array([Ue],dtype=complex)
        Mue=np.array([Mue],dtype=complex)
        S_K=(1+1j*w*beta)*STIF[i+1]
        S_M=(1j*w*alpha-w**2)*MASS[i+1]
        U_Obj_K[i]=(np.dot(np.dot(Mue,S_K),Ue.T))[0][0]
        U_Obj_M[i]=(np.dot(np.dot(Mue,S_M),Ue.T))[0][0]
    # Process sensitivities
    Ae=2*np.real(penal*Xe**(penal-1)*(U_Obj_M*(D1-D0)+U_Obj_K*(E1-E0)))
    return Obj,Ae

def Obj_Cal_MDR(ESM,Xe,penal,Mats,JOBName):
    l1=143;l2=429;l3=572
    GROSS_DOF=6*l1+3*(l2-l1)+6*(l3-l2)
    K,M,C,dN,Ld=Obj_Cal_MDR_READ(l1,l2,l3,GROSS_DOF,JOBName)
    C_STIF=ESM['ESMCORE_120_Elements.mtx']['STIF'];C_MASS=ESM['ESMCORE_120_Elements.mtx']['MAS
S'];C_NODENUM=ESM['ESMCORE_120_Elements.mtx']['NODENUM']
    T_STIF=ESM['ESMTOP_120_Elements.mtx']['STIF'] ;T_MASS=ESM['ESMTOP_120_Elements.mtx']['MASS
'] ;T_NODENUM=ESM['ESMTOP_120_Elements.mtx']['NODENUM']
    C_E0=Mats['Core']['E0'];C_E1=Mats['Core']['E1'];C_D0=Mats['Core']['D0'];C_D1=Mats['Core'][
'D1']
    T_E0=Mats['Top']['E0'];T_E1=Mats['Top']['E1'];T_D0=Mats['Top']['D0'];T_D1=Mats['Top']['D1'
]
    #load dynamic library
```

```
    flib = load_library("mdr","./");fun_1=flib.mdr_sen
    Ae= np.empty(shape=(len(Xe)),dtype='f8',order='f')
    Lf= np.empty(shape=(10),dtype='f8',order='f')
    # call function
    fun_1.argtypes =
[ndpointer(dtype='f8',ndim=1),ndpointer(dtype='f8',ndim=1),ndpointer(dtype='f8',ndim=1),c_int,
c_int,c_int,c_int,c_int,c_double,c_double,c_double,c_double,c_double,\
    c_double,c_double,c_double,ndpointer(dtype='f8',ndim=2),ndpointer(dtype='f8',ndim=2),ndpoi
nter(dtype='f8',ndim=2),ndpointer(dtype='f8',ndim=3),ndpointer(dtype='f8',ndim=3),\
    ndpointer(dtype='f8',ndim=3),ndpointer(dtype='f8',ndim=3),ndpointer(dtype='int',ndim=2),nd
pointer(dtype='int',ndim=2),ndpointer(dtype='int',ndim=1)]
    flib.mdr_sen(Ae,Lf,Xe,penal,GROSS_DOF,len(Xe),Ld,24,C_D0,C_E0,C_D1,C_E1,T_D0,T_E0,T_D1,T_E
1,K,M,C,C_STIF,C_MASS,T_STIF,T_MASS,C_NODENUM,T_NODENUM,dN)
    return 1/Lf[0],Ae

def Con_Constraint(x,y,z,l1,l2,l3):
    # Construct constrained vectors
    Master_P1=range(1,x*y+1)
    Master_P2=((np.kron(np.ones(y,dtype=int),range((x-1)*y*z+1,0,-
z*y))).reshape([y,x])+(np.kron(range(y-1,-1,-
1),np.ones(x,dtype=int))).reshape([y,x])).flatten()+l1
    Slave_P1=Master_P2+y
    Slave_P2=np.array(range(1,x*y+1),dtype=int)+l2
    Master=Master_P1;Master.extend(list(Master_P2))
    Slave=list(Slave_P1);Slave.extend(list(Slave_P2))
    return Master,Slave

def Node2DOF(Mnodes,l1,l2,l3):
    rem=[]
    for mm in Mnodes:
        if mm <= l1:
            rem.append((mm-1)*6)
        elif l1< mm <= l2:
            rem.append(l1*6+(mm-l1-1)*3)
        elif l2< mm <= l3:
            rem.append(l1*6+(l2-l1)*3+(mm-l2-1)*6)
    return np.array(rem,dtype=int)

def Result_Plot_BESO():
    # Display final design
    vp3 = session.Viewport('Final design', origin=(30,30),width=150, height=100)
    p = mdb.models['Model-1'].parts['Part-1']
    vp3.setValues(displayedObject=p)
    vp3.partDisplay.setValues(mesh=ON)
```

```
    vp3.partDisplay.displayGroup.remove(leaf=dgm.LeafFromSets(sets=(p.sets['vs'],)))

def Result_Plot_SIMP(mdb,Xe,Instance_Name):
    itern = len(mdb.customData.History['obj'])
    # Plot objective function history
    vp1 = session.Viewport('Objective history',origin=(20,20),width=150,height=100)
    try:
        xyPlot1 = session.XYPlot('Objective function')
    except:
        del session.xyPlots['Objective function']
        xyPlot1 = session.XYPlot('Objective function')
    chart1 = xyPlot1.charts.values()[0]
    objDat = [(k,mdb.customData.History['obj'][k]) for k in range(itern)]
    xydo = session.XYData('Objective function',objDat)
    chart1.setValues(curvesToPlot=[session.Curve(xydo)])
    chart1.axes1[0].axisData.setValues(title='Iteration')
    chart1.axes2[0].axisData.setValues(title='Objective function')
    vp1.setValues(displayedObject=xyPlot1)
    # Display final design
    opdb = session.openOdb(name= mdb.jobs.keys()[-1]+'.odb',readOnly=FALSE)
    frame=opdb.steps['Step-1'].frames[-1]
    MaterialDensity= frame.FieldOutput(name='MaterialDensity', description='Element Materials
Density',type=SCALAR)
    MyInstance=opdb.rootAssembly.instances[Instance_Name]
    elementLabels=range(1,len(MyInstance.elements)+1)
    elementValues=[[i]  for i in Xe]
    MaterialDensity.addData(position=WHOLE_ELEMENT, instance=MyInstance, labels=elementLabels,
data=elementValues)
    opdb.save()
    opdb.close()

def FinalRun(mdb, Xe, E0, E1, D0, D1, penal, Ele_NUM, possoin):
    # Final Run
    # Updating E, D, Obj, Volume
    E=Xe**penal*E1+(1-Xe**penal)*E0
    D=Xe**penal*D1+(1-Xe**penal)*D0
    # Assign solid and void elements to each section
    for i in range(Ele_NUM):
        mdb.models['Model-1'].materials['Material'+str(i+1)].Elastic(((E[i], possoin),))
        mdb.models['Model-1'].materials['Material'+str(i+1)].Density(((D[i],),))
    mdb.Job('Final_Design','Model-1').submit()
    mdb.jobs['Final_Design'].waitForCompletion()

def Topot_Main(Limit_iter):
```

```
    global mdb, elmts, nds, Ele_NUM
    global Part_Name, Instance_Name, ESM_Name
    global vf, rmin, penal, change, iter_num, Xei, vh, oh, Fm
    global w, alpha, beta, th, possoin
    global Xe, upp, low
    # Close Output Databases
    for i in range(len(session.odbs.keys())):
        session.odbs[session.odbs.keys()[0]].close()
    print 'VolFrac:{0} Rmin:{1} Penal:{2}  X_initial:{3}'.format(vf,rmin,penal,Xei)
    #print 'E_Strong:{0:.3e} E_Weak:{1:.3e} D_Strong:{2} D_Weak:{3}'.format(E1, E0, D1, D0)
    #print 'alpha:{0} beta:{1} wp:{2}Hz'.format(alpha,beta,w)
    # Start Time
    to=time.time()
    #-------------DOF Index-----------------#
    x=11;y=13;z=2
    l1=143;l2=429;l3=572
    Master,Slave=Con_Constraint(x,y,z,l1,l2,l3)
    TieDofNum=3;TieNodeNum=len(Master);
    Master=list(np.kron(Node2DOF(Master,l1,l2,l3),np.ones(TieDofNum,dtype=int))+np.kron(np.one
s(TieNodeNum,dtype=int),range(TieDofNum)))
    Slave
=list(np.kron(Node2DOF(Slave,l1,l2,l3),np.ones(TieDofNum,dtype=int))+np.kron(np.ones(TieNodeNu
m,dtype=int),range(TieDofNum)))
    #-------------Reading Matrix-------------#
    ESM={}
    for EN in ESM_Name:
        ESM[EN]={};ESM[EN]['NODESUM']=0;ESM[EN]['DOFNUM']=0
        ESM[EN]['STIF']=np.empty(shape=(len(Xe),24,24),dtype='f8',order='f')
        ESM[EN]['MASS']=np.empty(shape=(len(Xe),24,24),dtype='f8',order='f')
        ESM[EN]['NODENUM']=np.empty(shape=(len(Xe),24),dtype='int')
        Read_ESM(EN,ESM[EN]['STIF'],ESM[EN]['MASS'],ESM[EN]['NODENUM'],ESM[EN]['NODESUM'],
ESM[EN]['DOFNUM'], 24, l1, l2, l3, Slave, Master)
        print 'READ {0} ELEMENT MATRICES IN TOTAL: {1}'.format(len(ESM[EN]['STIF']),EN)
    #--------------FE Settings--------------#
    FE_Mdb(mdb,Mats,Ele_NUM,w)
    print "Optimization Start..."
    # MMA INITIAL PARAMETERS
    m=1;n=Ele_NUM;c0 = 1000;d = 0;a0 = 1;a = 0;
    xold1=np.zeros(n,dtype='f8');xold2=np.zeros(n,dtype='f8')
    xmin=0.001*np.ones(n,dtype='f8');xmax=np.ones(n,dtype='f8');Xmma=np.ones(n,dtype='f8')
    # Load dynamic library
    flib = load_library("mmsub","./");fmmsub=flib.mmsub
    fmmsub.argtypes =
[ndpointer(dtype='f8'),ndpointer(dtype='f8'),ndpointer(dtype='f8'),c_int,c_int,c_int,\
```

```
    ndpointer(dtype='f8'),ndpointer(dtype='f8'),ndpointer(dtype='f8'),ndpointer(dtype='f8'),nd
pointer(dtype='f8'),\
    c_double,ndpointer(dtype='f8'),c_double,ndpointer(dtype='f8'),c_double,c_double,c_double,c
_double]
    # Optimization iteration
    while change > 0.001 and iter_num < Limit_iter:
        # Run FEA
        print 'Run_FEA_Time comsumed:{0}s'.format(time.time()-to)
        odb_name=Run_FEA(mdb,iter_num)
        print 'Run_FEA_Time comsumed:{0}s'.format(time.time()-to)
        vh.append(np.sum(Xe)/Ele_NUM)
        # Calculate Objective and sensitivities
        #Obj,Ae=Obj_Cal_DISP(elmts,nds,STIF,MASS,w,alpha,beta,odb_name,Xe,penal,E1,E0,D1,D0)
        #Obj,Ae=Obj_Cal_DC(elmts,nds,STIF,MASS,w,alpha,beta,odb_name,Xe,penal,E1,E0,D1,D0)
        #Obj,Ae=Obj_Cal_PF(elmts,nds,STIF,MASS,w,alpha,beta,odb_name,Xe,penal,E1,E0,D1,D0)
        Obj,Ae=Obj_Cal_MDR(ESM,Xe,penal,Mats,odb_name)
        print 'Sensitivity_Cal comsumed:{0}s'.format(time.time()-to)
        oh.append(Obj)
        Ae=fltAe(Ae,Fm,Xe)
        # SIMP optimization
        #Xe=OC(vf,Xe,Ae,Ele_NUM)
        # MMA Algorithm
        f0val=Obj;df0dx=np.array(Ae,dtype='f8');fval=np.sum(Xe)-
vf*Ele_NUM;dfdx=np.ones(n,dtype='f8')
        fmmsub(Xmma,low,upp,m,n,iter_num,Xe,xmin,xmax,xold1,xold2,f0val,df0dx,fval,dfdx,a0,a,c
0,d)
        xold2 = xold1;xold1 = Xe;Xe=Xmma.copy();
        # ------------------Updating E, D, Obj, Volume ------------------#
        PN=Part_Name[0];part = mdb.models['Model-1'].parts[PN]
        E0=Mats[PN]['E0'];E1=Mats[PN]['E1'];D0=Mats[PN]['D0'];D1=Mats[PN]['D1']
        alpha=Mats[PN]['alpha'];beta=Mats[PN]['beta'];th=Mats[PN]['th'];possion=Mats[PN]['poss
ion']
        E=Xe**penal*E1+(1-Xe**penal)*E0
        D=Xe**penal*D1+(1-Xe**penal)*D0
        for i in range(Ele_NUM):
            mdb.models['Model-1'].materials['Material'+PN+str(i+1)].Elastic(((E[i],
possion),))
            mdb.models['Model-1'].materials['Material'+PN+str(i+1)].Density(((D[i],),))
        PN=Part_Name[1];part = mdb.models['Model-1'].parts[PN]
        E0=Mats[PN]['E0'];E1=Mats[PN]['E1'];D0=Mats[PN]['D0'];D1=Mats[PN]['D1']
        alpha=Mats[PN]['alpha'];beta=Mats[PN]['beta'];th=Mats[PN]['th'];possion=Mats[PN]['poss
ion']
        E=Xe**penal*E1+(1-Xe**penal)*E0
        D=Xe**penal*D1+(1-Xe**penal)*D0
```

```
        for i in range(Ele_NUM):
            mdb.models['Model-1'].materials['Material'+PN+str(i+1)].Elastic(((E[i],
possion),))
            mdb.models['Model-1'].materials['Material'+PN+str(i+1)].Density(((D[i],),))
        change=np.max(np.abs(Xe-xold1))
        if oh[-1] <1e16:
            iter_num += 1
            print 'iter: {3} vol:{0:.2f}, obj:{1}, change:{2:.6f}'.format(vh[-1],oh[-
1],change,iter_num)

        else:
            print 'Optimization faild for extreamly large obj.';break
        print "Optimization Finished!"
    print 'Time comsumed:{0}s'.format(time.time()-to)
    # Save results
    mdb.customData.History = {'vol':vh,'obj':oh}
    # Postprocess
    y=sorted(Xe,reverse=True)
    vt=y[int(np.floor((vf-0.001)*Ele_NUM/(1-0.001)))]
    Exa=np.where(Xe>=vt)
    Shr=np.where(Xe<vt)
    Xe[Exa]=1.0;Xe[Shr]=0.001
    # Display
    Result_Plot_SIMP(mdb,Xe,Instance_Name)
    #FinalRun(mdb, Xe, E0, E1, D0, D1, penal, Ele_NUM, possoin)
    # Cal Structural Identity
    #Cal_Identity(elmts,w)
    pass
```